TECHNICAL REPORT STANDARD TITLE PAGE

1. Report No.	2. Government Accession No.	3. Recipient's Catalog No.
FHWA/TX-88/1182-3		
4. Title and Subtitle Experimental and Analytical Study of a Post-Tensioned Bridge		5. Report Date February, 1992 6. Performing Organization Code
7. Author(s) Roschke, P.N., Pruski, K.R., and Sripadanna, N.		8. Performing Organization Report No. Research Report 1182-3
9. Performing Organization Name and Address Texas Transportation Institute The Texas A&M University System College Station, Texas 77843-3135		10. Work Unit No. 11. Contract or Grant No. Study No. 2-5-88/0-1182
12. Sponsoring Agency Name and Address Texas Department of Transportation Transportation Planning Division P. O. Box 5051 Austin, Texas 78763		13. Type of Report and Period Covered Intrim Report September, 1987-August, 1991 14. Sponsoring Agency Code

15. Supplementary Notes

Research performed in cooperation with DOT, FHWA

Research Study Title: Evaluation of Factors Affecting Slabs Due to Localized Post-Tension Forces.

16. Abstract

This is the third in a series of reports documenting a research program aimed at detailed investigation of bridge structures with moderately thick slabs resting directly on columns without bent caps. Post-tensioning is employed in the longitudinal and transverse directions. Longitudinal post-tensioning is uniformly distributed across the width of the bridge; transverse post-tensioning is employed only in column regions. Two scaled laboratory models, named Model One and Model Two, are being tested, along with instrumentation of an actual bridge in Wichita Falls, Texas. This report relates to the field study portion of this project.

The purpose of instrumenting the Brook Street Overpass bridge is to verify deflections and strains predicted by a finite element program, that is proposed as a general purpose design tool for flat plate bridges. Stresses in the field bridge are indirectly measured by a large array of strain gages attached to pencil bars that are embedded in the concrete. Deflections and temperatures of the slab are also monitored. Data due to dead load is acquired immediately after the concrete pour, after longitudinal prestressing, and for a period of two and one-half years. For live load testing, a three-axle dump truck is placed on the bridge at nine different locations.

Comparisons of deflections and strains that result from existing analytical methods and actual bridge responses are presented. Results indicate that a simplified analytical method does not yield predictions that are consistent with experimental measurements for service load conditions. Some assumptions often used in designing transverse prestressing are shown to be incompatible with experimental and finite element predictions. Simplified assumptions concerning distribution of transverse prestressing forces into the slab are evaluated. Placement of transverse post-tensioning exclusively on the column bents is evaluated and uniform distribution of transverse post-tensioning tendons is recommended to prevent occurrence of longitudinal cracking.

17. Key Words	18. Distribution Statement
Bridge, concrete, failure, finite elements, plate, prestressing, shear, slab, strain, stress, temperature	No restrictions. This document is available to the public through the National Technical Information Service 5285 Port Royal Road Springfield, Virginia 22161

19. Security Classif. (of this report)	20. Security Classif. (of this page)	21. No. of Pages	22. Price
Unclassified	Unclassified	146	

Form DOT F 1700.7 (8-69)

Experimental and Analytical Study of a Post-Tensioned Bridge

by

Paul N. Roschke
Assistant Research Engineer

and

Kevin R. Pruski
Narayana Sripadanna
Graduate Research Assistants

Research Report 1182-3

on

Evaluation of Factors Affecting Slabs Due to Localized Post-Tension Forces

Research Study No. 2-5-88-1182

Sponsored by

Texas Department of Transportation

in cooperation with

The United States Department of Transportation
Federal Highway Administration

February 1992

Texas Transportation Institute
The Texas A&M University System
College Station, Texas 77843-3135

METRIC (SI*) CONVERSION FACTORS

APPROXIMATE CONVERSIONS TO SI UNITS

LENGTH

Symbol	When You Know	Multiply By	To Find	Symbol
in	inches	2.54	centimetres	cm
ft	feet	0.3048	metres	m
yd	yards	0.914	metres	m
mi	miles	1.61	kilometres	km

AREA

Symbol	When You Know	Multiply By	To Find	Symbol
in^2	square inches	645.2	centimetres squared	cm^2
ft^2	square feet	0.0929	metres squared	m^2
yd^2	square yards	0.836	metres squared	m^2
mi^2	square miles	2.59	kilometres squared	km^2
ac	acres	0.395	hectares	ha

MASS (weight)

Symbol	When You Know	Multiply By	To Find	Symbol
oz	ounces	28.35	grams	g
lb	pounds	0.454	kilograms	kg
T	short tons (2000 lb)	0.907	megagrams	Mg

VOLUME

Symbol	When You Know	Multiply By	To Find	Symbol
fl oz	fluid ounces	29.57	millilitres	mL
gal	gallons	3.785	litres	L
ft^3	cubic feet	0.0328	metres cubed	m^3
yd^3	cubic yards	0.0765	metres cubed	m^3

NOTE: Volumes greater than 1000 L shall be shown in m^3.

TEMPERATURE (exact)

Symbol	When You Know	Multiply By	To Find	Symbol
°F	Fahrenheit temperature	5/9 (after subtracting 32)	Celsius temperature	°C

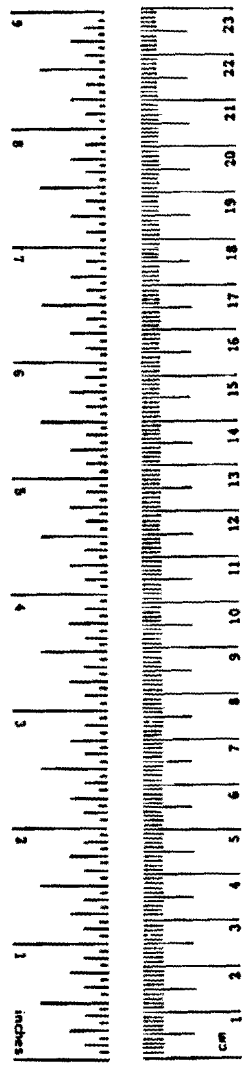

APPROXIMATE CONVERSIONS TO SI UNITS

LENGTH

Symbol	When You Know	Multiply By	To Find	Symbol
mm	millimetres	0.039	inches	in
m	metres	3.28	feet	ft
m	metres	1.09	yards	yd
km	kilometres	0.621	miles	mi

AREA

Symbol	When You Know	Multiply By	To Find	Symbol
mm^2	millimetres squared	0.0016	square inches	in^2
m^2	metres squared	10.764	square feet	ft^2
km^2	kilometres squared	0.39	square miles	mi^2
ha	hectores (10 000 m^2)	2.53	acres	ac

MASS (weight)

Symbol	When You Know	Multiply By	To Find	Symbol
g	grams	0.0353	ounces	oz
kg	kilograms	2.205	pounds	lb
Mg	megagrams (1 000 kg)	1.103	short tons	T

VOLUME

Symbol	When You Know	Multiply By	To Find	Symbol
mL	millilitres	0.034	fluid ounces	fl oz
L	litres	0.264	gallons	gal
m^3	metres cubed	35.315	cubic feet	ft^3
m^3	metres cubed	1.308	cubic yards	yd^3

TEMPERATURE (exact)

Symbol	When You Know	Multiply By	To Find	Symbol
°C	Celsius temperature	9/5 (then add 32)	Fahrenheit temperature	°F

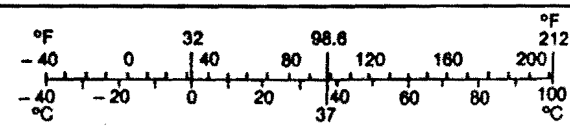

These factors conform to the requirement of FHWA Order 5190.1A.

* SI is the symbol for the International System of Measurements

ABSTRACT

This is the third in a series of reports documenting a research program aimed at detailed investigation of bridge structures with moderately thick slabs resting directly on columns without bent caps. Post-tensioning is employed in the longitudinal and transverse directions. Longitudinal post-tensioning is uniformly distributed across the width of the bridge; transverse post-tensioning is employed only in column regions. Two scaled laboratory models, named Model One and Model Two, are tested along with instrumentation of an actual bridge in Wichita Falls, Texas. This report relates to the field study portion of this project.

The purpose of instrumenting the Brook Avenue Overpass bridge is to verify deflections and strains predicted by a finite element program that is proposed as a general purpose design tool for flat plate bridges. Stresses in the field bridge are indirectly measured by a large array of strain gages attached to pencil bars that are embedded in the concrete. Deflections and temperatures of the slab are also monitored. Data due to dead load is acquired immediately after the concrete pour, after longitudinal prestressing, and for a period of 2.5 years. For live load testing, a three-axle dump truck is placed on the bridge at nine different locations.

Comparisons of deflections and strains that result from existing analytical methods and actual bridge responses are presented. Results indicate that a one-way procedure yields predictions that are not always consistent with experimental measurements for service load conditions. Some assumptions often used in designing transverse prestressing are shown to be incompatible with experimental and finite element predictions. Assumptions of the one-way procedure concerning distribution of transverse prestressing forces into the slab are considered. Placement of transverse post-tensioning exclusively on the column bents is evaluated, and a combination of banded and uniformly distributed transverse post-tensioning tendons is recommended.

DISCLAIMER

The contents of this report reflect the views of the authors who are responsible for the opinions, findings, and conclusions presented herein. The contents do not necessarily reflect the official views or policies of the Texas Department of Transportation. This report does not constitute a standard, specification, or regulation; it is not intended for construction, bidding, or permit purposes.

The engineer in charge of this project is Dr. Paul N. Roschke, who is a registered professional engineer in the State of Texas (Serial Number 53889).

KEYWORDS

Banded Tendon, Deflection, Finite Element, Post-Tensioning, Slab Bridge, Strain, Stress, Transverse Stressing

ACKNOWLEDGMENTS

This study was conducted under a cooperative program between the Texas Transportation Institute, the Texas Department of Transportation, and the Federal Highway Administration. Randy Cox, Tim Bradberry, and Richard Steger of TxDOT worked closely with the researchers, and their comments and suggestions are appreciated. VSL, Inc., supplied technical drawings. Epoxy coated bars for strain gages were supplied free of charge by Sunbelt, Inc.

IMPLEMENTATION STATEMENT

This report concentrates on one phase of a large study and needs to be read in the context of the other companion reports. Emphasis here is on a long-term field study of a full-scale bridge. Complementary work on a large laboratory model and a special finite element code (see reports 1182-1, 1182-2, and 1182-4) will be helpful for designers who analyze these structures. Placement of post-tensioning tendons can be optimized for reducing cracking of the slab and enhancing structural integrity.

Results of this study are available for immediate implementation by the Texas Department of Transportation.

TABLE OF CONTENTS

Page

LIST OF FIGURES

Figure *Page*

List of Tables

Table *Page*

1. Introduction and Objectives

1.1 General

Design of a structural system for slab and beam construction, which involves a limitation on overall depth of the structure, may require eliminating the beams altogether. For example, thickness of the structure becomes significant for overpasses at highway interchanges and bridges which have a minimum head-room requirement. In many cases the slab itself can be designed to withstand flexure, shear, and in-plane forces without supporting beams.

Texas Department of Transportation (TxDOT) engineers in Austin, Texas, have opted for a moderately-thick slab which rests directly on columns without bent caps. Post-tensioning is employed in longitudinal and transverse directions. While longitudinal post-tensioning is uniformly distributed across the width of the bridge, transverse post-tensioning is employed to stiffen only a small, banded region over each column line in order to act analogous to a stiffened beam (see Fig. 1).

Designers want to know if the current design method for this class of

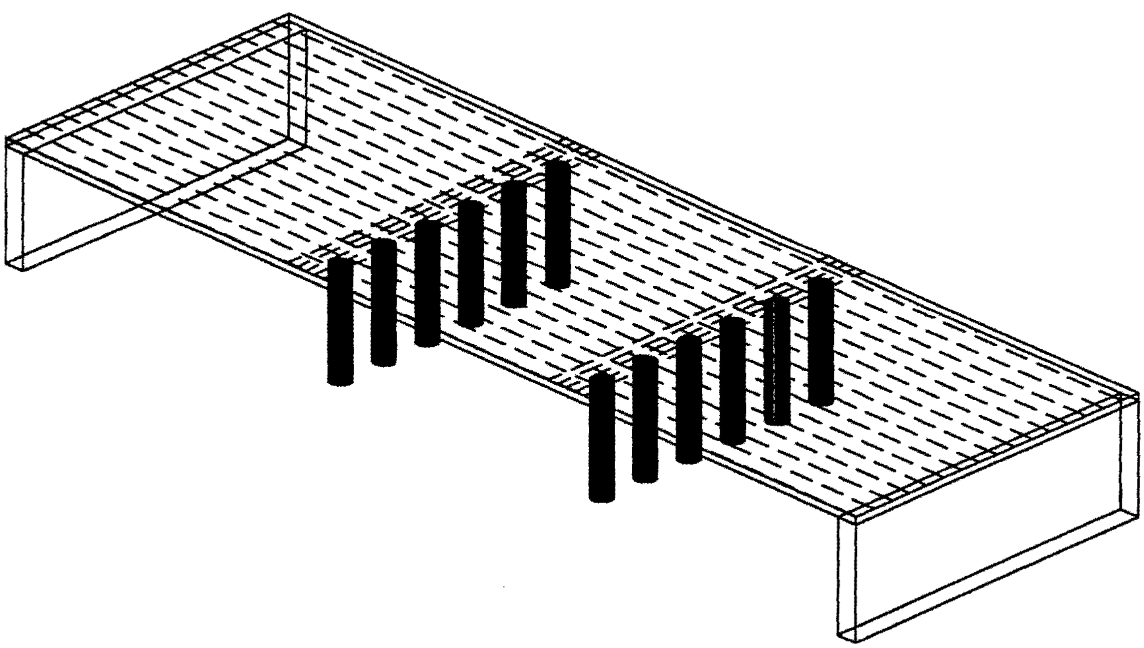

FIG. 1. Three-Span Bridge

structures is conservative or inadequate, degree of validity of the present assumptions, and distribution of prestressing force in the transverse direction. In recognition of the importance of post-tensioned slab bridges and the relative lack of experimental and analytical information pertaining to their behavior, Texas Transportation Institute is conducting a study entitled "Evaluation of Factors Affecting Slabs Due to Localized Post-Tensioned Forces." Two scaled laboratory models, Model One (Roschke 1989) and Model Two, are being tested. In addition, an actual bridge is being instrumented and monitored in Wichita Falls, Texas, as a third major component of the research. This report presents the field study portion of the project. Field data collected from the prototype bridge is used to track time-dependent behavior and validate the numerical simulation of a finite element analysis code.

1.2 LITERATURE REVIEW

Prestressed slab systems that are reinforced for flexure in more than one direction can be analyzed in accordance with American Association of State Highway and Transportation Officials' (AASHTO) specifications and code provisions of the American Concrete Institute (ACI). However, AASHTO does not recommend any special provisions for post-tensioned continuous bridges. An equivalent frame method of analysis (ACI 318-89) has been shown to satisfactorily predict factored moments and shears in prestressed slab systems by tests of large structural models (Scordelis 1959; Burns 1977). Tendons required in a design strip, i.e., center-to-center of adjacent spans, may be banded close to the column line in the transverse direction and uniformly distributed in the longitudinal direction (see Fig. 2). In the transverse direction, ACI calls for at least 2 tendons to be placed inside the design shear section along the column line. Predominant use of banded tendons in buildings by the construction industry has prompted research on this type of structure. The banded tendon layout has been successful in withstanding ultimate loads in a scale model slab (Burns 1985). In this regard, ACI-ASCE Committee 423 (1983) suggests the following:

> Within the limits of tendon distributions that have been tested, research indicates that the moment and shear strength of two-way prestressed slabs is controlled by total tendon strength and by the amount and location of non-prestressed reinforcement, rather than by tendon distribution. While

it is important that some tendons pass within the shear perimeter over columns, distribution elsewhere is not critical and any rational method which satisfies statics may be used.

In addition, ACI calls for a maximum tendon spacing of 6 to 8 times the thickness of the slab, but not to exceed the spacing that provides a minimum average prestressing of 125 psi (0.86 MPa). Even though no tendons are provided between bands in one direction, except near the slab edges, the majority of the area between bands is subjected to biaxial compression (ACI-ASCE 423 1983). This biaxial compression assumption is only true for slabs with an aspect ratio (long span to short span) less than 2. The approximate amount of prestressing required in each direction is obtained by satisfying the required minimum average compression in the slab and then positioning each tendon's vertical profile to withstand external moments (Lin 1981).

Instrumentation of a post-tensioned slab bridge (Burns 1988) shows that the conventional friction loss formula with recommended wobble and friction coefficients yields a reasonable estimation of holding end forces and tendon stress

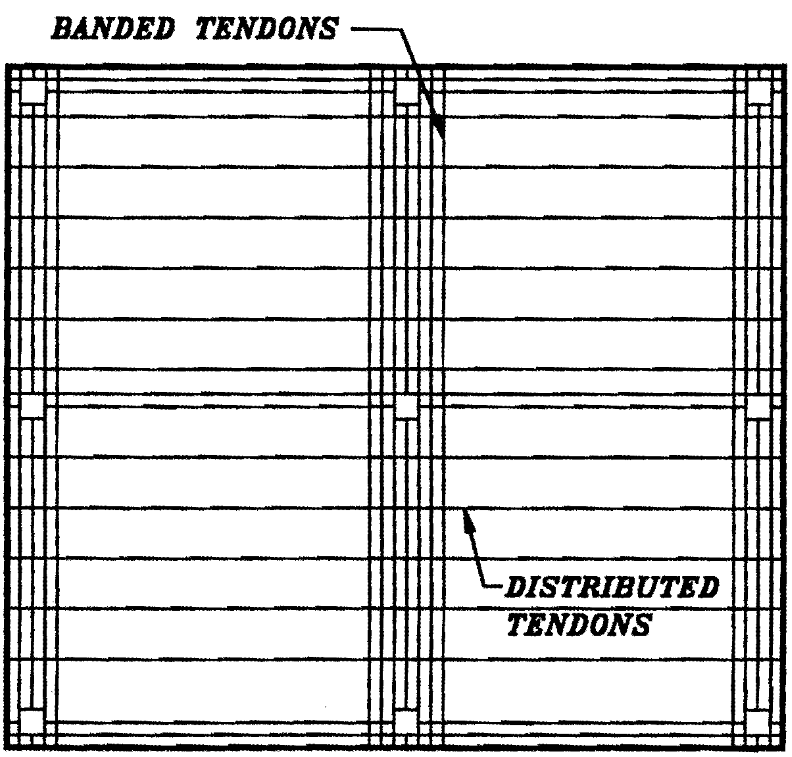

FIG. 2. Banded Tendons in a Flat Slab Supported by Columns

along the profile. However, no attempt is made to study structural response of the bridge.

ACI-ASCE 343 1988 committee comments that:

> Post-tensioned slabs using rigid, round, void forms sometimes exhibit longitudinal cracking over the conduits. This has been effectively controlled by using light transverse post-tensioning throughout the length of the bridge and limiting the longitudinal prestress force on the cross-section to an average value of $0.16\, f_c'$, where f_c' is the 28-day compressive strength of concrete.

Research on time-dependent behavior of concrete box girder bridges (Scordelis, Elfgren, and Larsen 1979) indicates that creep and shrinkage play an important role in strain and deflection levels of concrete bridges. Creep causes strains to increase, especially in negative moment zones. Final concrete strains can be 2.5 to 5 times greater than initial strains, which are due to dead and prestressing loads.

A three-span, haunched, post-tensioned slab bridge constructed in Kansas has uniform prestressing in both longitudinal and transverse directions (Govindaswamy 1989). Transverse prestressing improves the shear capacity of the concrete section. A longitudinal strip method is used for analysis in lieu of plate theory.

1.3 One-Way Design Procedure

A one-way (strip) design procedure for flat slab post-tensioned bridges, in which longitudinal and transverse prestressing are designed separately, has been developed by TxDOT (Bradberry 1987). For longitudinal design, the slab is assumed to act as a number of independent, thin, continuous beams which span from abutment to abutment and are supported at intermediate locations by columns. A typical longitudinal strip is checked for safety against maximum dead and live load stresses.

Design in the transverse direction is more complicated. The amount of load carried by transverse tendons is not calculated by simple statics using a strip. Instead, column reactions and transverse bending moments for dead and movable live loads are obtained from a flat plate analysis code such as SLAB49 (Panak 1979), which does not take prestressing forces into account. Tensile stresses caused by the transverse bending moments are either made equal to zero or kept within allowable limits by application of an appropriate amount of transverse post-tensioning. These tendons are straight and bisect the thickness dimension of the plate. Distribution of prestress force is assumed to spread at an angle of 25.6° in the plane of the plate from the outermost transverse tendon (see Fig. 2). A beam equation, which calculates final stresses in the transverse direction at various locations normal to the column line, is as follows:

$$\sigma = \frac{P_e}{A} \pm \frac{M_p Y}{I} \pm \frac{M_d Y}{I} \quad \text{....................} \quad (1)$$

where σ is the flexural stress, P_e is the total transverse prestressing force, M_p is the moment at a given section due to the prestressing force, M_d is the moment due to dead and live loads, Y is the distance from the neutral axis to the extreme cross-sectional fiber, I is the moment of inertia of the concrete section, and A is the area of concrete at a given cross-section. While calculating A and I, width of the concrete cross-section is assumed to vary according to the distribution of the prestressed force described earlier. In other words, transverse cross-sections of the bridge in column regions are designed by viewing each region as a continuous beam, which is supported at discreet column locations. The moment of inertia varies linearly in the direction of the column line.

Since current practice calls for construction of straight transverse tendons without eccentricity, moment due to transverse prestressing force vanishes. Therefore, Eq. 1 simplifies to:

$$\sigma = \frac{P_e}{A} \pm \frac{M_d Y}{I} \quad \text{....................} \quad (2)$$

or, rearranging to solve for the prestressing force:

$$P_e = A(\sigma \pm \frac{M_d Y}{I}) \quad \text{....................} \quad (3)$$

Eq. 3 shows that when the assumed region of influence of the prestressing force increases, the required prestressing force changes proportionately. That is, the

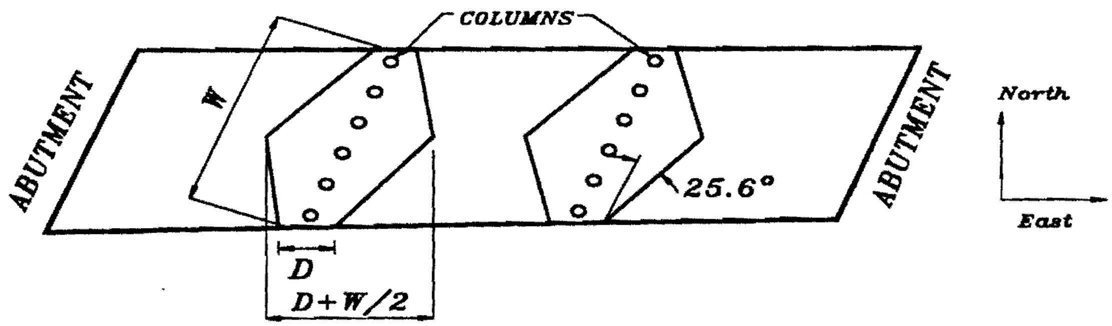

FIG. 3. Assumed Effective Regions of Transverse Stress in the One-Way Analysis

amount of required prestress force depends on the magnitude of the assumed cross-sectional area A. Therefore, the assumed distance $D + (W/2)$ (Fig. 3) is one of the controlling factors in the design of transverse prestressing.

The one-way method described above has been used to design the Brook Street Overpass in Wichita Falls, Texas, and other neighboring structures. In this one-way approach several important parameters such as skew can not be taken into account. Recent research on skewed box-girder bridges (Scordelis et al. 1980) indicates that non-orthogonal geometry leads to behavior which is markedly different from orthogonal bridges. Mid-span moments are generally reduced from their counterpart values in orthogonal plates. For simple-span structures there is the possibility of reducing dead load resisting moments by 50% and 70% in structures skewed 45° and 60°, respectively (Scordelis 1980). In addition to skew, the shape of the bridge in a plan view may not always be a perfect rectangle or parallelogram. On occasion, starting and ending widths are not the same due to entrance and exit ramps. Hence, the current assumption, that analysis of a thin longitudinal strip gives a fair representation of the behavior of the remaining portion of the bridge, may not be correct and can result in an unconservative or overly conservative design.

One means of overcoming some of these shortcomings is to analyze the structure by the finite element method (FEM). Not only can irregular geometry of the slab be taken into account, but biaxial material stresses resulting from simultaneous longitudinal and transverse prestressing can also be considered. Concrete exhibits approximately 27% more compressive strength when biaxially compressed (van Greunen 1979). In a two-way square slab the strain energy due to twisting moment reduces bending moments by about 25% compared to the maximum mid-span moment of a simply-supported one-way slab (Nilson 1972). For post-tensioned bridges, the slab is fully supported along the abutments but only at discrete column locations over the interior supports. This leads to complicated two-way slab action. With FEM, these special conditions can be analyzed.

Use of neoprene pads at abutments and column-bridge deck intersections reduces support stiffness for the slab. No consideration is made in routine design for settlement of supporting columns or compression of rubber pads. Increase of structural capacity due to passive reinforcing steel is often neglected for service load calculations. In reality this steel reduces the amount of required prestressing. Finally, concrete structures are subjected to varying temperatures during their lifetime. At the end of a hot summer day temperatures may reach 104° F (40° C) and subsequently fall to well below 32° F (0° C) during winter. The anticipated thermal strain for such a temperature range can be more than 300 microstrains (Hughes 1971). Simplified analytical approaches do not generally attempt to include these thermal effects.

1.4 OVERALL SCOPE OF THE PROJECT

The goal of this project is to collect and analyze information related to short and long-term behavior of a prototype, flat slab, post-tensioned bridge, under service load conditions. Specific objectives of the research are as follows:

- Develop and install suitable instrumentation to measure strains, deflections, and temperature effects of the Brook Street Overpass in Wichita Falls, Texas.
- Determine, through experimental measurement and analysis, effects due to transverse post-tensioning in the Brook Street Overpass.
- Observe changes in deflections and strains due to temperature and time-dependent effects such as creep and shrinkage on Brook Street Overpass for a period of more than two years from concrete pour.
- Validate the ability of FEM to predict structural response of the prototype bridge under service load conditions.
- Make suggestions to prevent or minimize development of longitudinal cracking.

2. Construction

2.1 General

Construction of a post-tensioned slab bridge in Wichita Falls, Texas, on U.S. Highway 82 began during the summer of 1988. This bridge is the third of its kind constructed in Wichita Falls. At the time of construction of the Brook Avenue Overpass, two Taft Street structures, which are similar in form and construction, were complete and open to traffic. The narrative contained herein, together with accompanying photographs, constitutes a fairly complete description of the construction process. Figs. 4 and 5 show the nearly-completed eastbound Brook Avenue Overpass and a close-up view of the banded tendon region, respectively. Fig. 6 shows the column region of the neighboring Taft Street Overpass.

A pair of bridges for eastbound and westbound traffic is planned at the Brook Avenue site. The eastbound structure is a continuous three-span post-tensioned bridge, which measures 297.2 ft (90.59 m) from abutment to abutment along its centerline. The center span is 97.20 ft (29.63 m) with two 100.0 ft (30.48 m) end spans (see Fig. 7).

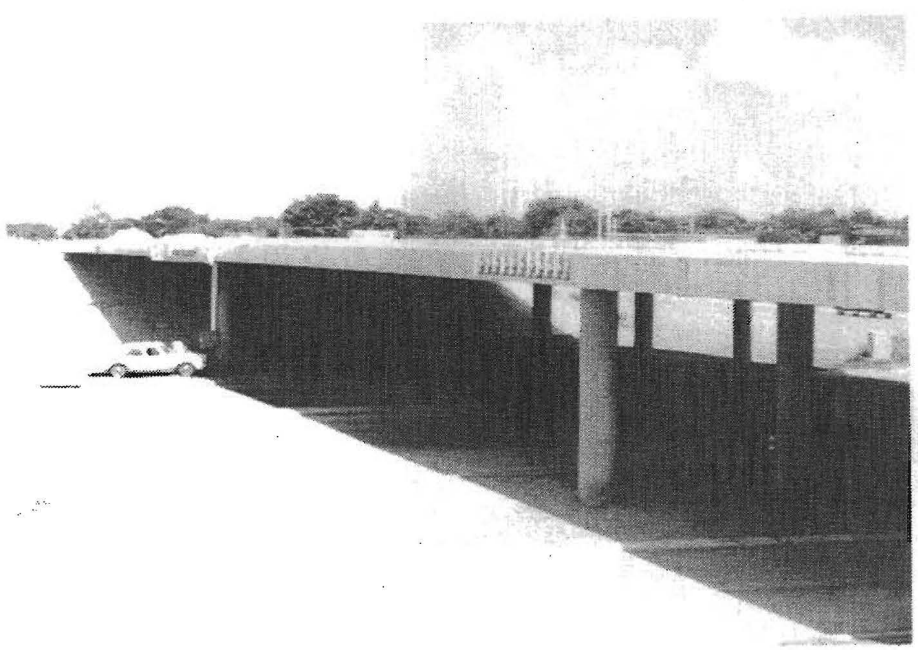

FIG. 4. Brook Street Overpass

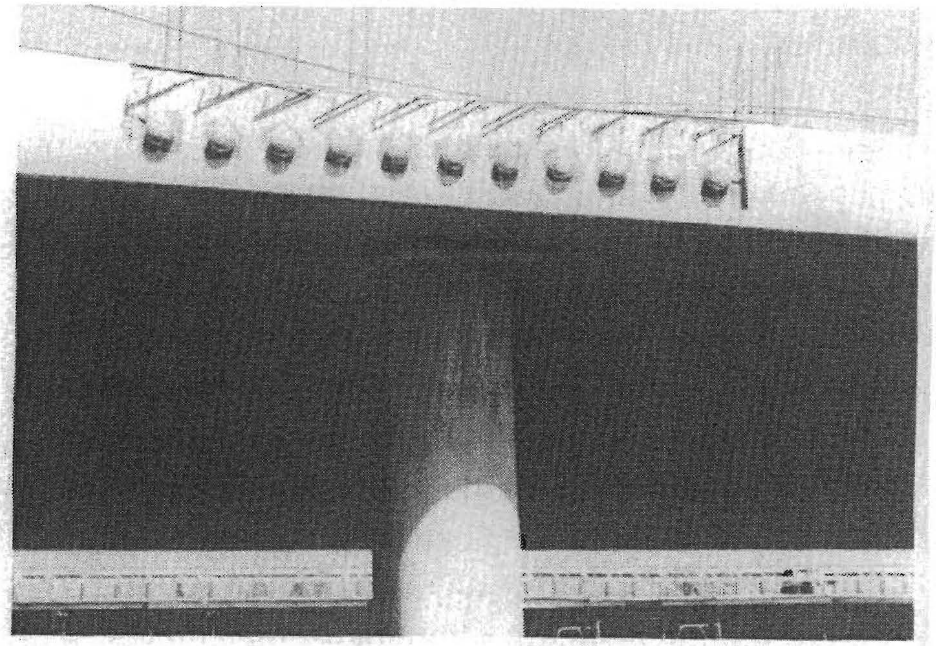

FIG. 5. Banded Transverse Post-Tensioning

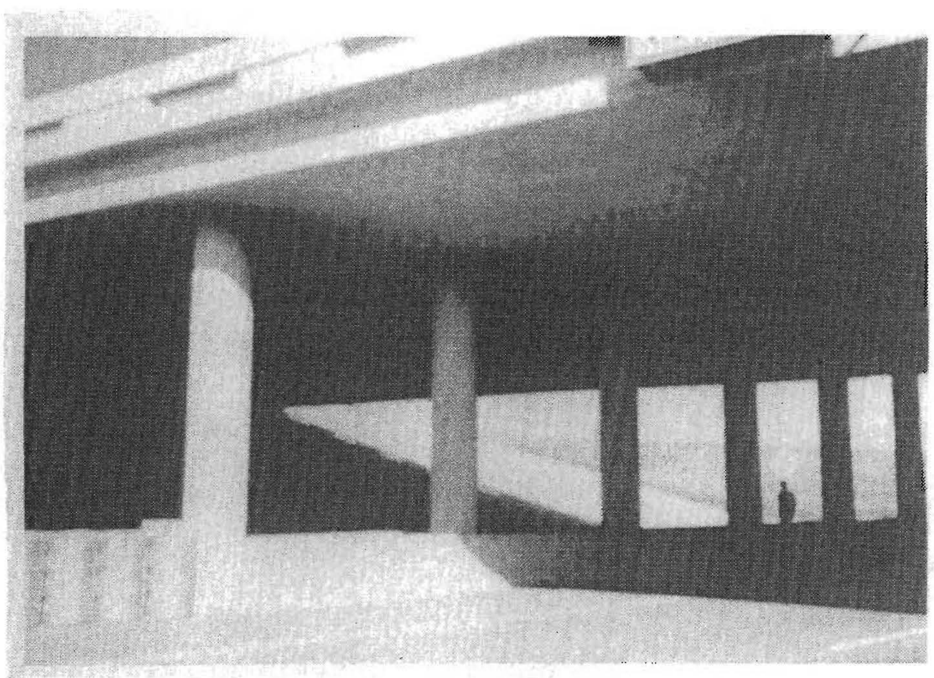

FIG. 6. Column Region of Taft Street Overpass

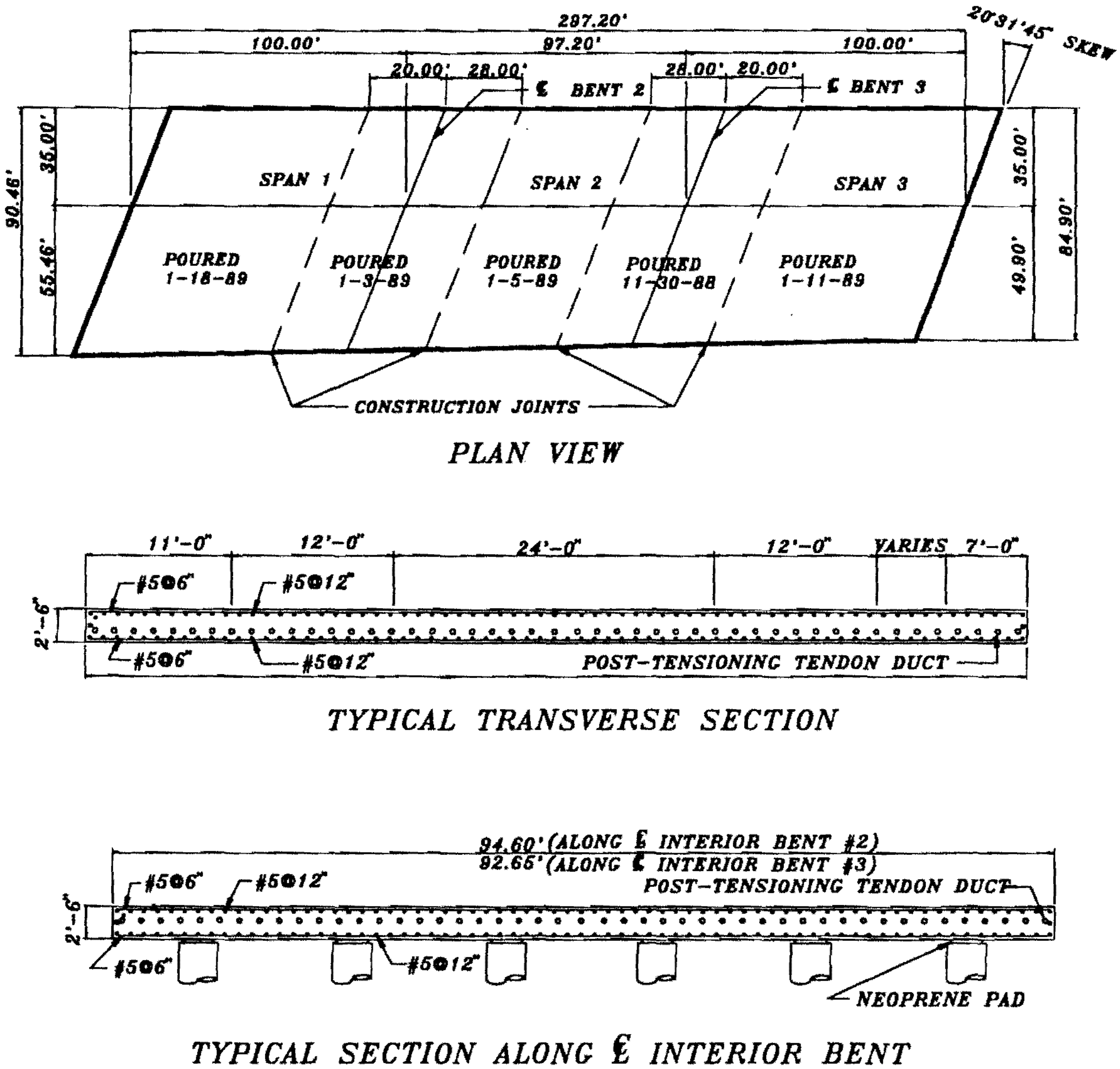

FIG. 7. Plan View and Cross-Section Details

The slab rests on abutments at the outer supports and on 6 columns along each of 2 interior support lines. Its width varies linearly from 90.46 ft (27.57 m) at the west end to 84.90 ft (25.88 m) at the east end. Design thickness of the concrete plate is 30.0 in. (0.762 m). Abutments and columns are skewed by 20°31'45" from a perpendicular to the longitudinal direction. The deck has a 7.0-in. (177.8-mm) crown at the center of the transverse cross-section. It rests directly on neoprene pads that surmount the columns, which are not rigidly connected to the slab by means of reinforcing steel. Instead, a single 2.0-in. (50.8-mm) dowel bar, which extends approximately 6 in. (152.4 mm) into the slab, provides the only steel connection between the column and slab. A neoprene pad separates the bridge slab from each column and cushions the interface. Details of the tendon profile and end-section are shown in Fig. 8. Fig. 9 shows a typical dowel bar and neoprene pad along with the bottom mat of reinforcing steel.

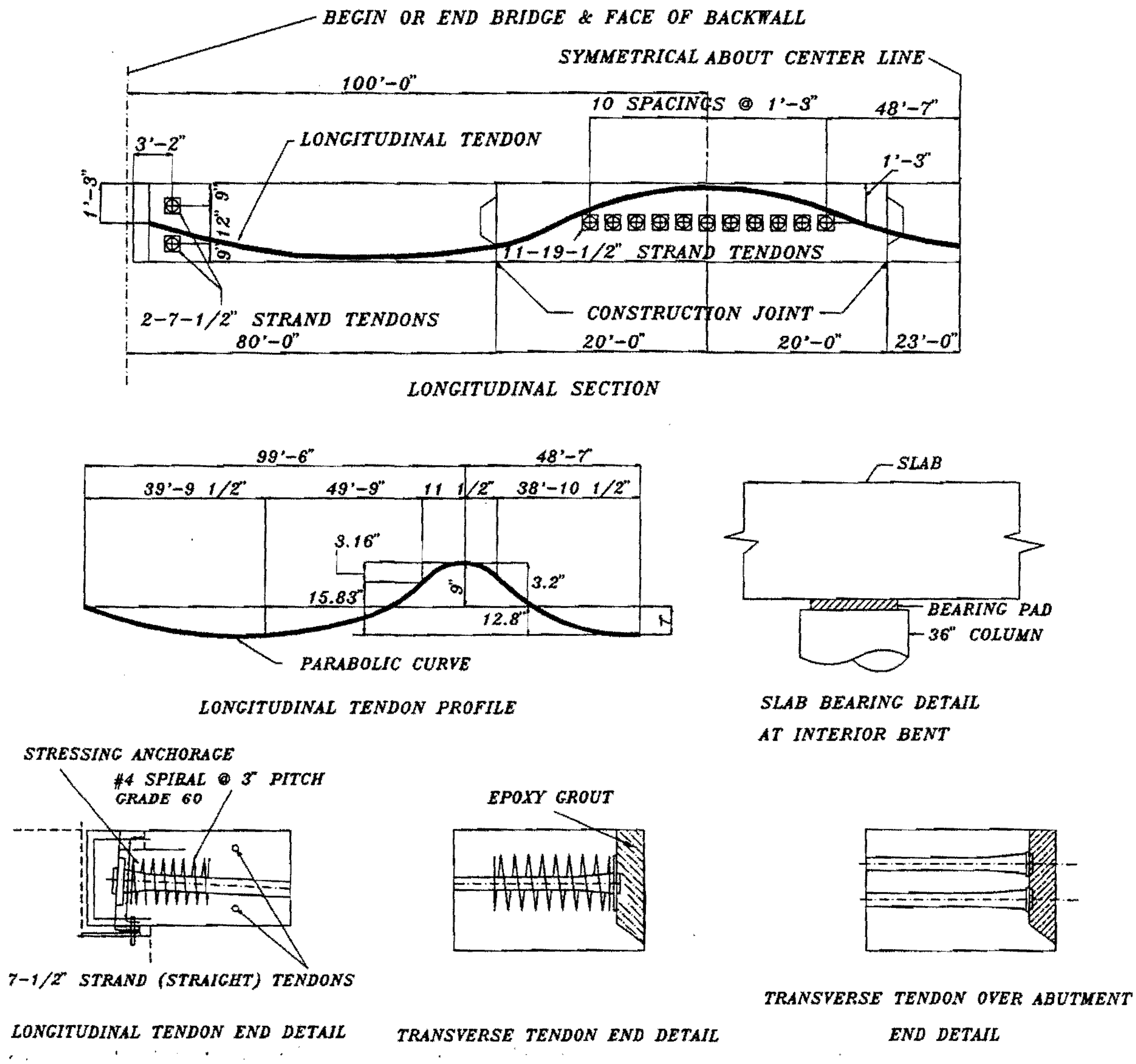

FIG. 8. Prestressing and Column Details

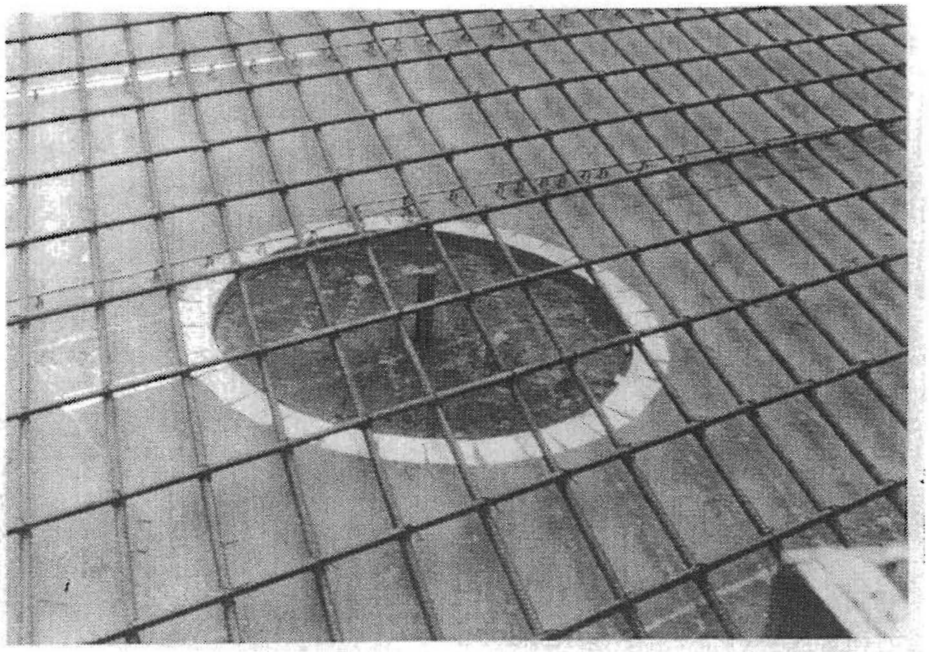

FIG. 9. Neoprene Pad and Dowel Bar

Pouring of the concrete slab began on November 30, 1988. Fig. 10 shows workmen casting the bridge. Concrete pours were made in 5 separate stages. The location of 4 construction joints and dates of each pour are shown in Fig. 7. By January 18, 1989, the entire bridge slab was in place; at the end of February, 1989, stressing of longitudinal and transverse tendons was complete. TxDOT engineers allowed a slump of 9 in. (228.6 mm) for the first casting (see Fig. 11) but changed the maximum allowable slump to 6 in. (152.4 mm) for the four remaining pours. During the first pour, buoyancy of tendon ducts caused portions of the reinforcing steel to rise 2 in. (50.8 mm). TxDOT engineers called for placement of a 2-in. (50.8 mm) thick overlay on this area (pour 1) to provide adequate cover for the reinforcement steel. However, application of the overlay was delayed for 8 months. In the meantime thicknesses of the remaining pours were gradually adjusted (see Fig. 12) to match the new target thickness of 32 in. (812.8 mm) for pour 1. Pours 1, 2, and 3 cured for 59, 25, and 23 days, respectively, before prestressing operations began. However, pours 4 and 5 cured only 10 and 17 days, respectively.

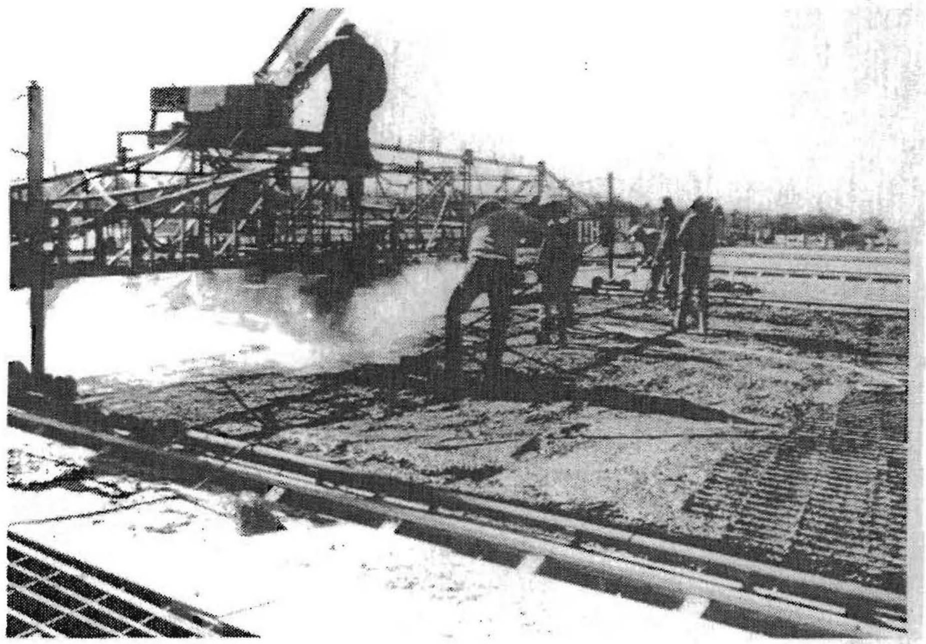

FIG. 10. Concrete Pour

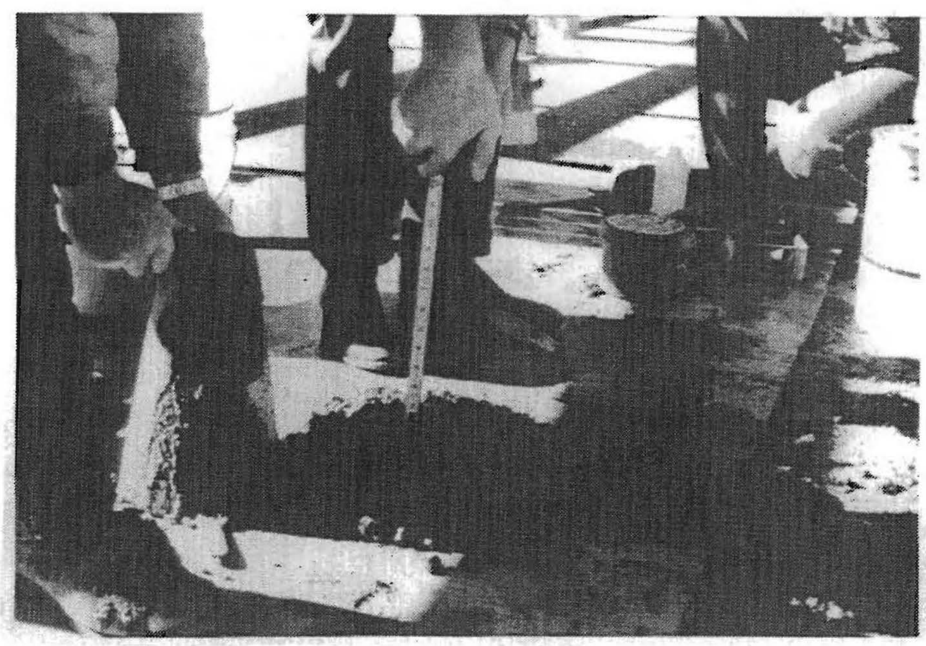

FIG. 11. Slump Test

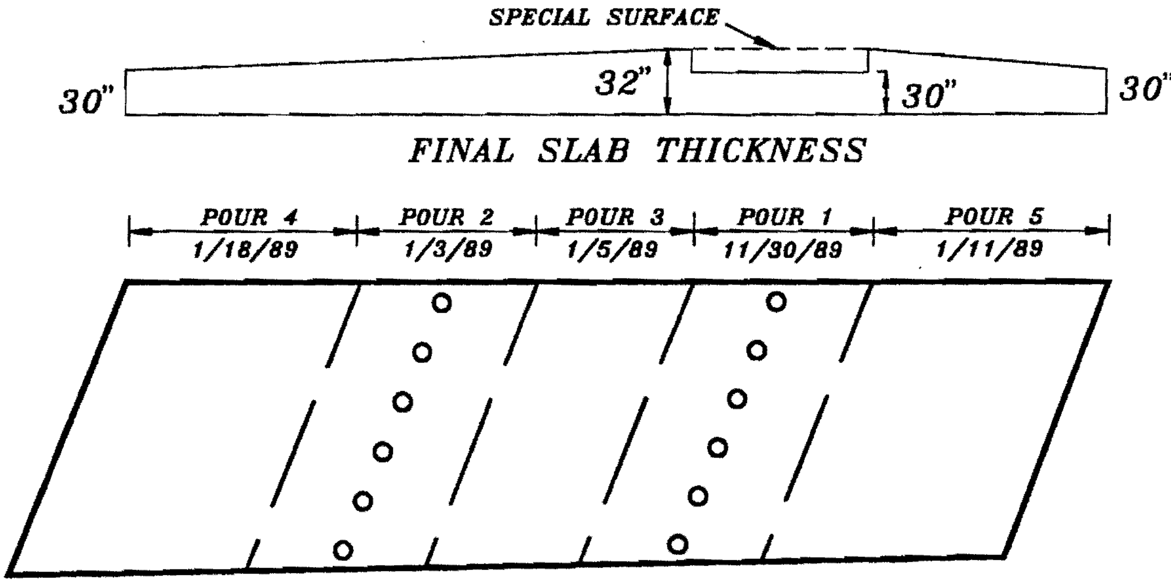

FIG. 12. Final Bridge Profile and Concrete Pours

In addition to transverse tendons above the column lines, 2 transverse tendons near each abutment were installed to control bursting stress developed during longitudinal post-tensioning. Transverse tendons near abutment ends were stressed first, followed by those over the interior column lines. In each case tendons were stressed by jacking from alternating edges of the slab. Out of 11 tendons near each column line, 5 were stressed from one edge of the bridge and 6 were stressed from the other. All transverse tendons were tensioned prior to stressing the longitudinal tendons, which were jacked from both ends. Grout vents were placed on the longitudinal tendon ducts along each column line.

During stressing of the transverse tendons, cracks appeared parallel to the column line approximately 1.0 ft (0.30 m) from the outermost transverse tendon. These cracks extended completely through the slab thickness. During stressing of longitudinal tendons these cracks closed and became invisible to the naked eye. It was reported by the construction crew that the bridge deck lifted off of the formwork at the midsection of each span during longitudinal stressing, creating a gap between the formwork and slab. Longitudinal cracks were observed and measured along tendon ducts approximately one month after longitudinal prestressing was applied (see Figs. 13, 14, and 15). These cracks extend from top to bottom of the slab thickness. This is apparent as rainwater trickles through these cracks. However, there is no evidence that the prestressing forces caused the cracking. Shrinkage of restrained concrete from adjacent pours of concrete is the most probable cause. Diagonal shrinkage cracks were observed in regions of acute angles of the third, fourth, and fifth concrete pours (see Figs. 13). Water also passes through the slab along a small length of one construction joint. Slab-supporting formwork was removed 21 days after stressing of longitudinal tendons.

Nearby Taft Street bridge, which was constructed 1 year earlier, shows only minor signs of cracking or leaking. One possible explanation for an absence of cracks in the Taft structure is that the concrete slab is covered by an asphaltic concrete protection (ACP) surface. In addition, the Taft Street bridge has less post-tensioning force and lower strength concrete than the eastbound Brook Avenue bridge. The westbound Brook Avenue Overpass structure also manifests some cracks, but they are not as extensive as in the eastbound structure. The westbound bridge was constructed during warm weather; improved curing conditions helped the concrete gain strength more rapidly and reduced visible cracking.

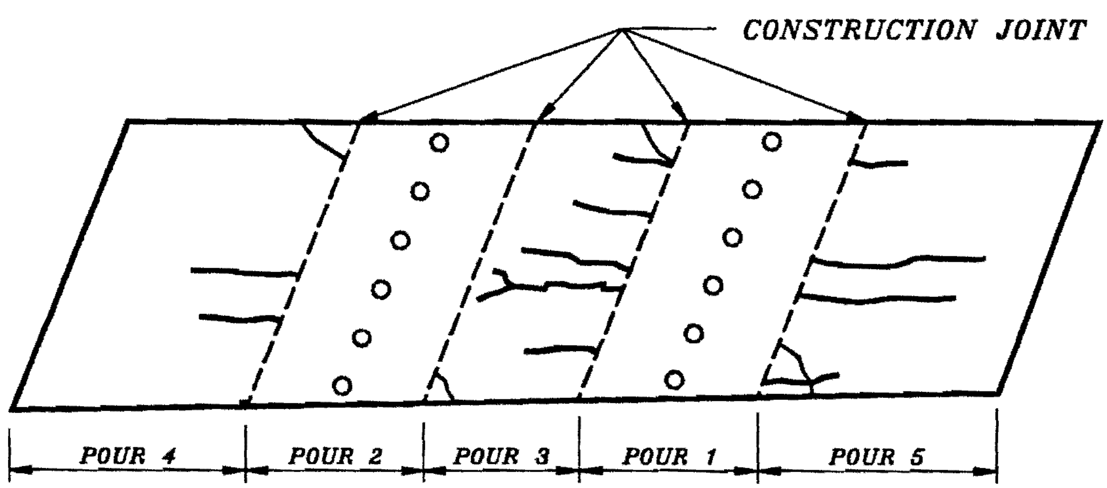

FIG. 13. Plan View of Longitudinal Cracks

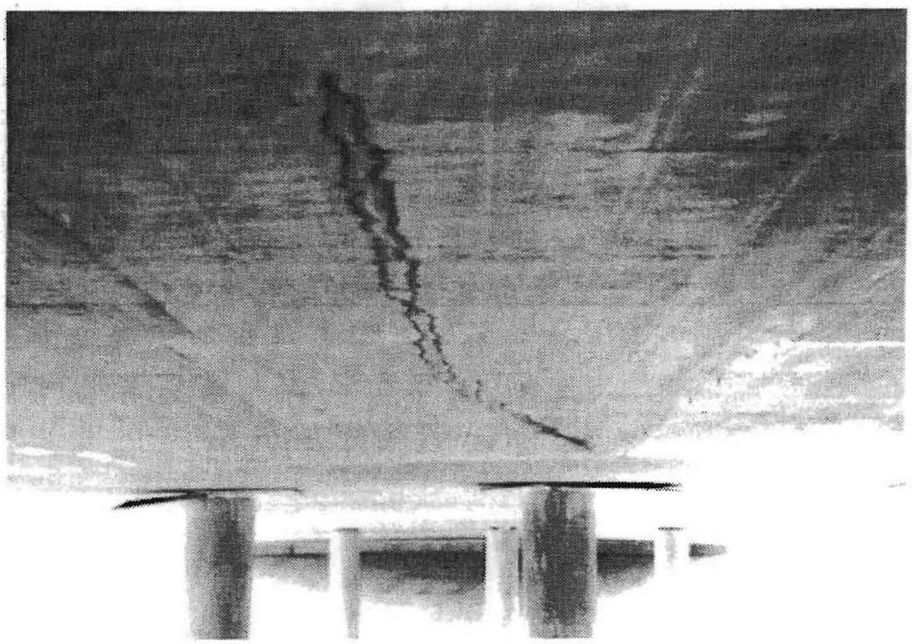

FIG. 14. Longitudinal Slab Cracks

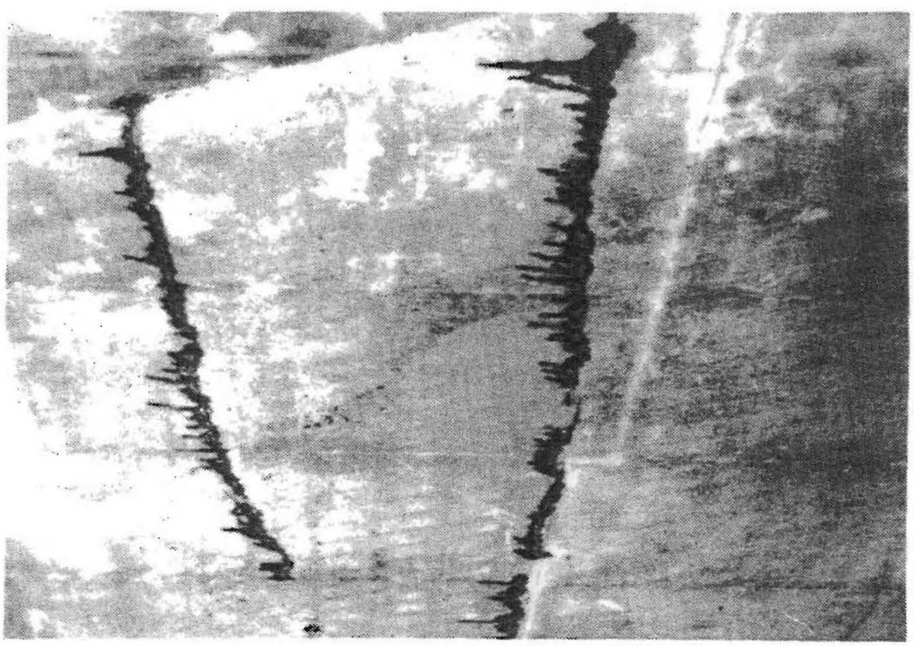

FIG. 15. Close View of Longitudinal Cracks

2.2 MATERIALS

2.2.1 Concrete

Concrete used for the bridge slab has a minimum 28-day compressive strength requirement of 6,000 psi (41.37 MPa). The average compressive strength, f_c', on the 28th day is 7,594 psi (52.01 MPa) (Steger 1989). More detail is available in section 4.3.

2.2.2 Passive Steel

Grade 60 reinforcement steel is located near the top and bottom surfaces with the top bars being epoxy-coated (Fig. 7). In the longitudinal direction, #5 (15.87 mm) bars were spaced at 12 in. (0.30 m), while in the transverse direction, #5 bars are placed on 6-in. (152.4-mm) centers with a design clear cover of 1.5 in. (38.1 mm) and 2.0 in. (50.8 mm) for the bottom and top layers, respectively.

2.2.3 Post-Tensioning System

VSL Corporation supplied the post-tensioning anchorage system, conduit, and stressing equipment for the bridge and performed the actual stressing operation. The multi-strand tendons consist of Grade 270, seven-wire, low relaxation, strand conforming to ASTM-A-416. Each tendon is enclosed in a rigid, galvanized, metal conduit. The anchorage assembly consists of a cast bearing plate, a permanent anchor block, a transition cone, and sets of wedges (see Fig. 8). Steel spirals provide passive reinforcement to accommodate anchorage zone stresses for each anchorage assembly. Post-tensioning materials, equipment, and the jacking operation are shown in Figs. 16-19.

To achieve the necessary longitudinal prestressing force, 73 tendons are spaced at 1.17-ft (0.36-m) centers on the west edge and at 1.14-ft (0.35-m) centers along the east edge. Each longitudinal tendon consists of nineteen, 0.5-in. (12.7-mm) diameter, low relaxation strands, which is prestressed to approximately 70% of yield strength. Tendon profiles (Fig. 8) are parabolic with a 9.0-in. (0.23-m) maximum eccentricity in the exterior span and a 7.0-in. (0.17-m) eccentricity in the interior span. At each abutment, the tendon profile is placed at the center of the concrete slab. Eleven straight tendons with a 1.25-ft (0.38-m) spacing are placed along each column line in the transverse direction. Center of gravity of each transverse conduit is designed to be 15 in. (38 mm) above the bottom of the slab.

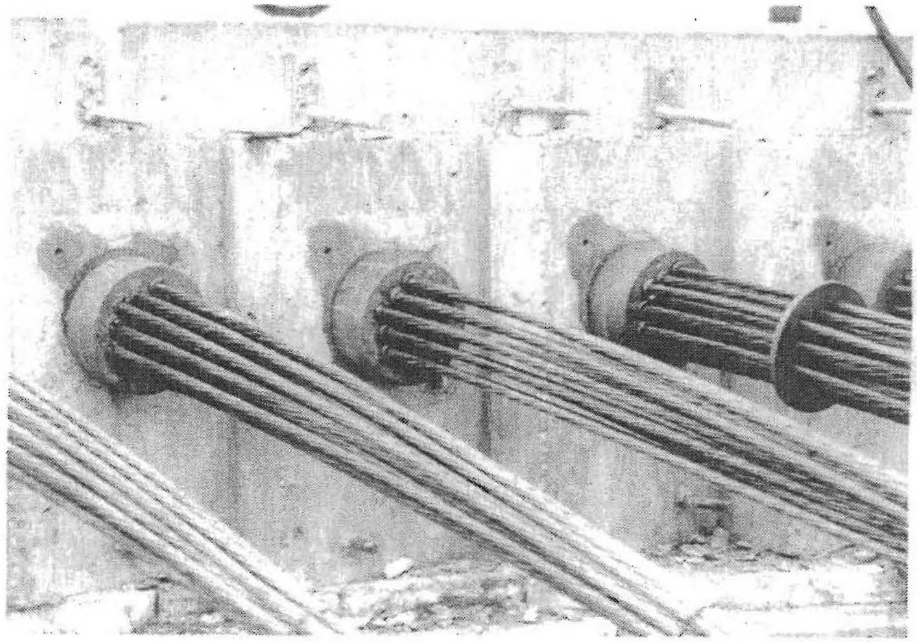

FIG. 16. Anchor Heads

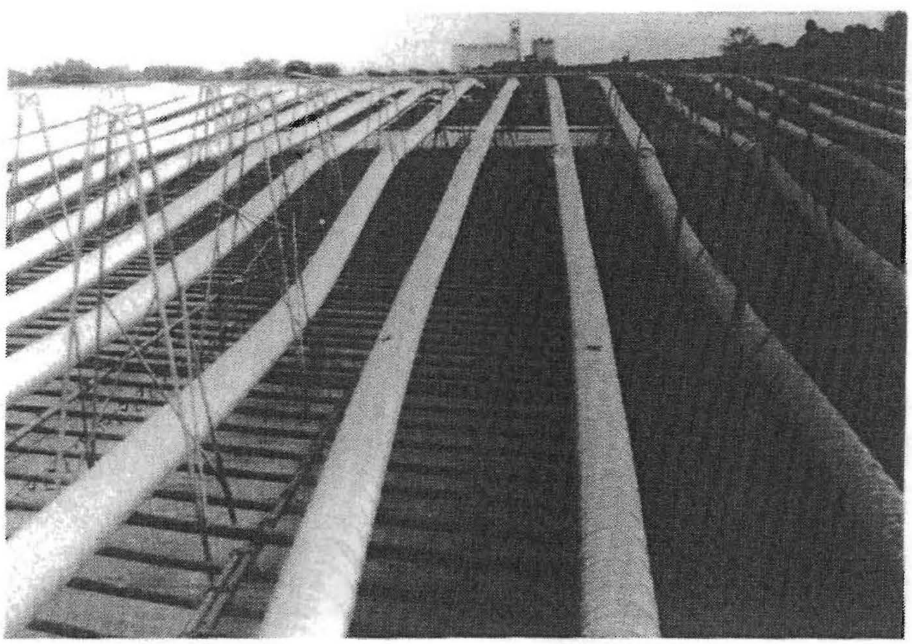

FIG. 17. Longitudinal Tendon Ducts

FIG. 18. Tendon Stressing Jack

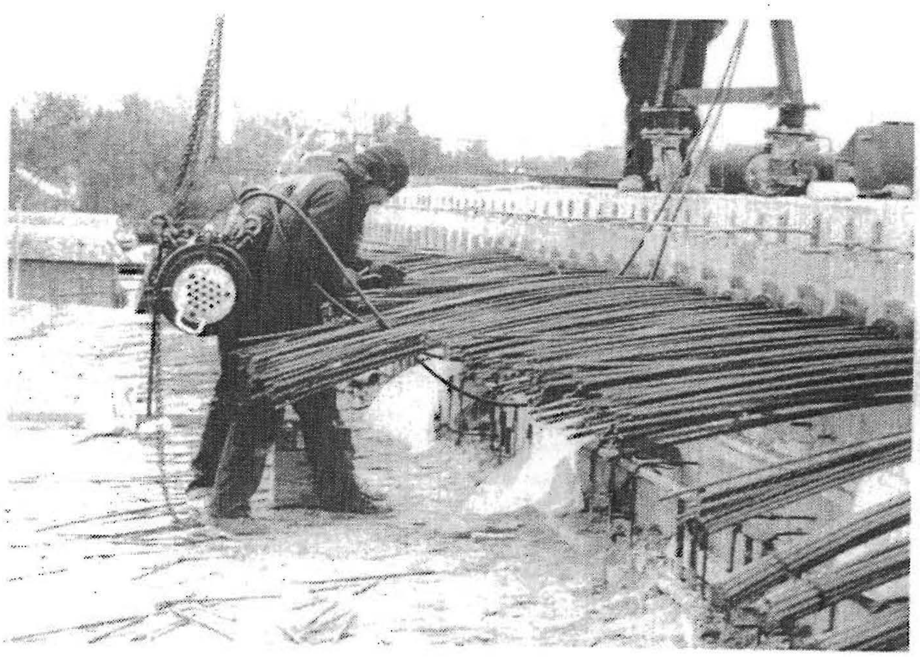

FIG. 19. Tendon Stressing

3. INSTRUMENTATION

3.1 GENERAL

To validate computer simulation of the construction sequence and imposition of external loads, it is necessary to know deflections and strains of the bridge. Deflection measurements at discrete locations on the bridge deck were taken with surveying equipment. Sensors were placed in the slab to record strains due to dead and live load, shrinkage, creep, and temperature change. A total of 170 active strain gages were attached to 2.5 ft- (0.76-m) #4 (12 mm) bars and connected by shielded lead wires to a data acquisition system. In the discussion that follows these bars are referred to as "pencil bars." Concrete strains due to time dependent effects and dead and live loads are assumed to be completely transmitted to each pencil bar.

3.2 DATA ACQUISITION SYSTEM

Development and implementation of a suitable instrumentation system is of utmost importance to this field study. After considering a number of alternatives, an HP-3497A was selected for acquiring strain gage data. The HP-3497A is known for its repeatability and immunity from noise as it is powered separately from the microcomputer. The instrument reads a total of 30 channels at a time by means of 3 strain-gage cards. Each card has two RS232 connectors that interface with a total of 10 strain gages. Channels 0-4 and 5-9 of each card attach to individual RS232 connectors. Channel 10 indicates excitation voltage.

IBM PC-based software, Lotus Measure (*Lotus Measure* 1986), controls the HP-3497A. Raw test readings are acquired, converted to useful units, and stored directly in a worksheet. Lotus Measure initiates data acquisition, stores data in a vertical row, and converts voltage data into equivalent strains. After completion of 30 readings, a chime sounds and a macro command procedure halts execution for the next hook-up of RS232 connectors. This sequence is repeated until all gages are read. Gage identification numbers and initial readings are stored in columns adjacent to the raw data. After acquiring data from all gages the computer saves the information to a file on a harddisk marked with the current date. Reduction of data and graphical display of results are done using Microsoft Excel (*Microsoft* 1990).

3.3 STRAIN GAGE INSTALLATION

Application of strain gages to pencil bars was done in the structures laboratory at Texas A&M University. Epoxy-coated pencil bars were used in the top reinforcing mat. They were supplied to the researchers by Sun Belt Works Inc., free of charge. 6-mm, 120-Ω, FLA-6 foil strain gages, manufactured by Tokyo Sokki Kenkyujo Co., LTD, were glued to ground surfaces of the bars and protected by 3 different coating layers. A rubber pad was placed on the top of the gage to protect it from mechanical damage; this was followed by a bituminous compound, and a metal foil coating. Finally, gages were sealed with a joint sealer. Strain gage installation was done using M-bond 200 Adhesive, supplied by M-Line Accessories. Figs. 20-23 show the sequence of steps for strain gage installation on the pencil bars. For more information regarding installation procedures, refer to Instruction Bulletin B-127-9 supplied by the above-mentioned company.

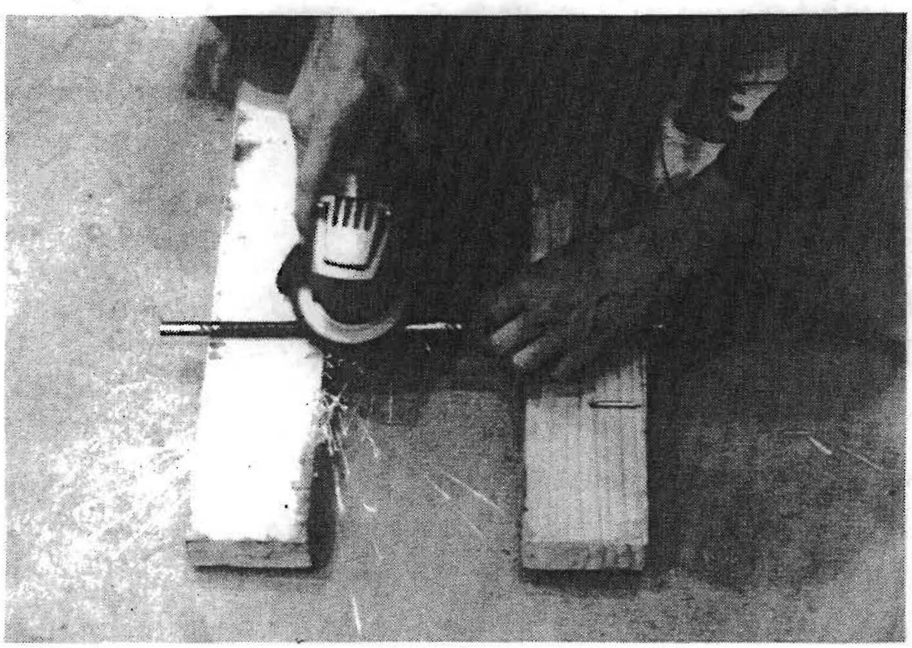

FIG. 20. Rebar Surface Grinding

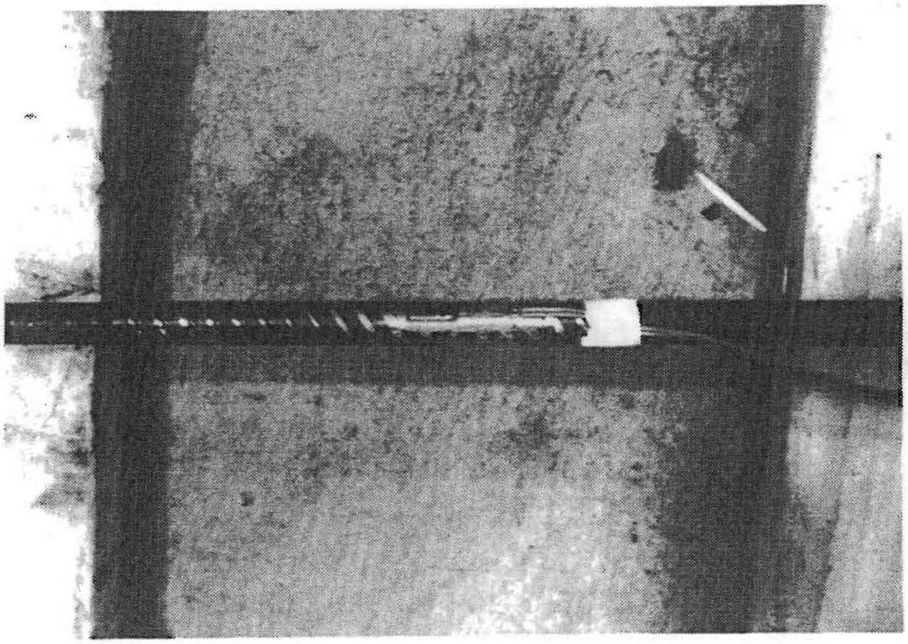

FIG. 21. Placement of Foil Gage

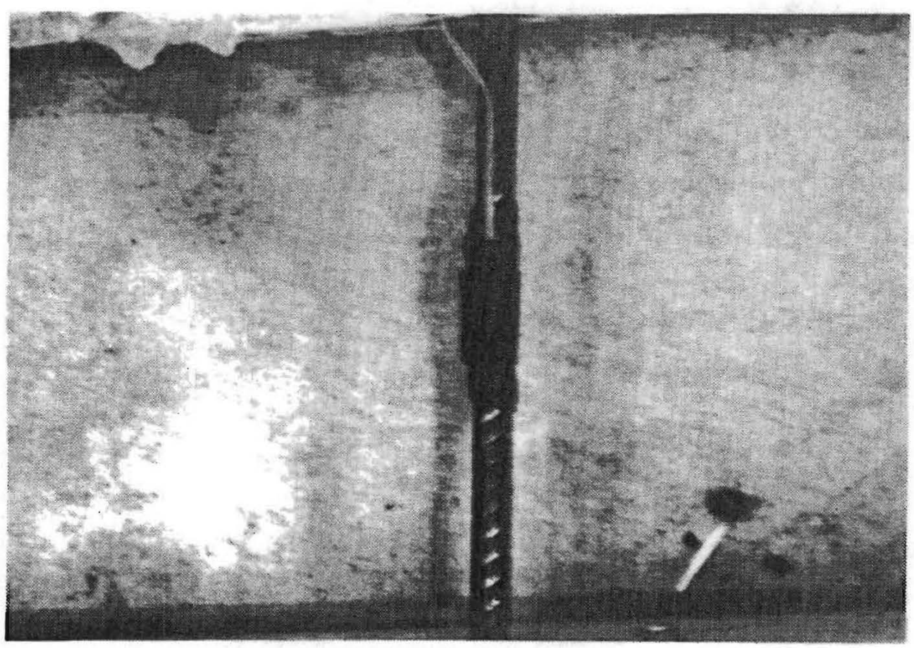

FIG. 22. Bituminous Coating on Strain Gage

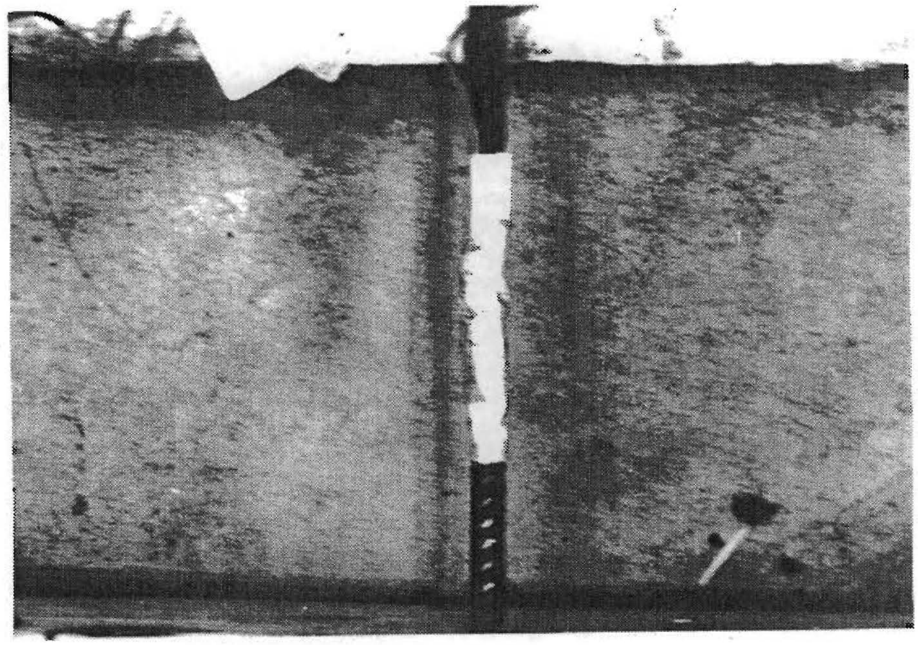

FIG. 23. Foil Shield on Strain Gage

3.4 GAGE EMBEDMENT

Numerical predictions showed that strains would not be symmetrical in the slab due to skew, and hence, gages were placed in regions of interest and where maximum and minimum strains are predicted to occur. That is, strain gages were not placed symmetrically in the bridge. A total of 167 strain gages, 10 temperature gages, and 3 strain-free gages were employed. Each gage was assigned a unique number as indicated in Fig. 24. Strain gages were secured in pairs to the top and bottom tiers of nominal steel. Abutment and column line skew necessitated that strain gages be placed parallel to the abutments in the transverse direction and parallel to the roadway in the longitudinal direction.

Before concrete was poured, positions of the strain gages were determined and their reference numbers written on the formwork. Fig. 25 shows strain gage lead wire being placed. Each lead wire was marked with a reference number on the strain gage and connection ends of the wire. Wires were tied to the bottom tier of reinforcement and bundled together when feasible. Two openings in the vertical formwork on the north side of the bridge allowed passage of the lead wires from within the slab to a terminal box located near the ground on a column. Strain gage lead wires located east and west of the east column line were pulled through the east and west openings, respectively, with two exceptions: gages 78 and 159 passed through the west opening.

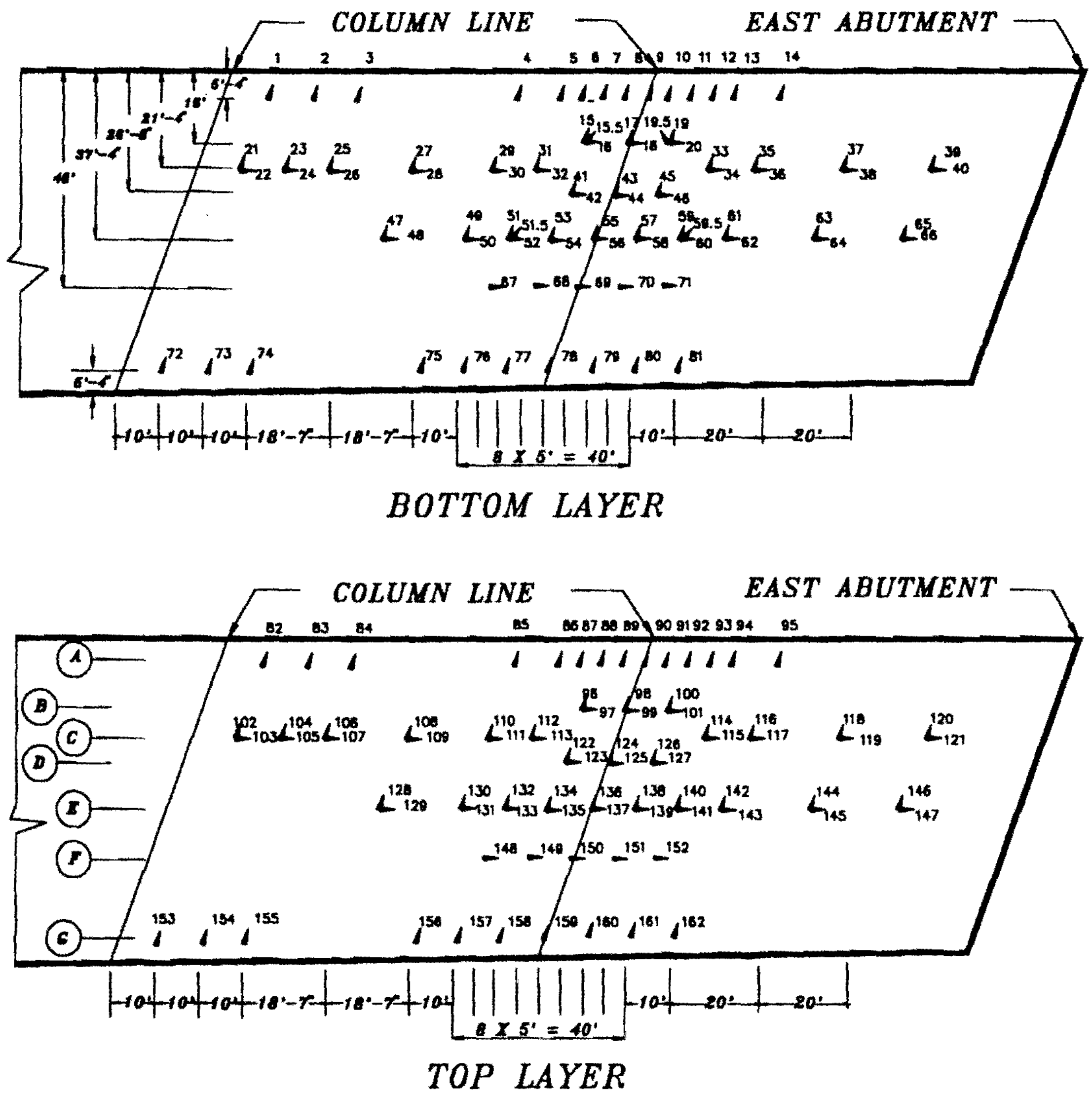

FIG. 24. Strain Gage Locations

After all strain gages that were attached to 2'-6"- (0.76-m) long pencil bars were soldered to lead wires, pencil bars were tied to the nominal steel in the bridgedeck. Finally, 3 gages, intended as strain-free gages, were loosely placed in a steel tube which was embedded in the slab so that the gages were isolated from concrete strain. These gages, numbered 001, 002, and 003, check temperature, shrinkage, and creep effects on the remaining gages. Their lead wires were pulled through the eastern duct near the column line.

Strain gages were checked against errors in numbering and wiring before RS232 connectors were soldered to lead wires at the data acquisition end. HP-3497A channel numbers were marked on the male and female parts of RS232 connections so that the same connection sequence can be followed each time readings are taken. Some strain gage bars were accidentally disconnected by construction workers during the course of placing reinforcement steel and needed to be reattached. Occasionally, soldering at RS232 connectors needed to be repaired. Figs. 26, 27, and 28 show strain gages placed before the concrete pour, the junction box, and RS232 connectors, respectively.

FIG. 25. Strain Gage Lead Wires

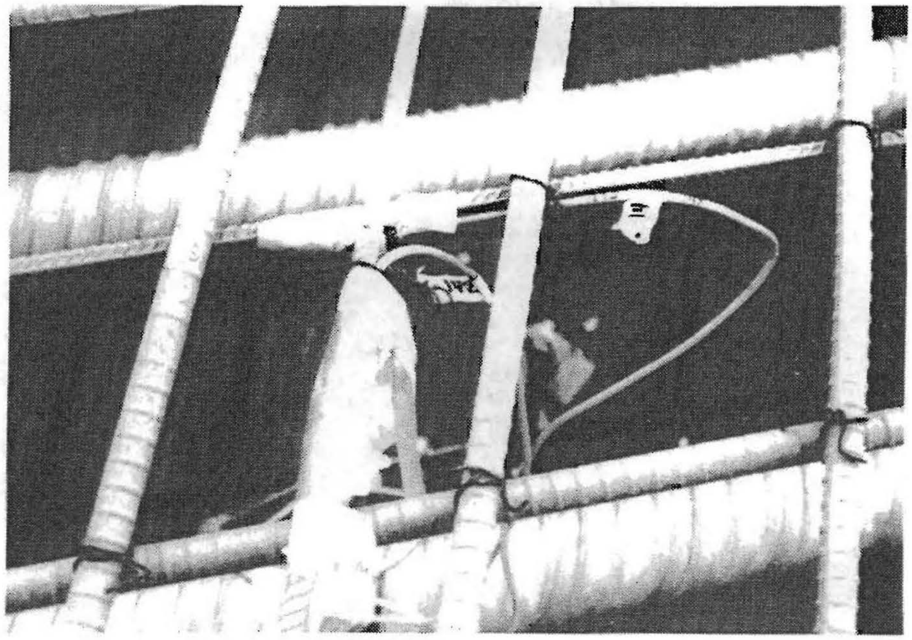

FIG. 26. Strain Gages before Concrete Pour

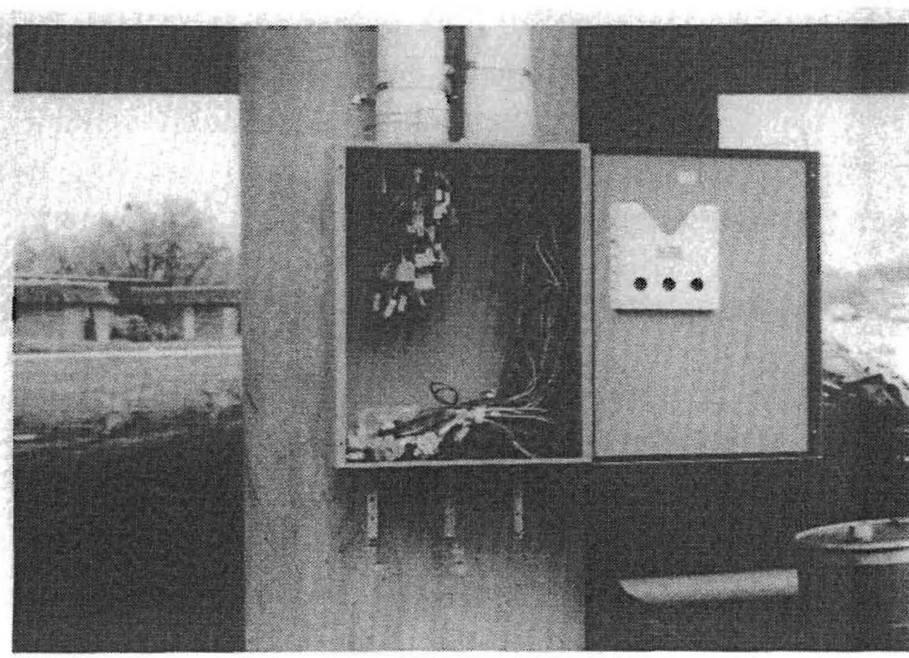

FIG. 27. Connection Box

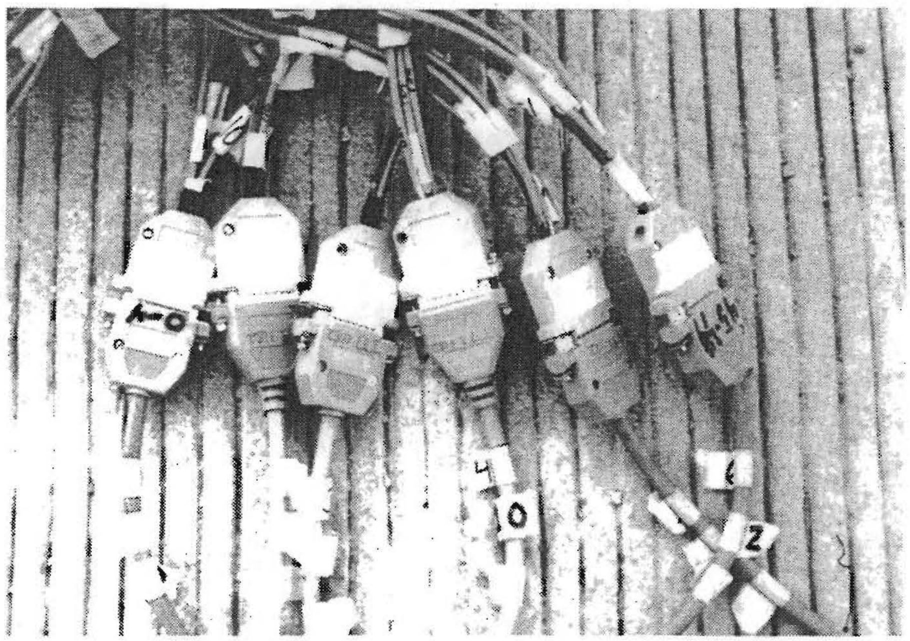

FIG. 28. RS232 Connectors

3.5 THERMAL INSTRUMENTATION

Transducers used for collection of temperature data were located within the slab. Two sets of 5 National Semiconductor LF335 temperature sensors, numbered T1 through T10, were placed in the deck. In plan they were placed on the east and west sides of the east column line 5 ft (1.52 m) from the north edge. Each set of five gages is distributed vertically through the depth of the slab. A separate card in the HP-3497A reads these sensors. Temperature gages require excitation of 5 volts, and, therefore, a separate power supply is required. See Fig. 29 for vertical distribution of temperature sensors.

3.6 DEFLECTION INSTRUMENTATION

On January 25, 1989, a total of 35 brass implants, 0.19 in. (4.76 mm) in diameter and 1.88 in. (47.63 mm) long, were embedded in the slab by drilling holes and attaching with cement mortar. They were located at 25-ft (7.62-m) intervals in the longitudinal direction (see Fig. 30). From 75 ft (22.86 m) to 150 ft (45.72 m) from the east end, no deflection implants were installed as the concrete overlay was not complete in that region. Deflections of the bridge slab were measured with a Wild Na2 level and a Philadelphia rod (see Figs. 31 and 32). Accuracy of deflection measurements is ±0.012 in. (±0.30 mm). The benchmark used by TxDOT engineers during construction was also taken as the benchmark for deflection measurements.

A leveling rod was placed on one of the brass implants and elevations were taken with the leveling instrument. Elevations were recorded in a field book and later transferred to an electronic spreadsheet.

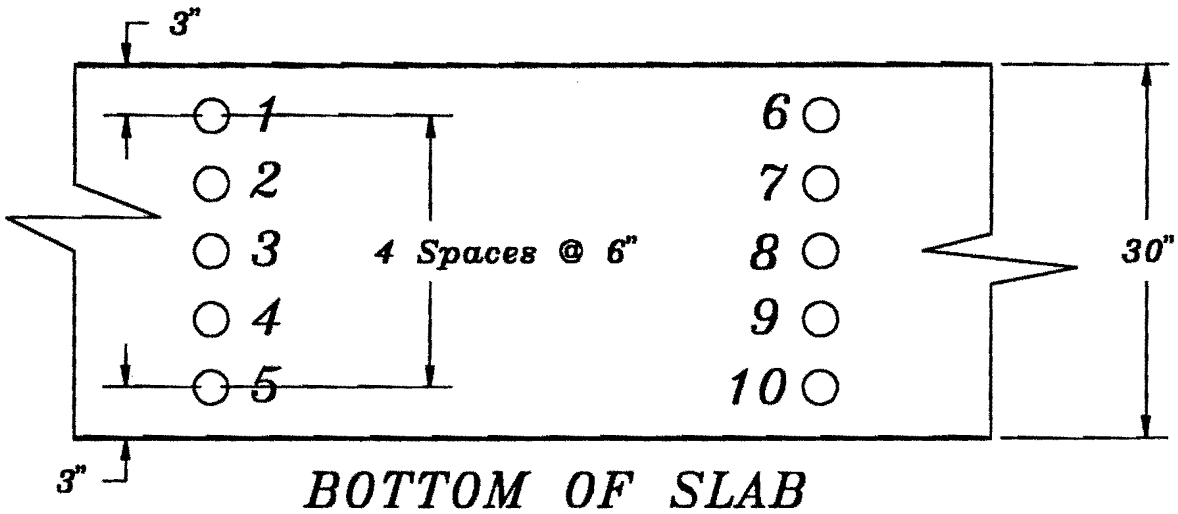

FIG. 29. Vertical Distribution of Temperature Sensors

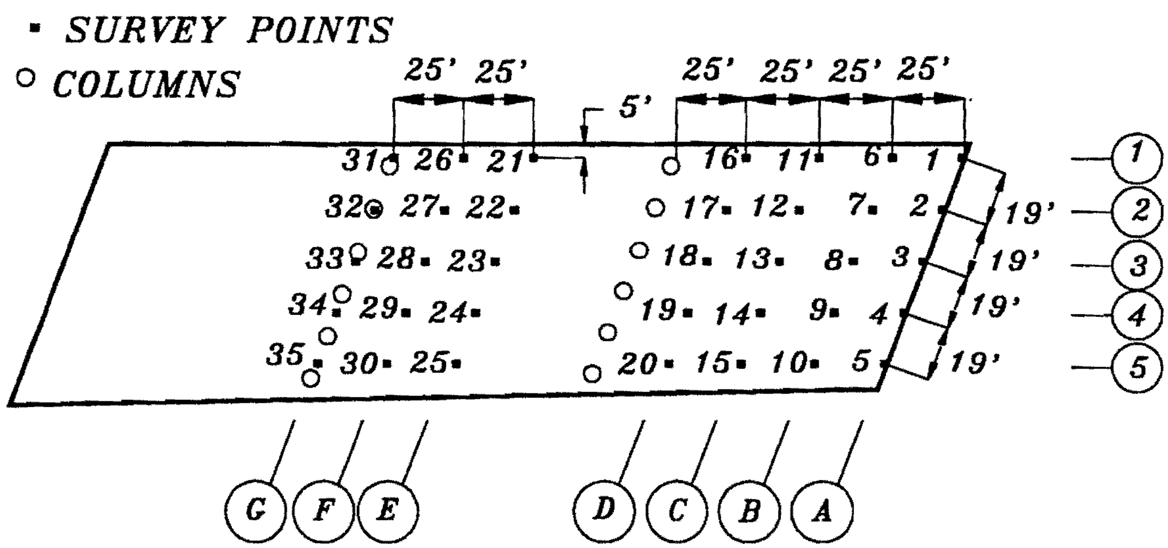

FIG. 30. Deflection Implants

FIG. 31. Leveling

FIG. 32. Leveling Rod on Deflection Implants

4. Auxiliary Laboratory Experiments and Data Collection

4.1 General

Strain and temperature gages were tested and calibrated in the laboratory prior to installation in the bridge. Concrete cylinders were also tested to confirm results supplied by TxDOT. Motivation for the laboratory tests described in this chapter is to provide accurate data on material properties for the computer simulation.

4.2 Pencil Bars

Three pencil bars mounted with strain gages were selected at random for testing the gage's ability to predict a known magnitude of strain. Each bar was loaded in tension, during which time the applied load and strain in the bar were monitored. Mean value of modulus of elasticity was found to be 28.69×10^6 psi (198 kN/m^2), which compares well with a commonly assumed elastic modulus of 29×10^6 psi (200.1 kN/m^2).

In order to determine long-term effects, the strain gages were tested for adequacy of protection against water infiltration. Toward this end, two #4 rebars were instrumented with strain gages. Following manufacturer's instructions, the gages were protected by M-COAT F which is manufactured by Micro-measurements, Inc. One sample was protected with special care (instructions supplied by the manufacturer were followed meticulously). The second gage was protected by the same material but in a less meticulous manner. After allowing the samples to cure for one day, both were submerged in a water bath. One month later both gages were examined for damage and checked for proper functioning. The gage with careful application of water proofing material gave correct readings. By comparison, the gage with less careful application did not function properly. After peeling away several protective layers, water was found to surround the gage. In addition, the gage was no longer attached to the rebar. Therefore, careful gage installation plays a key role in the life of a strain gage embedded for a long period of time in a humid environment such as concrete.

Effects of using a long lead wire were also investigated. A tensile load test was performed on a pencil bar by sequentially using a 5-ft (1.524-m), 50-ft (15.24-m), and 100-ft (30.48-m) long lead wire. The bar was tested in a 20-kip (88-kN)

MTS machine for strain and elastic modulus. No significant difference in elastic moduli and/or strains was observed between data from the 5-ft (1.52-m), 50-ft (15.2-m), and 100-ft (30.5-m) long lead wires.

4.3 CONCRETE CYLINDERS

Average compressive strengths of concrete cylinders at 7, 15, and 28 days are obtained from tests that were carried out by an independent testing laboratory in Wichita Falls, Texas. The cylinders were cured by immersion in a water bath in an air-conditioned room. Table 1 lists averages of 28-day compressive strengths determined for each pour.

TABLE 1. Strength of 28-Day Cylinders

Pour Number (1)	Date Poured (2)	Date Tested (3)	Age (day) (4)	Compressive Strength (psi) (5)
1	11/30/88	12/28/88	28	8,201
2	1/3/89	1/31/89	28	7,834
3	1/5/89	2/2/89	28	6,873
4	1/11/89	2/8/89	28	7,744
5	1/18/89	2/15/89	28	7,320

Six additional concrete cylinders were cured in a tank near the construction site and transported from the bridge site to the structures laboratory at Texas A&M University. These cylinders were poured on November 30, 1988, and tested at an age of 135 days on April 15, 1989. Three of these cylinders were tested for crushing strength, while the remainder were used to observe the stress-strain relationship of the material. Cylinders set aside for elastic modulus determination were tested in an MTS machine. Vertical deformation of each cylinder under compression was measured by a linear variable differential transformer (LVDT). Applied load was measured by the MTS itself. An example stress-strain relationship obtained from these measurements is shown in Fig. 33.

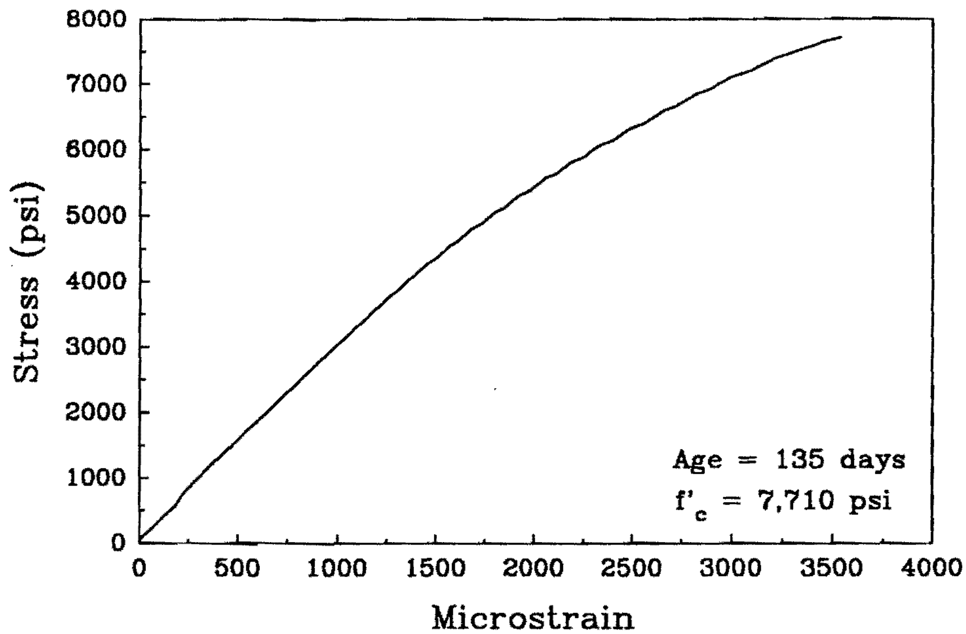

FIG. 33. Typical Stress-Strain Curve of a Concrete Test Cylinder Cured at the Bridge Site

Compressive test results from these cylinders show strengths of 5,354 psi (36.91 MPa), 6,123 psi (42.21 MPa), and 7,345 psi (50.64 MPa). Each of these strengths is less than the average 28-day compressive strength of 7,594 psi (52.01 MPa) furnished by TxDOT in Table 1. However, since cylinder strength results furnished by TxDOT are quite extensive, TxDOT results are used in the numerical modeling. Further discussion of concrete strength is presented in Section 5.2.7.

4.4 TEMPERATURE SENSORS

Five temperature sensors, similar to those described in Chapter 3, were used to calibrate the thermal transducers. Each temperature sensor was soldered to a 4,500 Ω resistor. A thermocouple was used to calibrate the temperature sensors, which were immersed in a 3.2 °C cold water and a 70 °C hot water bath; similarly, two more intermediate readings were taken. As per the manufacturer's specifications, the temperature sensor should register approximately 3 volts on an HP-3497A when a 5 volt excitation is applied at 25 °C and should increase by 10 millivolts for every 1 °C rise in temperature. On testing, the voltage reading showed exactly 3.00 volts at 25 °C. The following equation, which was derived from a linear regression of experimental data, supplies temperatures from voltages of the bridge transducers:

$$T = -284.975 + 103.386\,V \quad (4)$$

where T is the predicted temperature, and V is the sensor voltage.

4.5 NEOPRENE PAD

As the bridge slab is separated from its supporting columns and abutments by neoprene pads, tests were conducted in the laboratory to verify behavior of a three-tenths scale neoprene pad. The neoprene pad tested was 9 in. (228.6 mm) in diameter and reinforced with 3 layers of steel. It was placed in an MTS machine between two rigid metal blocks that displace vertically. Deflections of the rigid blocks were measured by two dial gages located on opposite sides of the diameter. A load-deflection curve for the experimental data is plotted in Fig. 34.

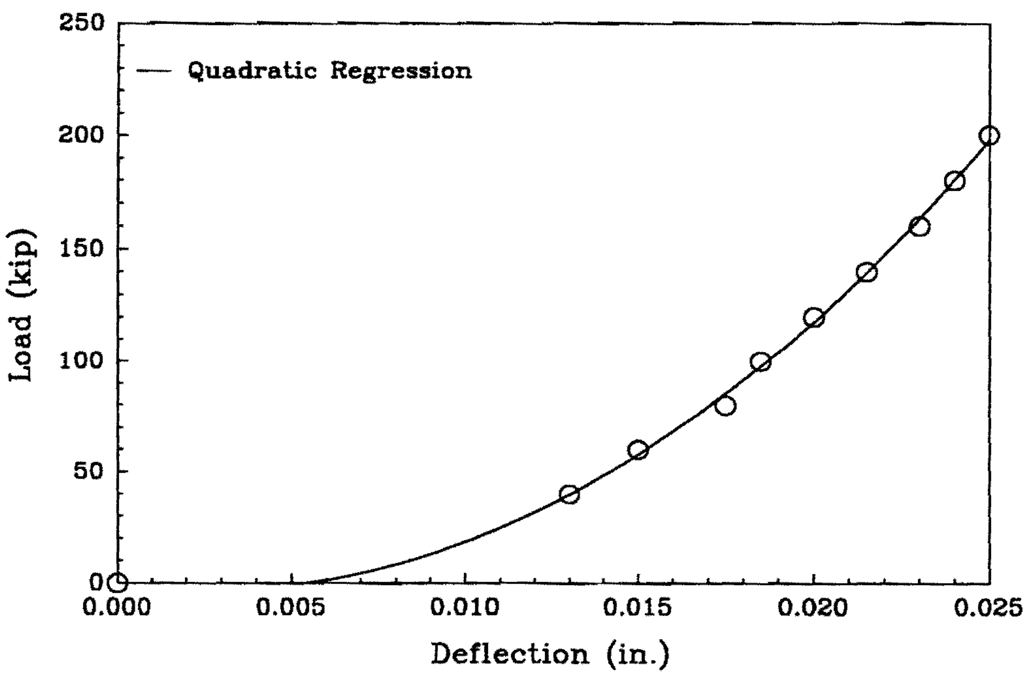

FIG. 34. Load versus Deflection Curve for Elastomeric Bearing Pad

4.6 DATA ACQUISITION AND REDUCTION

A field trip was made to the Wichita Falls bridge site whenever a significant event took place such as a concrete pour or stressing of tendons. More frequent visits could not be made as the bridge site is 300 miles (540 km) from Texas A&M University. An IBM AT-compatible microcomputer was used to acquire data into a spreadsheet and operate the HP-3497A as described in Chapter 3. A portable generator supplied power to the computer and 2 volts to the strain gages according to manufacturer's specification.

The data acquisition system was set up either on the bridge deck or on the shoulder of the road beneath the bridge. Since the system read only 30 strain gages at a time, RS232 connectors were frequently disconnected and reattached to a different set of connectors. RS232 connectors at the bridge site were protected from moisture by a metal box and plastic bags. Refer to Figs. 27 and 28.

In general, deflection and strain data were collected approximately once a month at the field site for a period of more than two years. Table 2 lists dates of visitation to the site and time in days from the average date of the five pours to the date that each event occurred. Initial pouring of concrete occurred during December, 1988. Prestressing began near the end of January, 1989. Days after casting for jacking of the prestressing tendons is taken as 30. The remaining days after casting at which data acquisition is carried out are 56, 70, 102, 136, 193, 231, 294, 319, 320, 400, 472, 591, 681, and 878. Live load testing is performed at 193 and 319 days after casting. Monitoring of thermal and strain gages was halted after the reading taken on the 400th day due to unreliability of the readings caused by moisture and the harsh environment of the concrete slab. Details of the deflection and strain gage readings are listed in Appendices III and IV, respectively.

Voltages from strain gages are converted to units of microstrain for a one-quarter strain gage bridge by the following relationships:

$$V_r = \frac{V_{out}}{V_{ex}} - \frac{V_{ini}}{V_{ex}} \qquad (5)$$

and

$$\varepsilon = \frac{4V_r}{G_f(1+2V_r)} \qquad (6)$$

where V_{out} is final voltage, V_{ini} is initial voltage, V_{ex} is excitation voltage, G_f is the gage factor, and ε is the measured strain in the material in microstrains.

TABLE 2. Schedule of Events

Date (1)	Days after Casting (2)	Event (3)
10/28/88	—	Lead wire placed for strain gages
11/4/88	—	Pencil bars, lead wires, and RS232 connectors installed
11/20/88	—	Base strain gage readings taken
12/20/88	—	Strain gage readings taken after first pour over bent 3
1/5/89	—	Strain gage readings taken after second pour
1/30/89	30	Deflection and strain gage readings during transverse post-tensioning; longitudinal post-tensioning begins
2/25/89	56	First set of deflection and strain gage readings taken
3/14/89	70	Two sets of temperature and strain gage readings are taken to verify effect of slab temperature on gages.
4/12/89	102	Deflection, temperature, and strain gage readings taken
5/16/89	136	Deflection, temperature, and strain gage readings taken
7/11/89	192	Deflection, temperature, and strain gage readings taken; live load testing of the bridge (two trucks)
8/19/89	231	Deflection, strain, and temperature gage readings taken
10/21/89	294	Deflection, strain, and temperature gage readings taken
11/15/89	319	Second phase of live load testing; deflection, temperature, and strain gage readings taken
11/16/89	320	Deflection readings taken; second phase of live load testing (one truck)
2/4/90	400	Final temperature and strain gage readings taken; deflection readings taken
4/17/90	472	Deflection readings taken
8/14/90	591	Deflection readings taken
11/12/90	681	Deflection readings taken
5/28/91	878	Deflection readings taken; monitoring ceases

5. NUMERICAL SIMULATION

5.1 GENERAL

Measurements from actual, full-size, slab bridges and experimentation with laboratory models provide important data predicting behavior of similar structures. However, expense and time considerations render an experimental approach impractical for most slab structures. Numerical simulation, albeit replete with assumptions and limitations, provides a viable alternative for prediction of structural response to prestressing forces and externally imposed loads. Only a small number of computer codes have sufficient material and geometrical nonlinearities incorporated in their algorithms to be considered as candidates for prediction of elastic and failure behavior of prestressed plates.

The code used in this study, NOPARC, is a nonlinear finite element program (van Greunen 1979; Roschke and Pruski 1992) which traces the quasi-static response of reinforced and prestressed concrete slabs of arbitrary geometry that undergo instantaneous and sustained normal and in-plane loadings. Time-dependent environmental phenomena, such as creep and shrinkage, are considered in order to follow changes in field variables in the elastic and inelastic regimes. Input to the code consists of geometry of the structure, boundary conditions, various concrete material properties, reinforcing steel material properties and their locations, post-tensioning details, and location and magnitude of loads. The following sections give a detailed description of important parameters used for numerical simulation of the Brook Avenue overpass. Refer to Appendix VI for a slightly abbreviated form of a sample input data listing.

5.2 INPUT DATA

5.2.1 Geometry

An independent FORTRAN program has been written to generate the finite element mesh. For the present study, 637 nodes and 1,152 triangular elements model Brook Avenue overpass (see Fig. 35). The bridge model consists of 49 and 13 lines of nodes in the longitudinal and transverse directions, respectively.

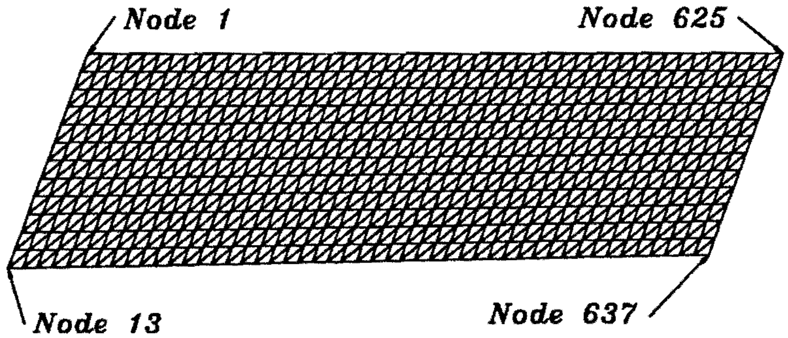

FIG. 35. Finite Element Mesh

5.2.2 Convergence Parameters

The analysis assumes constant stiffness within each load step, i.e., element stiffness matrices are reformed only for the first iteration of each load step. Effects of nonlinear geometry and creep and shrinkage are taken into account. From a choice of two convergence norms, the displacement norm is used. Absolute values of displacement convergence tolerances are specified.

5.2.3 FEM Analysis Output Controls

Due to large file sizes, displacements, unbalanced forces, and strains are typically requested only at the end of all load steps and iterations. Displacements are calculated in terms of local element coordinates. Strains are output instead of stresses so that they can be readily compared with experimental data obtained from the pencil bars. Limits of 15 in. (381 mm) and 1.0 radian are placed on the maximum allowable displacement and rotation, respectively.

5.2.4 Time Dependent Study

Data collection dates determine a series of ages in days after casting at which an analysis is required. Prestressing began near the end of January, 1989, which corresponds to the first load record in the computer simulation (see Table 2). Days after casting for jacking of the prestressing tendons is taken as 30. The remaining days after casting at which analyses are requested are as follows: 56, 102, 136, 193, 231, 294, 319, 320, 400, 472, 591, 681, and 878. Live load testing is performed at 193 and 319 days after casting. The program divides each concentrated load into a specified number of fractional loads and conducts the analysis. In the present case the specified fraction is unity. When very high concentrated loads are placed on the nodes it is advisable to stipulate that the code apply the load in small increments. In the first load step, prestressing forces are applied, while the remaining steps analyze the bridge at intermediate days when data is collected.

5.2.5 Nodal Point Data

Global coordinates of the boundaries of the model are as follows:

Node 1:	0.0, 0.0 in. (0.0, 0.0 m).
Node 13:	381.5, 1,019 in. (9.69, 25.88 m).
Node 625:	3,566, 0.0 in. (90.58, 0.0 m).
Node 637:	3,973.0, 1,086.0 in. (100.91, 27.58 m).

Nodes are not rigidly fixed at abutment and column support locations. Instead, they are supported by numerical springs called boundary elements (see Section 5.2.15).

5.2.6 Material Properties

A single concrete and a single steel type are selected for the entire bridge. That is, identical steel and concrete layer systems are used throughout the bridge. Two prestressing steel data cards are used, one for longitudinal and transverse tendons over the columns, and the other for transverse tendons near the abutments.

5.2.7 Concrete Material Properties

ACI formulae are used in the program for creep and shrinkage analysis. Mean concrete compressive strength at 28 days obtained from TxDOT is 7,594 psi (52.35 MPa). The concrete pours occurred during cold-to-mild weather with temperatures ranging between 37 °F (3 °C) and 60 °F (16 °C). Since compressive test results from cylinders, which are cured by immersion in water at room temperature, often do not agree with the actual compressive strength of concrete in a structure, compressive strength used in the numerical simulation is scaled down using the concept of maturity (Mindess and Young 1981). A curve proposed by Nurse and Saul (1978) reduces compressive strength down to 6,300 psi (43.43 MPa) from 7,594 psi (52.35 MPa) at 28 days after casting, which is a net reduction of 27% of mean compressive strength. Poisson's ratio and concrete density of 0.15 and 0.087 lb/in.^{3} (24,000 N/m^3), respectively, are used. The cracked shear constant is taken to be 1.0. Default ultimate shrinkage strain is 0.008. Although initial slump measured at the site was 9.5 in. (241.3 mm), an average slump of 7.1 in. (180.34 mm) is obtained by averaging field slump data supplied by TxDOT. Average annual relative humidity for the year 1988 is used in the analysis. Thermal expansion of concrete is assumed to be 5.5×10^{-6} (Mindess and Young 1981). Minimum size of the member is specified as 30.0 in. (762 mm), which is the design depth dimension of the slab.

5.2.8 Steel Material Properties

Modulus of elasticity, modulus for strain hardening, and an ultimate allowable stress for reinforcing steel are taken to be 29×10^6 psi (2×10^5 MPa), 6×10^4 psi (413.7 MPa), and 34.6×10^4 psi (2385.67 MPa), respectively (Burns and Lin 1981).

5.2.9 Prestressing Steel Properties

Grouting of tendons in the field bridge necessitates use of the bonded option for post-tensioning. Area of each tendon is 2.907 in.^{2} (187.5 mm^2). Wobble and curvature friction coefficients for semi-rigid galvanized metal ducts are 0.0002 lb/ft (0.0004 N/mm) and 0.25 (Lin 1981), respectively. Offset yield stress at 0.1% strain is 25.0×10^4 psi (1,723.75 MPa) (Burns and Lin 1981), and a relaxation coefficient of 1.0 is used.

5.2.10 Stress-Strain Curve

To describe the material properties of post-tensioning strands, four points on a stress-strain curve are required by NOPARC. These points are obtained from the plot shown in Fig. 36, which is obtained for 0.5-in. (50.8-mm) strand from Post-Tensioning Institute manual (PTI 1985).

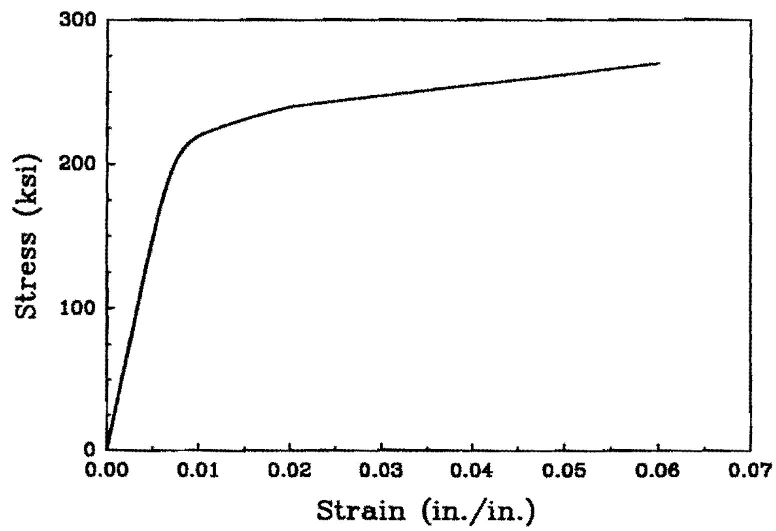

FIG. 36. Ultimate Load Test of Post-Tensioning Strand

5.2.11 Concrete Layer System

The bridge thickness is divided into ten continuous layers of concrete. Strains are calculated at the centroid of each layer. In the Brook Avenue structure, pencil bars with attached strain gages were placed at the centroid of the top and bottom layers of passive steel (see Section 5.2.12). Hence, layer thicknesses in the numerical simulation are specified so that penultimate top and bottom layers report strains at the same level as the field strain gages (see Fig. 37).

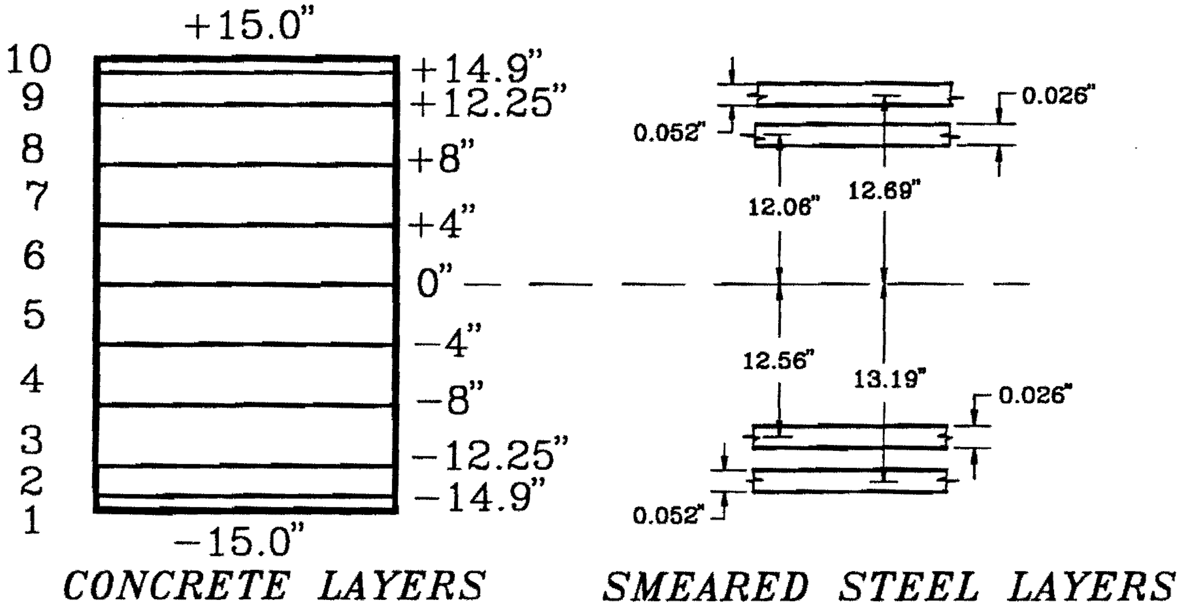

FIG. 37. Concrete and Steel Layer System

5.2.12 Steel Layer Systems

Four anisotropic steel layers are used in this bridge: one each in the longitudinal and transverse directions at the top and bottom of the slab. Number 5 bars are spaced at 6 in. (152.4 mm) and 12 in. (304.8 mm) in the transverse and longitudinal directions, respectively. Finite element analysis in NOPARC requires that discrete passive steel be represented in the form of an equivalent "smeared" continuum. To convert the total steel area into a smeared layer, the steel area of a single bar is divided by the spacing of the reinforcement in that direction. This gives a 0.026-in. (0.66-mm) thick layer in the longitudinal direction, and a 0.051-in. (1.29-mm) thick layer in the transverse direction. Transverse steel is oriented 69.5° from the bridge centerline, i.e., it is parallel to the abutments and not orthogonal to the longitudinal steel.

5.2.13 Triangular Finite Elements

A total of 1,152 triangular plate finite elements are selected for the analysis. Since there are 6 columns across the bridge at each column line, a total of 13 nodes are specified in transverse direction so that 6 nodes are located at the column locations, 5 nodes lie between column locations, and the remaining 2 nodes denote the outer edges of the slab. In the longitudinal direction each span is divided into 16 equal divisions. The number of elements is limited to 1,152 for the sake of convenience, since a larger number of elements results in intractably large output files.

Nodes describing element connectivity are specified in a counterclockwise order about an axis normal to the plane of the element. The local coordinate system is defined by the node sequence. An initial temperature is specified on each element data record. Here, the average temperature during December, 1988, and January, 1989, is taken as 48 °F (8.8 °C) (A&M Climatologists). An option of placing a distributed load on specified elements can be used to impose lane loads. As per section 3.7.6 of AASHTO (*Standard* 1989), 64 psf (3.06 kN/m^2) is to be provided for lane loading.

5.2.14 Gravity Load Multiplier

Gravity loads calculated in the vertical direction are set equal to the unit weight of concrete multiplied by the corresponding gravity load multiplier. For this structure, the unit weight of concrete is taken as 0.087 $lb/in.^3$ (23.62 kN/m^3). Concrete cylinders obtained from the bridge site were weighed for density before confirming the above values, which are widely accepted for normal weight concrete.

5.2.15 Boundary Elements

Boundary elements are used in NOPARC for three purposes: to limit nodal displacements or rotations to prescribed values, to compute support reactions, and to provide linear-elastic supports for nodes. Direction of a boundary element at a given node is specified in two ways: (1) two nodes define the positive direction of the boundary element from a primary node of interest to a second node, or (2) two vectors are defined by specifying nodes lying along their directions. For a detailed description of this approach, refer to the NOPARC reference manual, pages 254 and 274 (van Gruenen 1979).

Boundary elements simulate normal and in-plane reactions of the columns and abutments on the slab. The Wichita Falls bridge is supported on 36-in. (0.91-m) diameter columns at the interior supports. If each column is assumed to act as a cantilever beam which is embedded in the ground, an approximation of the stiffness contribution of a column to the slab is obtained from the following equation:

$$\Delta = \frac{PL^3}{3EI} \qquad (7)$$

or, rearranging gives:

$$P = \frac{3\Delta EI}{L^3} \qquad (8)$$

where P is the horizontal force of the column acting on the slab, Δ is the column deflection, E is the transformed modulus of the reinforced column, I is the transformed moment of inertia, of the reinforcing bars, and L is the equivalent length of a cantilevered column, which is assumed to be fixed at some depth below the surface of the ground. Transformed moment of inertia is obtained by converting steel area into concrete area by multiplication with an appropriate coefficient. The column is assumed to be fixed at 1/6th of the pier length below the ground surface. With these assumptions, stiffness of the boundary element in the plane of the slab becomes 56,620.5 lb/in. (8,395,000.0 N/m). Two boundary elements in two non-orthogonal directions are used to simulate the column stiffness.

The slab is supported at the abutments on 15 reinforced neoprene pads that are 18-in. (457.2-mm) square and on a 36-in. (0.9144-m) diameter pad at each column. To simulate these pads, vertical boundary elements are placed at the abutments and at the columns. To verify stiffness, 9-in. (228.6-mm) neoprene pads were tested in laboratory (see Section 4.5). Stiffness of a uniaxial pad element is given by:

$$\Delta = \frac{PL}{AE} \qquad (9)$$

or

$$P = \Delta\frac{AE}{L} \qquad (10)$$

where k represents the material stiffness, E is the elastic modulus, A is cross-sectional area of the pad, and L is the pad thickness. In this case modulus for the elastomer is 53,000 psi (36.58×10^4 kN/m^2), area of the bearing pad on each column is 1,017.8 in.^{2} (0.65 m^2), and material thickness is 1.75 in. (44.45 mm). Hence, the stiffness is 30.83×10^6 lb/in. (83.75×10^8 N/m). Similarly, at the abutments the area of each pad is 324 in.^{2} (0.02 m^2) which gives a stiffness of 9,815.00 kip/in. (26.66 N/m) per pad.

5.2.16 Prestressing Tendon Data

A total of 99 longitudinal tendons were placed in the Wichita Falls slab. There are six inflection points per tendon. Average anchor slip noted by field engineers was 0.125 in. (1.52 mm). The average prestressing force is 588 kips (2,615 kN) for longitudinal tendons and 596 kips (2,650 kN) for transverse tendons. "Slab" tendons are used in NOPARC since all prestressing ducts are straight in a plan view. Field jacking is employed sequentially. In the numerical simulation, input data for locations of 13 longitudinal tendons is explicitly specified, while the remaining longitudinal tendons are automatically generated. Elements crossed by each tendon are obtained by using an independent FORTRAN program. All transverse tendons are straight in plan and elevation, and are explicitly entered without generation. For convenience the tendon generation capability of the program is used.

5.2.17 Load Data

Maximum number of iterations permitted in this simulation for one load step, such as a prestressing load or a time-dependent analysis, is 20. If the program does not converge in 20 iterations, execution terminates. Loading of nodes is not included in the prestressing load record, but rather they are included in a later input record input to simulate live load testing of the bridge. Application of prestressing causes elastic deformation of the structure at the time of transfer. If elastic deformation of the structure is not ignored the tendons are numerically shortened and tendon forces reduce accordingly. A factor ranging from 1.0 to 0.0 is used in the code to account for the phenomenon. In the present case this factor is taken as 0.5. This is a widely accepted notion in design of prestressed concrete structures (Nilson 1978).

5.2.18 Temperature

Temperatures collected from thermal gages embedded in the bridge deck are used in the time-dependent analysis. The number of finite elements undergoing temperature change is 1,152. Temperature gradient between the top and bottom surfaces is negligible since data collection is usually done during the morning when the bridge has a relatively uniform temperature. A temperature for the slab is input at each time step in the analysis. Although NOPARC provides the option, no thermal gradient through the thickness of the slab is used. See also section 6.2 for additional detail.

5.2.19 Concentrated Nodal Loads

A three axle dump-truck was used in the live load testing. Axle loads were calculated using portable scales. Truck dimensions approximately match those of the finite element grid. Concentrated nodal loads of 23,880 (106.21 kN), 23,880 (106.21 kN), 5,800 (25.79 kN), and 5,800 lb (25.79 kN) are used to simulate wheel forces of the first truck on the bridge. Similarly, concentrated nodal forces for the second truck are: 1,140 (50.72 kN), 1,140 (50.72), 3,980 (17.70 kN), and 3,980 (17.70 kN) lbs. Live load testing was carried out in two stages: the first on July 11, 1989, and the second on November 15, 1989. In the second phase only one truck was used. This is the same vehicle as the 59.36-kip (263.99-kN) truck used in July. Truck details are described in Section 7.2.

5.3 OUTPUT

NOPARC generates strains and stresses at three integration points, which are at mid-points of concrete and steel layers (refer to Sections 5.2.12 and 5.2.13), and nodal displacements. Upon request, it also lists stress resultant quantities such as bending moments and in-plane forces per unit length of mid-plane surface. Stresses, strains, and deflections are viewed graphically with PATRAN II (PDA 1988) on a VAX mini-supercomputer or SUPERVIEW (Algor 1990) on an IBM personal computer. PATRAN II is a graphics package that runs on a VAX 8800 computer. It is specifically written to view output from finite element codes. Similarly, SUPERVIEW is a graphics post-processor that runs on an IBM personal computer. Finite element analysis gives results at three integration points within each element. Appendix VII shows a condensed output file from NOPARC for dead loads at 319 days after casting.

6. Results of Prestressing and Environmental Loads

6.1 General

Self weight, thermal, and prestressing forces were the only loads that existed on the Brook Avenue bridge for the first year of this study. Traffic loads were not allowed until approximately one year after the structure was cast. Due to the large volume of concrete required by the flat slab, dead load is more significant than for typical beam-and-slab bridges. Deflections and strains change with time due to creep and shrinkage of concrete, change in ambient temperature, and loss of prestressing force in the bridge. Temperatures measured by strain gage sensors embedded in the slab are used in the time-dependent analysis.

Vertical deflections and material strains, measured by a survey and strain gages, respectively, were taken 30 days after longitudinal prestressing (56 days after concrete pour in Table 2). This data provides the first set (chronologically) of experimental information used in comparison with numerically predicted results. As explained in Section 5.2.4, data collection and complementary finite element analyses are carried out at 56, 102, 136, 193, 231, 294, 319, 320, 400, 472, 591, 681, and 878 days after casting. Salient deflection, strain, and stress quantities are presented in graphical form via fringe and x-y plots in this chapter. More complete listings of data are available in the appendices.

6.2 Variation of Temperature

Each day on which readings were taken for strain gages attached to pencil bars, a temperature profile through the thickness of the slab was determined by monitoring the 10 thermal gages embedded in the slab. Table 2 lists the dates when these temperatures were taken. Fig. 45 shows the variation of temperature through the slab thickness for selected days on which data are recorded in March, April, May, July, and August. Each curve in the plot represents the average of the two gages at a particular depth in the slab. At a given moment, temperature variation through the thickness is generally in the range of 5-15 °F (2.8-8.3 °C). An average of the readings from the 10 gages is used as the temperature for the entire slab in the FEM analyses.

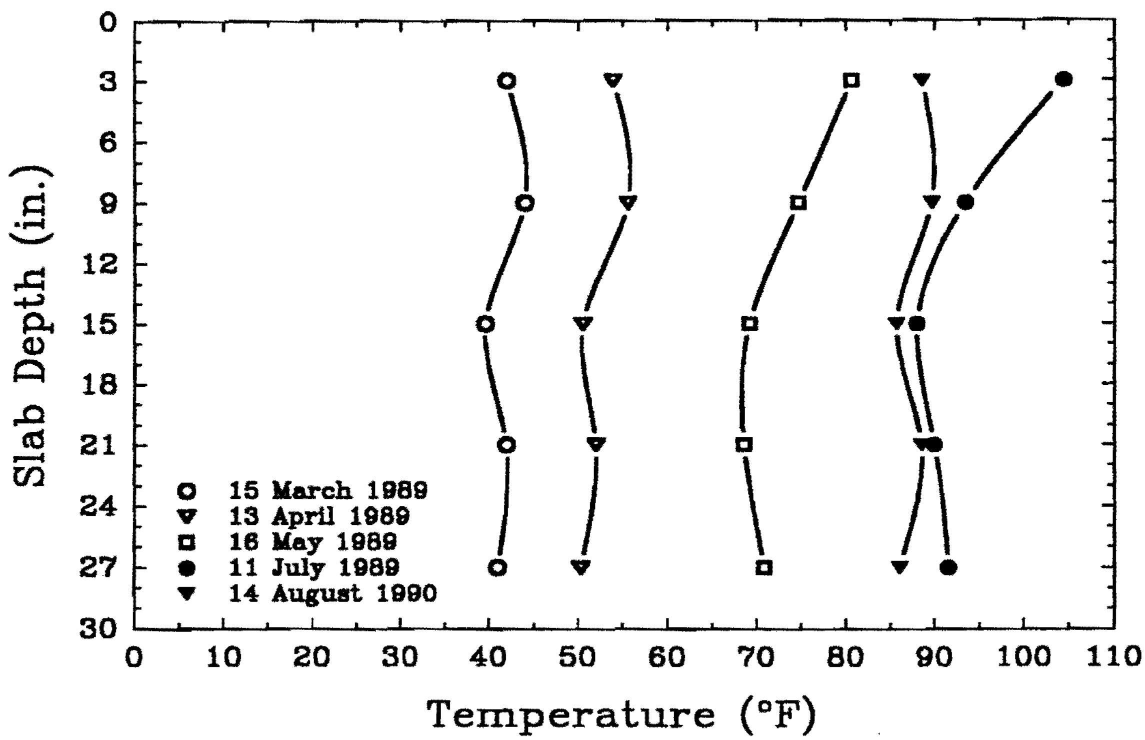

FIG. 38. Variation of Temperature Through the Thickness of the Slab with Time

Not only seasonal changes in ambient temperature effect changes in deformation of the slab, but daily warming and cooling cycles lead to changes in elevation. On August 13 and 14, 1990, a series of elevation readings were taken on implants 11 and 21 (see Fig. 30), that lie on the north edge and at the center of the east and center spans, respectively. Over a period of 20 hours four sets of data were taken with a surveying instrument. The first reading occurred at 8 p.m. with an ambient temperature of 75 °F (24 °C). Succeeding air temperatures at the other times of data collection on August 14 were 80 °F (27 °C), 90 °F (32 °C), and 95 °F (35 °C). Fig. 39 shows the variation of the vertical deflection at implants 11 and 21, respectively, relative to the 9:30 a.m. elevations taken on August 14. The range of change in elevation for both the east and center spans is approximately 0.2 in. (5.1 mm). Moreover, the spans move in opposite directions: the survey point on the east span undergoes an increase in elevation during the hottest part of the day while the center span decreases.

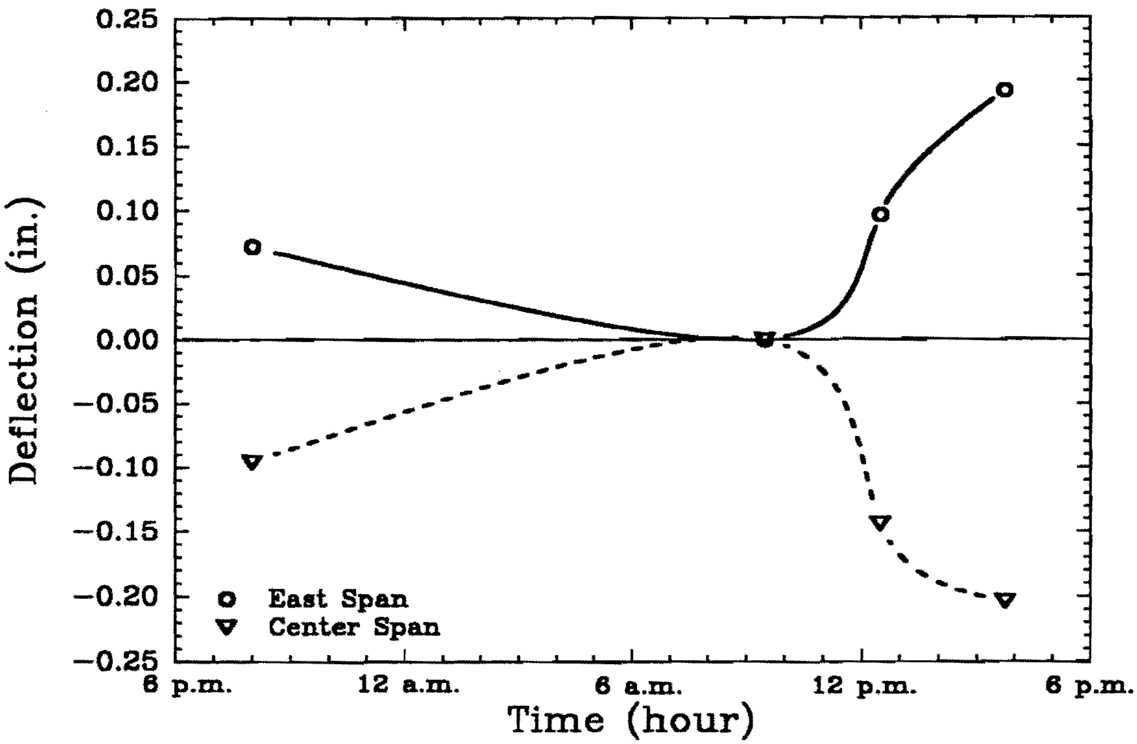

FIG. 39. Deflection in Center and East Spans Due to Temperature

6.3 VERTICAL DEFLECTION

6.3.1 Short- to Moderate-Term

Application of post-tensioning forces during construction caused the bridge to deflect upward at the center of each span. Table 4 in Appendix III tabulates vertical deflections at the implant locations for each date on which survey data were collected. To highlight important trends in data, Fig. 40 compares vertical deflections obtained from surveying, FEM, and the one-way procedure at 56 days after the concrete pour. Each of the three plots follows a sequence of deflection implants along the length of the bridge that is parallel to the roadway. Refer to Fig. 30 for location of implants. Fig. 40(a) shows experimental and predicted deflections along section 1 of Fig. 30. Likewise, Figs. 40(b) and 40(c) compare deflections at 56 days along sections 3 and 5, respectively. A gray-scale fringe plot summarizes prediction of the deflected shape by FEM at the 56-day period (Fig. 41).

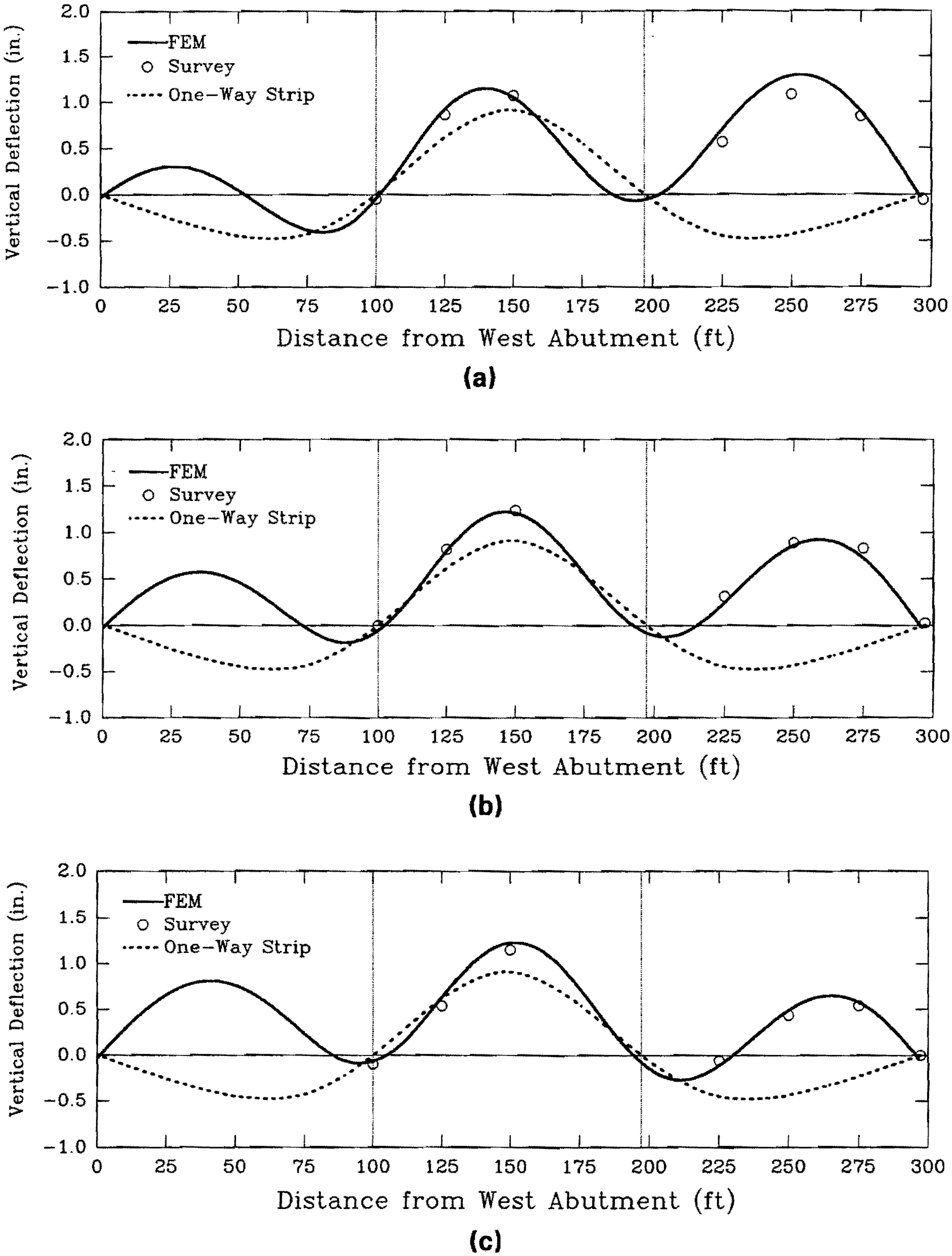

FIG. 40. Experimental and Analytical Bridge Deflections 56 Days after Pour: (a) North Edge; (b) Middle; (c) South Edge

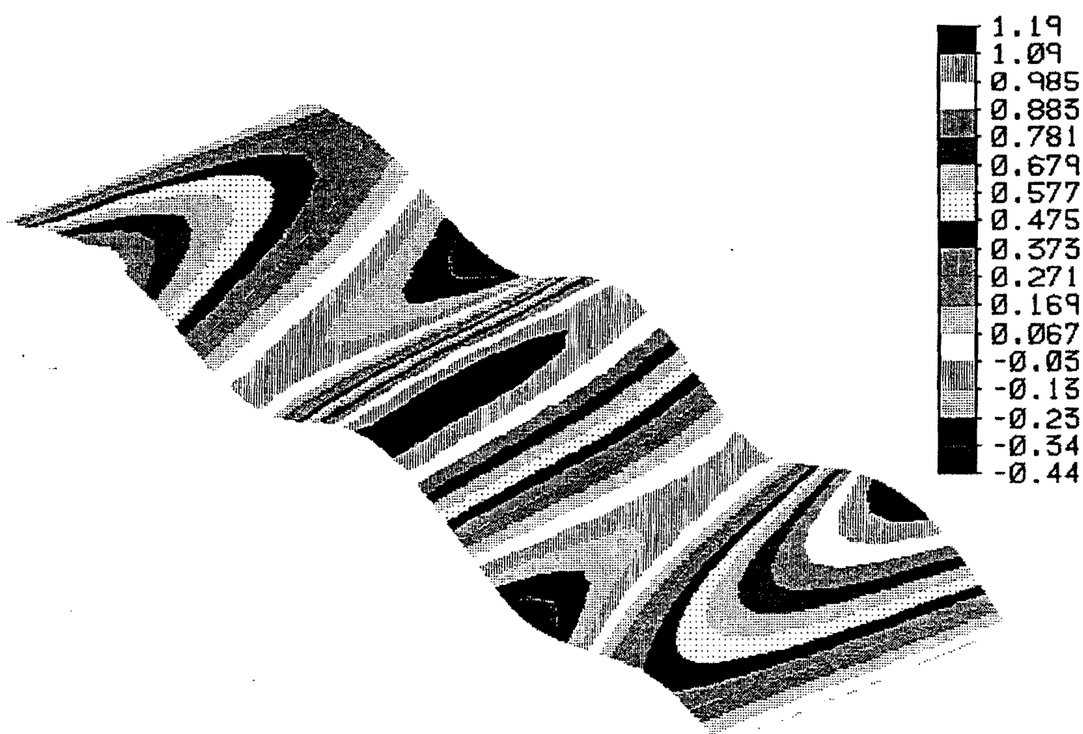

FIG. 41. Deflected Shape 56 Days after Concrete Pour

As a consequence of assumptions inherent in the unit strip approach, the one-way procedure predicts the same deflected shape for all longitudinal cross-sections and all periods of time. That is, it disregards any effects of skewed geometry, such as twisting, and lumps effects of long-term creep, shrinkage, and relaxation together. The center span is predicted to rise approximately 0.91 in. (23.2 mm), and the elevation of each end span is expected to decrease by 0.46 in. (11.7 mm).

The deflected shape of the one-way procedure differs markedly from that measured in the field and predicted by FEM. An additional inflection point occurs in each end span according to the FEM approach. FEM and surveyed values of deflection are nonzero at the columns due to compliance of the column and the neoprene pads. For all 3 longitudinal cross-sections in Fig. 40 the measured and FEM deflections noticeably exceed those of the one-way procedure in the center span and, especially, the east span. For example, along the north edge of the slab the maximum upward deflection measured by the survey instrument exceeds 1.06 in. (26.9 mm) in the east and center spans, whereas the one-way procedure predicts a decrease of 0.46 in. (11.7 mm). Twisting in the end spans due to skew of the bridge is clearly evident in Fig. 41 and also by comparison of the north and south edges of the west span in Figs. 40(a) and 40(c).

Deflections at the 319 day period emulate the same trends, especially those attributed to skew, as at the 56-day mark. At 319 days total in-plane deflection of the slab in the longitudinal direction relative to the dimensions of the slab on the date of pour is shown in Fig. 42 with the vertical deflected shape as the surface on which the fringe plot is displayed. Displacement of the slab at each of the abutments due to all factors (temperature, creep, shrinkage, etc) is predicted to be approximately 0.9 in. (23 cm). Vertical deflection throughout the slab is shown by means of a fringe pattern in Fig. 43. The general pattern of undulating deflection is very similar to that of 56 days (see Fig. 41), except that magnitudes of rise and fall have increased.

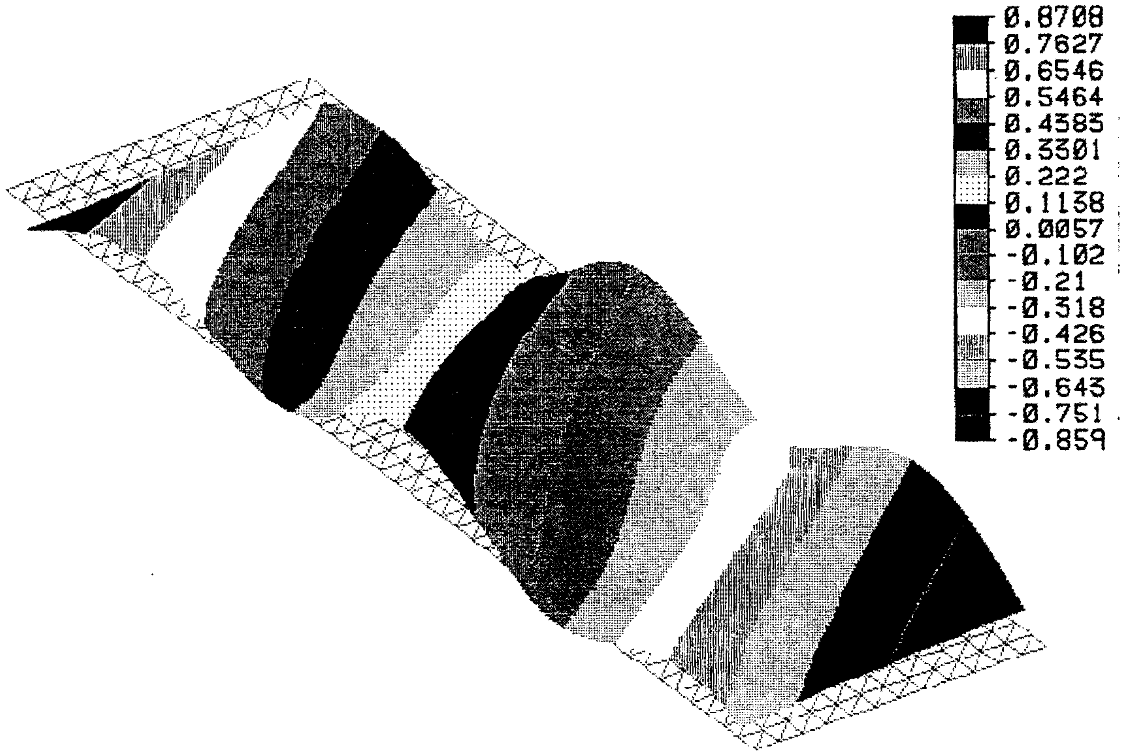

FIG. 42. In-Plane Displacement of the Slab in the Longitudinal Direction at 319 Days

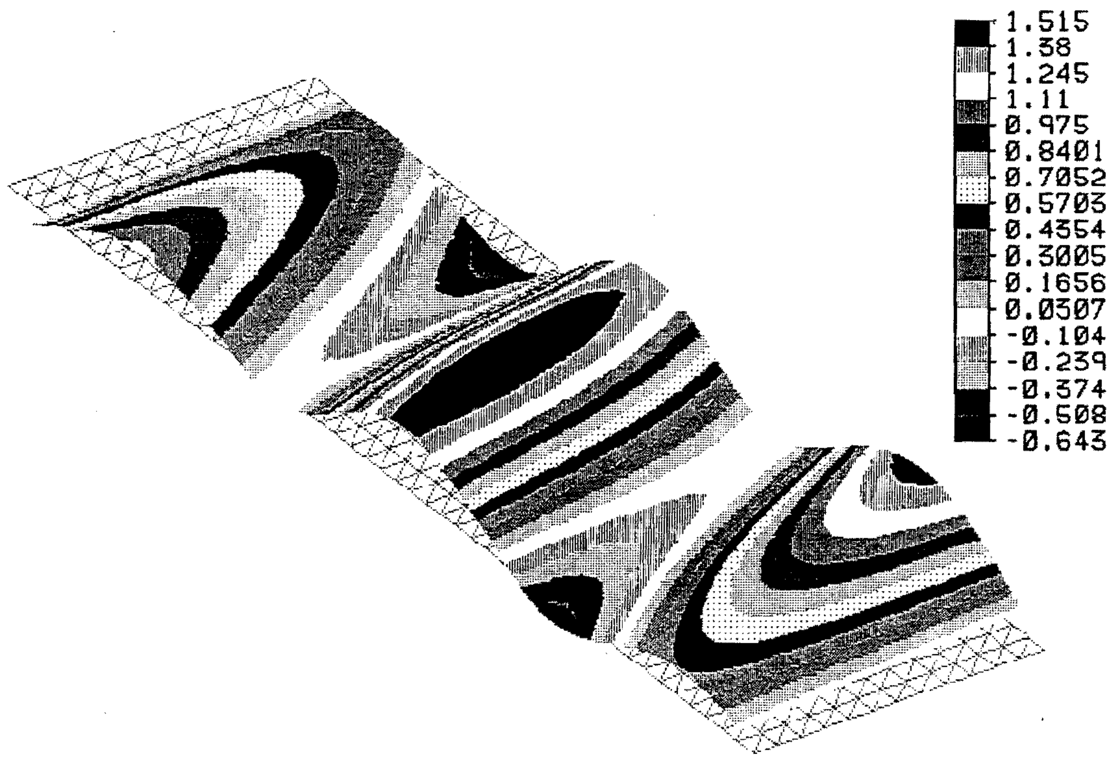

FIG. 43. Vertical Displacement of the Slab at 319 Days

Fig. 44 compares deflections at 319 days by the same methods used in Fig. 40: survey, one-way analysis, and FEM. While the one-way analysis does not change with time, the survey and FEM values for the vertical deflection of the midpoint of center span are now greater than 1.5 in. (38.1 mm). That is, between the 56th and 319th days, the increase in deflection at this central location is approximately 0.5 in. (12.7 mm) as reported by the survey instrument.

Again, deflections estimated by the one-way procedure do not compare favorably with experimental or FEM results. Especially noteworthy is that end span deflections predicted by the one-way procedure show a downward deflection, while FEM predictions and measured deflections show generally upward movement. In addition, although the one-way procedure's prediction of deflections in the mid-span region agrees reasonably well with that of FEM predictions and survey values at the 56-day reading, the agreement deteriorates for all regions at 319 days after pour. Since temperatures are nearly the same on the 56th and 319th days, thermal effects are negligible and differences in deflections can be attributed to prestressing losses, creep, and shrinkage effects. Results from numerical simulation are acceptable in that trends due to skew are in agreement with experimental findings, and peak magnitudes are acceptably close to each other.

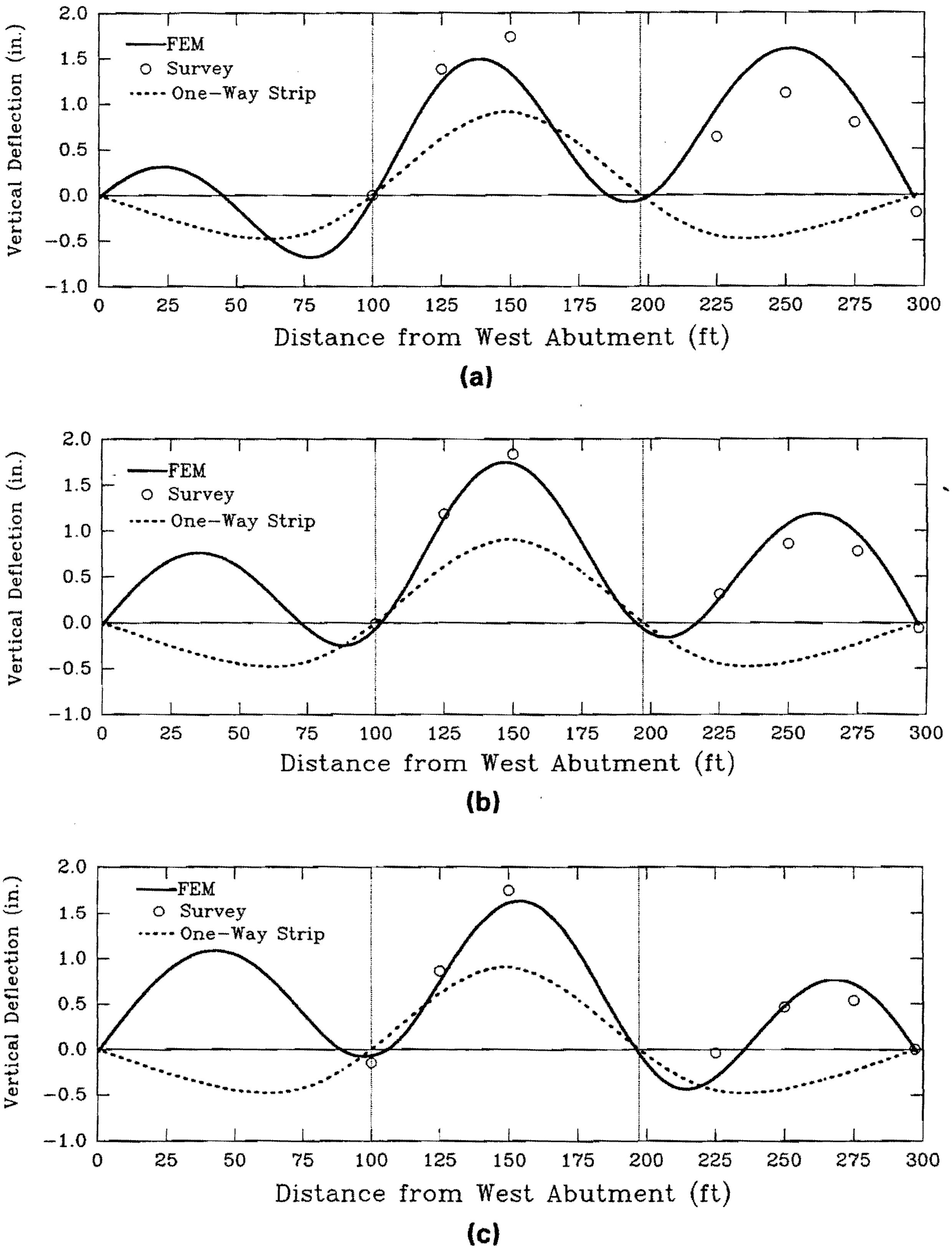

FIG. 44. Experimental and Analytical Bridge Deflections 319 Days after Pour: (a) North Edge; (b) Middle; (c) South Edge

6.3.2 Long-Term

One of the important goals of this phase of the research study is to observe long-term effects of the construction materials, methods, and environment on a full-scale field bridge. As described in Table 2, visits to the site of the Brook Avenue bridge in Wichita Falls, Texas, continued for approximately 2.5 years. Although reading of strain gages had to be discontinued after 400 days due to unreliable data, survey measurements on the top surface of the slab continued throughout the entire period. Vertical deflections at each implant location obtained from these visits are listed in Table 4 (see Appendix III) according to the number of days after the concrete slab was poured.

Fig. 45 presents results of vertical deflection at the center of the center and east spans for a total period of 878 days from the date of pour. For an initial period of approximately 200 days after the pour, the center of each slab rises at a rate of approximately 0.25 in. (6.35 mm) per month. This is followed by a relatively slow rate of change in the vertical deflection. The maximum deflection for the center and end spans is measured to be 1.93 in. (49.0 mm) and 0.88 in. (22.4 mm), respectively, or more than twice that predicted by the one-way procedure. FEM results predict this trend relatively well. In summary, long-term effects show that deflection at the center of the middle span is continuing to increase, albeit slowly, even two years after construction.

6.4 STRAIN

Strain gage readings reflect effects of shrinkage and creep as well as strains caused by prestressing, thermal, and dead loads. Formats used for presentation of results in this section include x-y plots and gray-scale fringe plots. Changes in strain due to truck loads are described in section 7.3.2.

Figs. 46 and 47 compare bottom and top layer strains, respectively, in the longitudinal direction obtained from strain gages, FEM, and the one-way procedure at 319 days after the concrete pour. Chronologically, data from gages in the prototype is acquired approximately 11 months after the concrete pour. Each plot on these graphs follows a sequence of strain gages (see Fig. 24 for gage locations) along the length of the bridge that is parallel to the roadway. The one-way strip procedure developed by TxDOT does not consider strains. However, in order to make a comparison with FEM and gage readings from the prototype, a transformation of the bending moments predicted by the one-way procedure is carried out. Strains corresponding to the one-way procedure are obtained using moments at various cross-sections due to dead and prestressing loads and, subsequently, Hooke's Law.

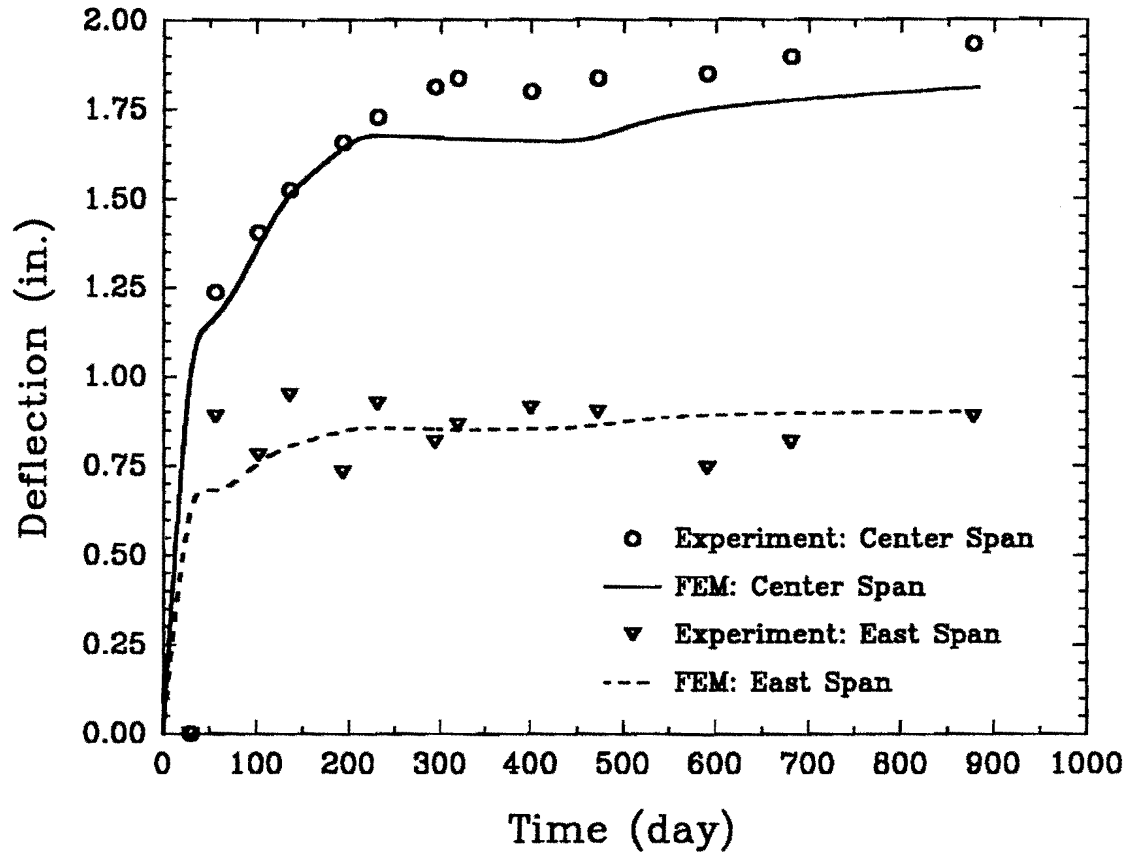

FIG. 45. Vertical Deflection versus Time for Center and East Spans

These graphs show that strains predicted by the one-way design procedure that uses elastic analysis deviate by as much as 600 microstrains from gage readings and FEM analysis. There are a number of factors that may contribute to this difference. The one-way procedure follows AASHTO (*Standard* 1989) and lumps time-dependent effects of creep and shrinkage together. Two-way slab action is neglected. Also field readings of anchor set loss are less than the standard value (0.25 in. (25.4 mm)) taken for design purposes to estimate the loss. During construction the anchor set loss recorded was as low as 0.06 in. (1.52 mm) and averaged approximately 0.10 in. (2.5 mm) during the longitudinal and transverse post-tensioning operations.

Trends of the predicted and measured strains correlate well with the counterpart deflection plots at 319 days (see Fig. 44). Plots of deflection show the bridge moving upward at the middle section of each span. Strains predicted in the longitudinal direction at the bottom layer of mild steel reinforcement show high magnitudes of compression at the midspans and relatively low values at the supports (Fig. 46). Corresponding strains at the top level of reinforcement in the longitudinal direction (Fig. 47) show low midspan strains and relatively high strain levels at the supports. Measured strains compare well with FEM results in both the midspan and support regions in the top and bottom layers but far exceed magnitudes of strain predicted by the one-way procedure. A complete tabulated listing of all strain gage data and FEM results is presented in Table 6 (Appendix IV).

An average gage reading of normal strains in the transverse direction at the level of the top and bottom layers allows a helpful comparison with FEM and the one-way procedure. This average strain provides a means of comparison with the approach used by the one-way procedure during design of the transverse area of the slab over the columns. Factors that contribute to bending in the slab such as unequal creep, shrinkage, and dead load are removed from consideration of strain by the averaging process. The governing constitutive equation from two-dimensional elasticity for plane stress is as follows (Timoshenko and Goodier 1951):

$$\varepsilon_t = \frac{1}{E_c}(\sigma_t - \nu\sigma_l) \qquad (11)$$

where ε_t is the normal strain in the transverse direction, σ_t and σ_l are normal stresses in the transverse and longitudinal directions, respectively, ν is Poisson's ratio, and E_c is the modulus of elasticity of the material. Since the tendon force in the slab in each direction is known, the corresponding normal stress can be computed and, in turn, the normal strain can be determined. Neglecting effects of skew, substituting constants for material properties of concrete according to chapter 5, computing the average normal stress due to longitudinal post-tensioning, dividing the force applied by the transverse post-tensioning tendons by the area indicated in Fig. 2, and applying Eq. 11 gives the one-way procedure's prediction of average in-plane strain. These strains are computed at sections A, B, C, D, E, and G (see Fig. 24) and listed in Table 3.

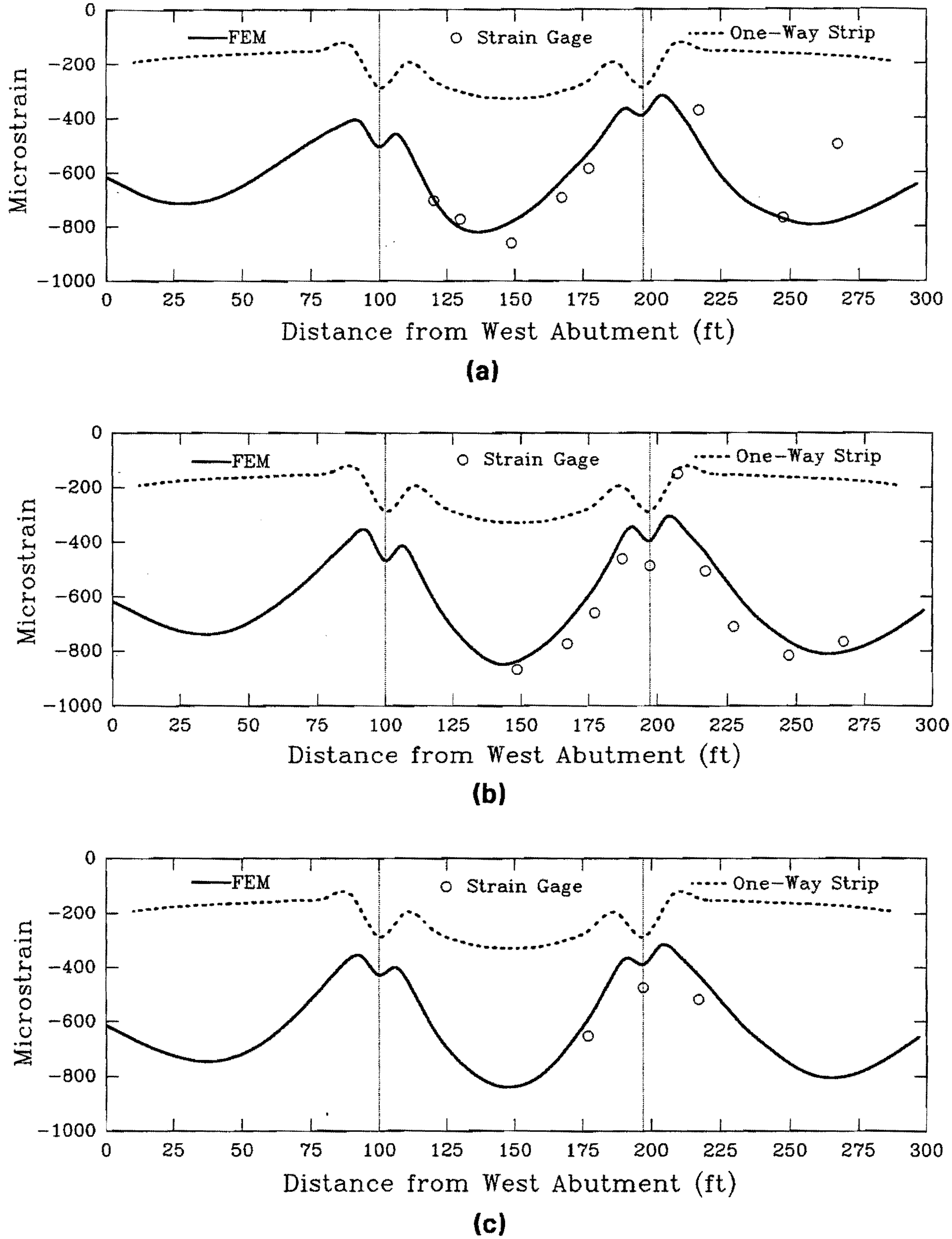

FIG. 46. Comparisons of Bottom Layer Longitudinal Strains 319 Days after Pour: (a) Section C; (b) Section E; (c) Section F

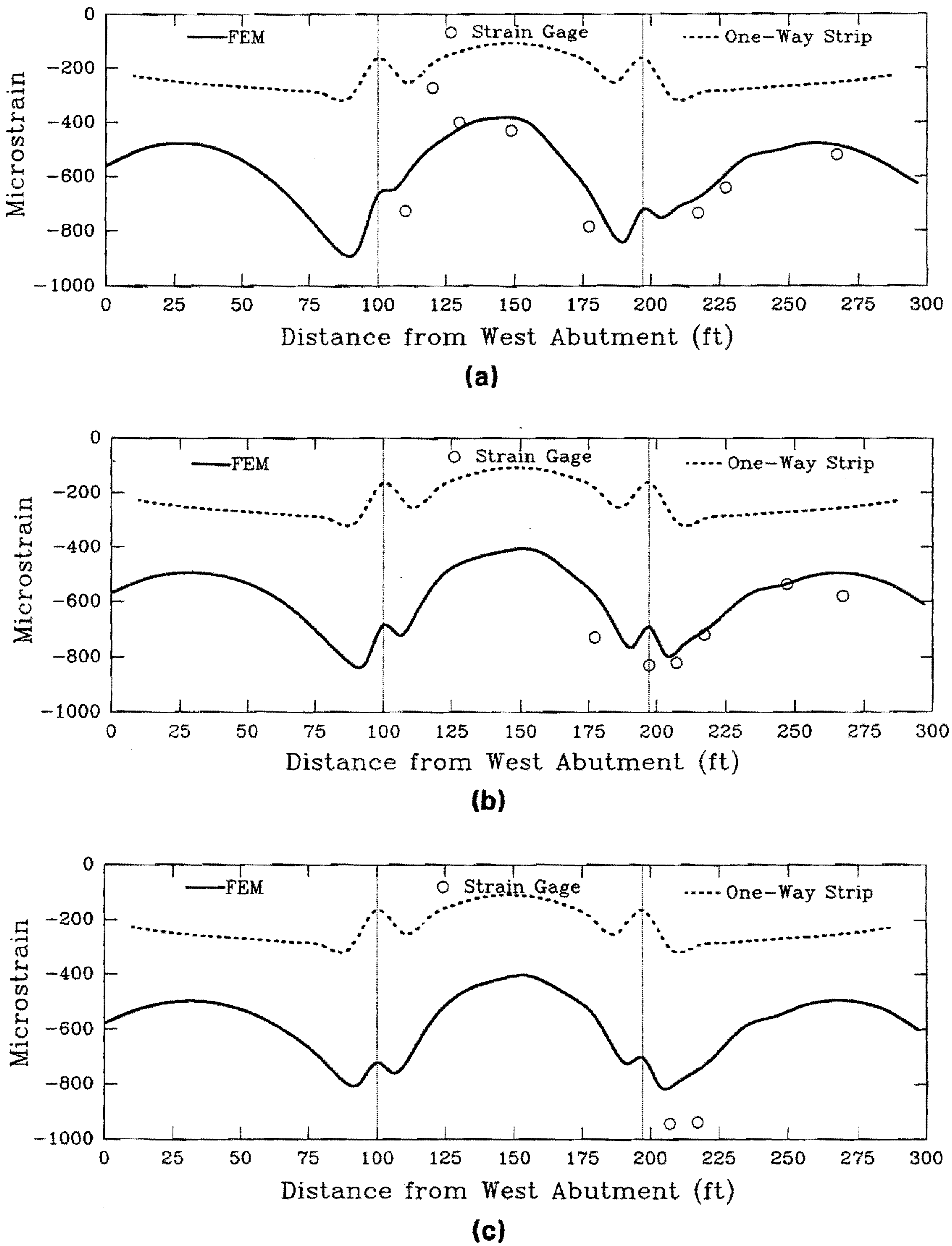

FIG. 47. Comparisons of Top Layer Longitudinal Strains 319 Days after Pour: (a) Section C; (b) Section E; (c) Section F

TABLE 3. Transverse Normal Strain at Cross-Sections A, B, C, D, E, and G

Section (1)	Width (in.) (2)	Transverse Normal Stress (psi) (3)	Longitudinal Normal Stress (psi) (4)	Transverse Normal Strain (10^{-6} in./in.) (5)
A	261.4	-658	-962	-105.3
B	484.1	-355	-962	-36.8
C	595.5	-289	-962	-21.8
D	706.9	-243	-962	-11.5
E	929.6	-185	-962	1.7
G	261.4	-658	-962	-105.3

Note: 1 in. = 0.0254 m; 1 psi = 6.895 kPa

To enable a graphical comparison of one-way, FEM, and averaged strain gage readings in the transverse direction, Fig. 48 is constructed for values at sections A, E, and G. Sections A and G are near the post-tensioning anchor heads, while section E is near the centerline of the bridge traffic lanes. In all cases the one-way procedure predicts less strain in the transverse direction than is measured by the strain gages or predicted by FEM. Predictions by the one-way procedure are especially poor along section E where FEM and average gage readings all exceed 125 microstrain while the one-way values are slightly tensile. Compressive strain gage readings along section A near the north edge of the structure are at least twice as large as the one-way procedure anticipates at 319 days. FEM predictions agree reasonable well in magnitude and trend with strain gage readings for each of these sections.

It should be noted that measured longitudinal strains (see Figs. 46 and 47) are in better agreement with FEM results than with transverse strain data from gages. This can be attributed to several factors. First, the magnitude of transverse strain is generally much less than that of the corresponding longitudinal strain. Foil strain gages are unable to make accurate predictions in the range of 0-50 microstrain. Also, some scatter in the readings is expected from connection and disconnection of RS232 connectors (see Fig. 28).

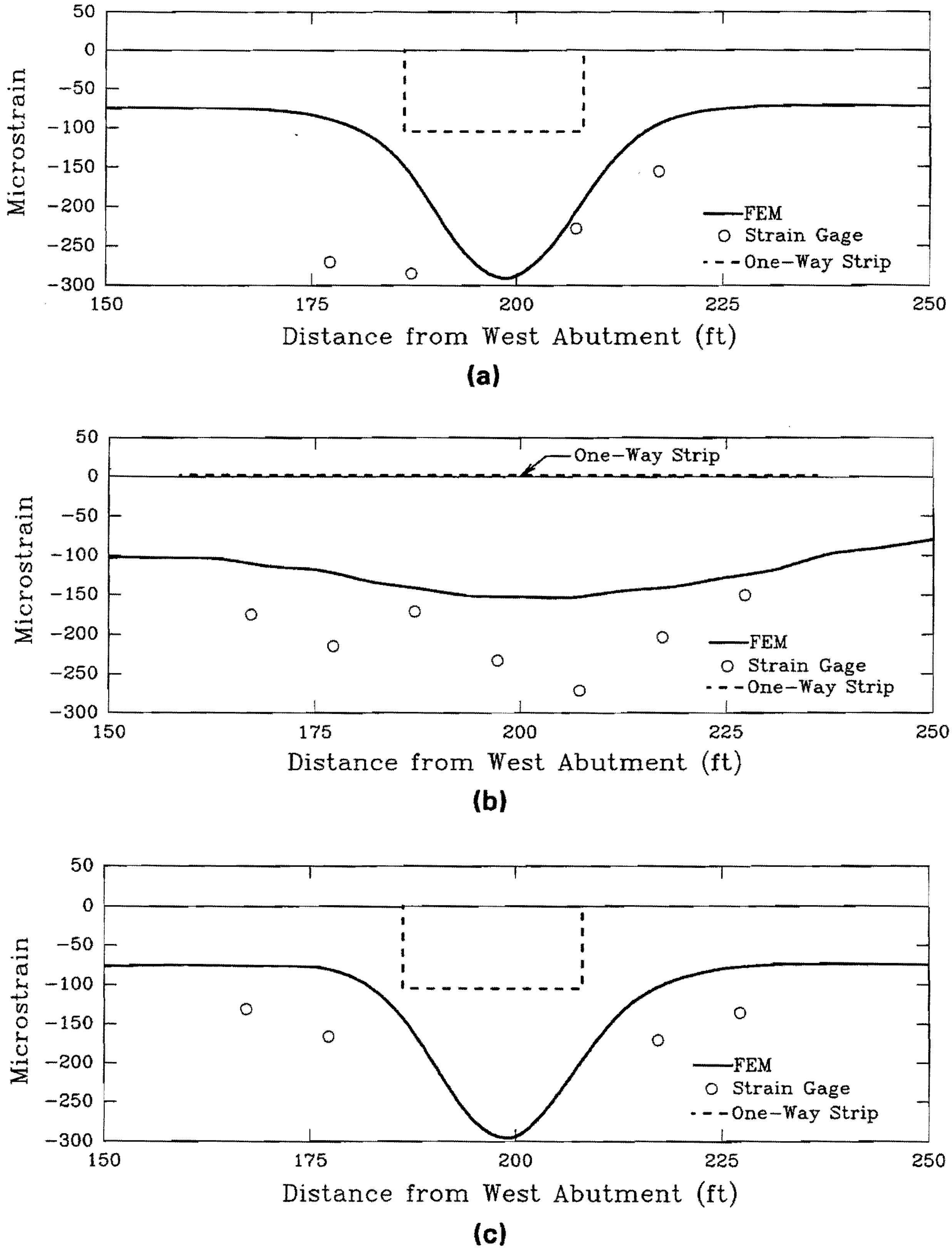

FIG. 48. Comparisons of Midplane Transverse Strains 319 Days after Pour: (a) Section A; (b) Section E; (c) Section G

6.5 STRESS

Section 6.4 reports measured and predicted strains for the slab. However, bridge designers usually work in terms of resultant moments, forces, and stresses rather than strains. Toward this end, a series of figures that show gray-scale fringe plots of a plan view of the bridge deck from numerical simulation by FEM are presented in this section. Each figure displays a single stress component throughout the slab at a specific level of the slab thickness. In this section, the notation "bottom" and "top" refer to quantities computed at the center of layers one and ten, respectively, of the concrete layering system used by NOPARC (see Fig. 37). By comparison, in section 6.4 these labels refer to strain quantities at the levels of the mild steel reinforcement. Order of presentation here parallels that used to discuss the strains: longitudinal components are treated first followed by transverse stresses. To aid this process eight fringe plots from FEM analyses showing stresses in the extreme top and extreme bottom layers of the bridge are plotted in Figs. 49-56. Since cracks were observed in the bridge (see Figs. 13, 14, and 15) parallel to the longitudinal direction, transverse stresses in this section are plotted for an axis that is perpendicular to the longitudinal direction rather than parallel with the skew.

6.5.1 56 Days after Pour

Fig. 49 shows the distribution of stresses at the level of the bottom layer of concrete in the longitudinal direction at 56 days after concrete pour. That is, these stresses are present on the first date of data collection after the post-tensioning operation was complete (Table 2). Magnitudes of stress range from -306 psi (-2.11 MPa) to -2,012 psi (-13.86 MPa). Maximum stress in the center of the west span (-1,784 psi (-12.29 MPa)) is approximately 228 psi (1.58 MPa) less than the maximum stress in the center of the east span (-2,012 psi (-13.87 MPa)). This reduction is expected due to the change in width of the bridge along its length as discussed in section 6.4. The maximum compressive stress in the middle of the interior span is also -2,012 psi (-13.96 MPa). Effects of skew and column reactions are visible. Magnitudes of compressive stress are the smallest directly above the columns and along the north and south edges.

FIG. 49. FEM Longitudinal Bottom Layer Stresses at 56 Days after Pour

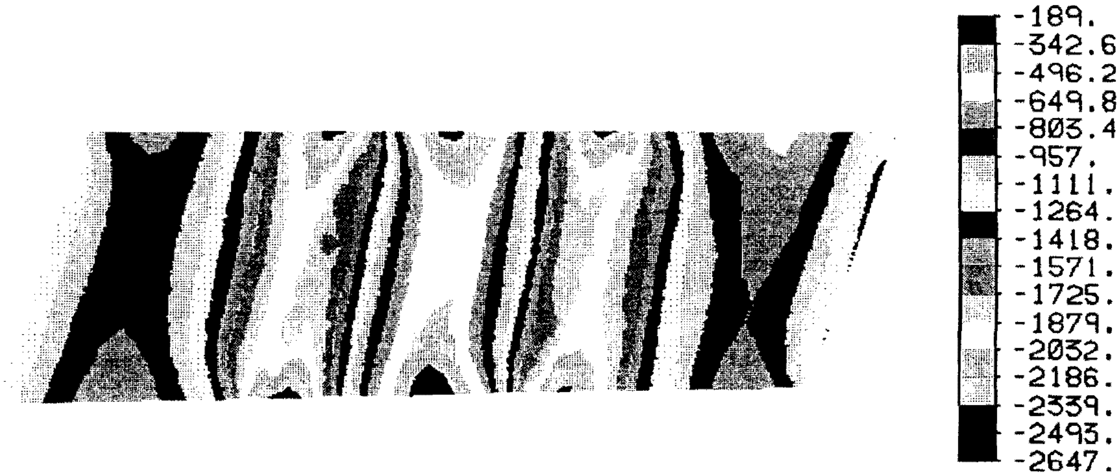

FIG. 50. FEM Longitudinal Top Layer Stresses at 56 Days after Pour

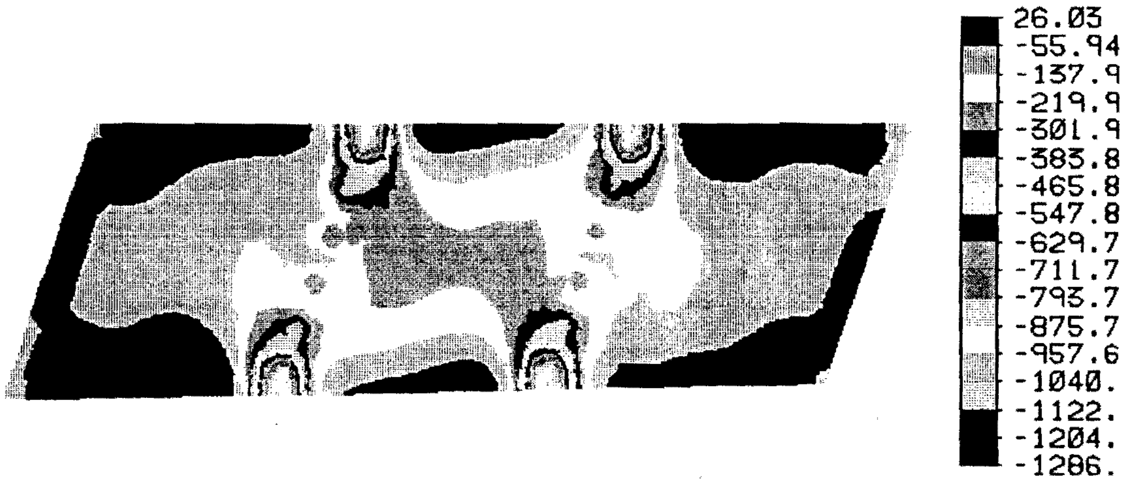

FIG. 51. FEM Transverse Bottom Layer Stresses at 56 Days after Pour

FIG. 52. FEM Transverse Top Layer Stresses at 56 Days after Pour

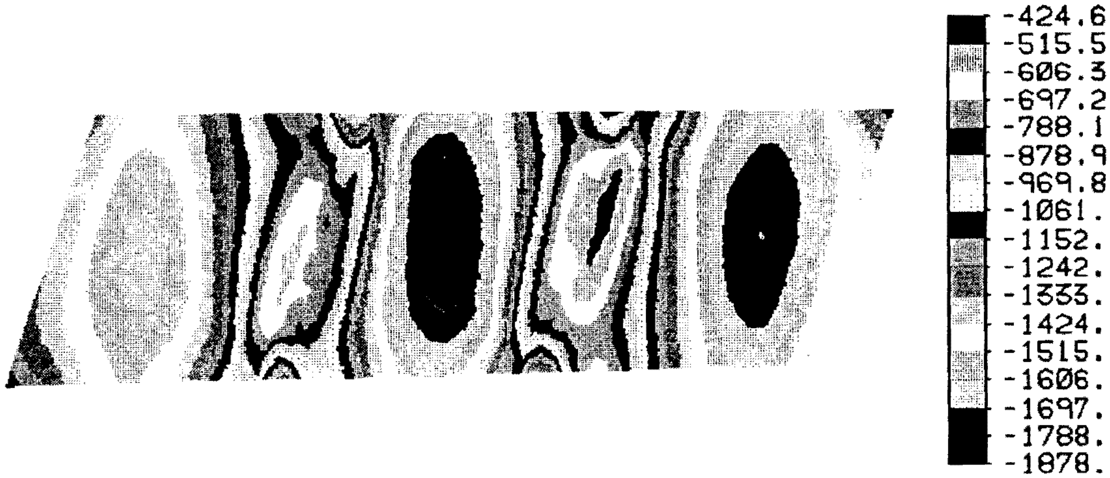

FIG. 53. FEM Longitudinal Bottom Layer Stresses at 319 Days after Pour

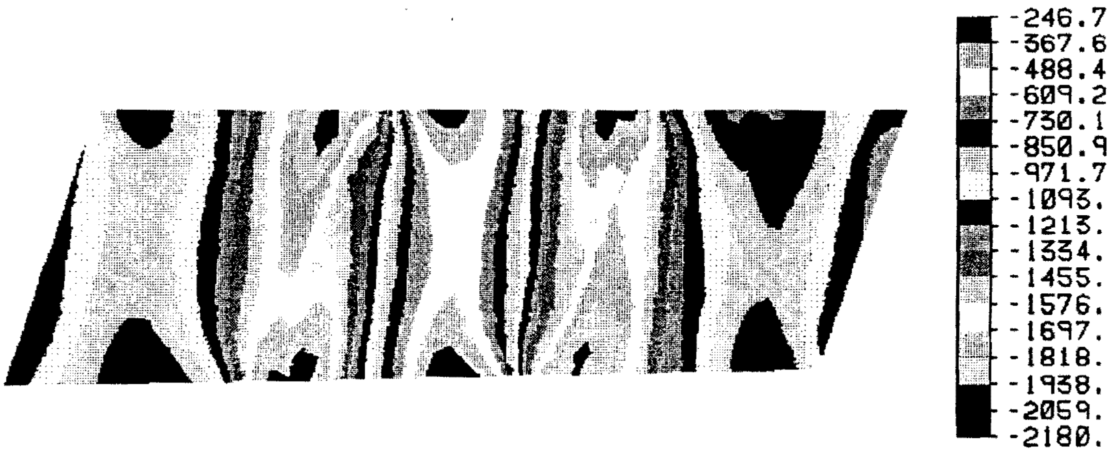

FIG. 54. FEM Longitudinal Top Layer Stresses at 319 Days after Pour

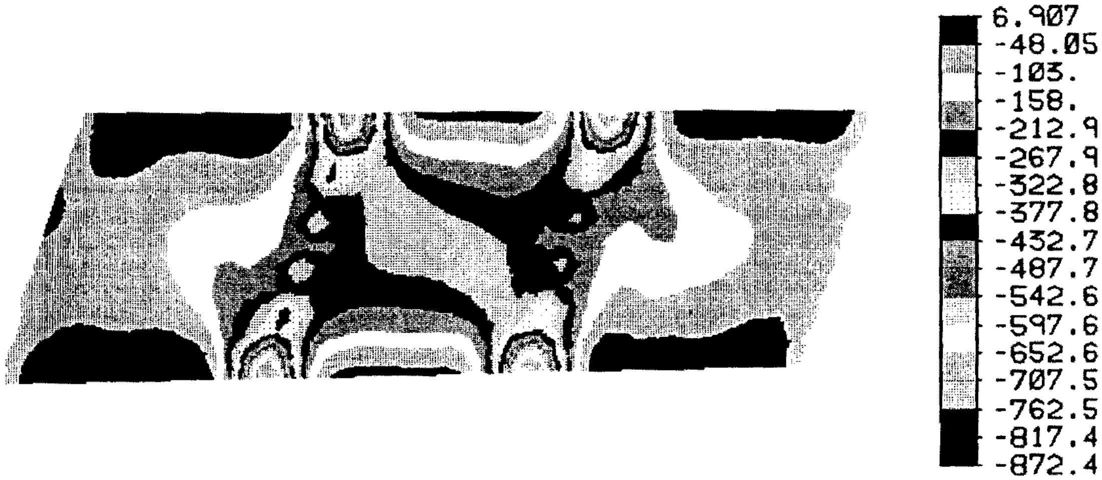

FIG. 55. FEM Transverse Bottom Layer Stresses at 319 Days after Pour

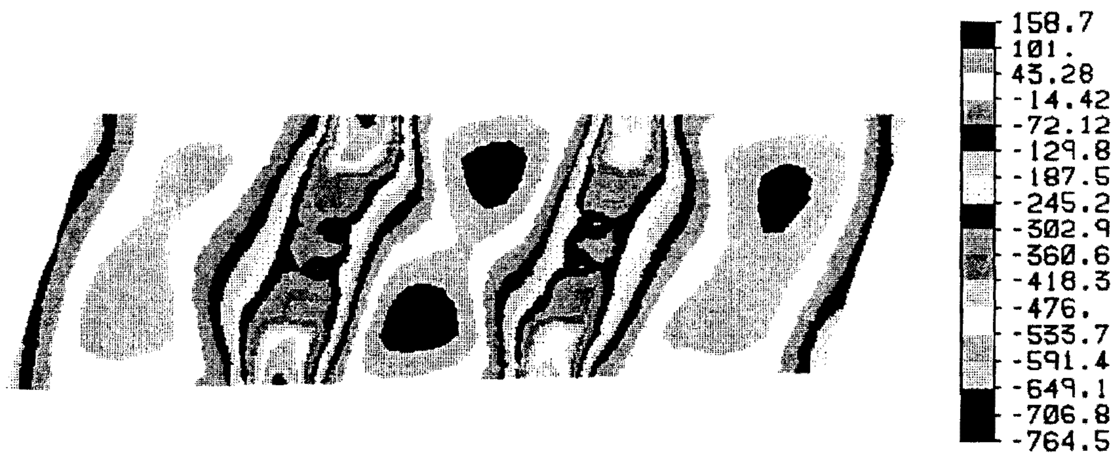

FIG. 56. FEM Transverse Top Layer Stresses at 319 Days after Pour

Fig. 50 is a gray-scale representation of the distribution of longitudinal stresses in the topmost layer of concrete at 56 days after pour. Upward deflection of the structure between supports causes compressive stresses in the top layer at the middle of each span to decrease. However, midspan longitudinal stresses are still compressive in nature and do not decline below -217 psi (-1.50 MPa). Compressive stress in the middle of the interior span is approximately -582.5 psi (-4.04 MPa). As is the case with longitudinal strains, normal stress magnitudes decrease with proximity to the north or south edge. Compressive stress reaches the greatest magnitude near each line of columns.

Figs. 51 and 52 describe predictions of transverse stress in the bottom and top layers of concrete, respectively. Transverse stress in the bottom layer (Fig. 51) ranges from 24.1 psi (0.16 MPa) to -990 psi (-6.82 MPa). A high gradient in stress is predicted between the post-tensioning anchors and the center of each column line: a maximum of -990 psi (-6.9 MPa) near the anchor heads to -44 psi (-0.30 MPa) at the center of the column lines. Away from the column lines the transverse stress varies from 24.1 psi (0.16 MPa) in tension along the edges of the slab to approximately -200 psi (-1.38 MPa) in the middle of each span. In many areas of the slab, stresses are below the minimum compression recommended by (ACI 1989).

Transverse stresses in the top layer are important because of potential for cracking and moisture penetration. Although the modulus of rupture is not exceeded, Fig. 52 shows a large portion of the east and center spans having tensile stresses as high as 135 psi (0.93 MPa). Beneficial compressive stresses along the north and south edges that are near tendon anchors dissipate rapidly. Tensile stresses in the transverse direction are, to a large extent, caused by Poisson's effect, which is not considered in the one-way design procedure. Due to construction sequencing, the prototype structure has an additional complicating factor in these regions of tensile stress: restraint due to unequal shrinkage of concrete in adjacent pours.

6.5.2 319 Days after Pour

While Figs. 49-52 present stresses occurring shortly after transfer of post-tensioning forces, the long-term behavior is also important. Figs. 54-56 present gray-scale plots of FEM stress components at 319 days after the pour. In comparison with its counterpart at 56 days (Fig. 49), Fig. 54 shows that longitudinal stresses at the bottom layer of concrete have the same general distribution for both dates. The entire structure remains in compression even after significant prestressing loses due to creep, shrinkage, and relaxation. However, the maximum compressive stress is reduced from -1,965 psi (-13.5 MPa) to -1,878 psi (-12.9 MPa). Predictions for the longitudinal stress in the top layer of the slab are similar, with the maximum compressive stress reducing from -2,647 psi (-18.3 MPa) to -2,180 psi (-15.0 MPa). In summary, there is a net decrease of compressive stress in the top and bottom layers in the longitudinal direction. As a final example, the top layer compressive stress in the middle of interior span reduces by approximately 50 psi (0.34 MPa).

Transverse stresses in the bottom layer of concrete do not change appreciably between the 56th and 319th day after concrete pour (Fig. 54). However, top layer stresses in the transverse direction show increases in maximum tension (from 135 psi to 150 psi) and compression (from -863 psi (-5.95 MPa) to -999 psi (-6.88 MPa)) over this period of time (Fig. 56). The above-mentioned reduction in longitudinal stresses also effects a redistribution in the transverse stress (Figs. 54 and 56) due to the Poisson's effect. In the middle region of the outer spans, the tensile stress in the transverse direction is reduced slightly, while the corresponding stress in the middle span is increased slightly.

7. LIVE LOAD

7.1 GENERAL

Results of tests on the Brook Avenue bridge using heavy trucks to impose live load are presented in this section. Design vehicles currently used in AASHTO specifications (*Standard* 1989) were adopted in 1944. Loadings consist of four weight classes, namely: H15-44, H20-44, HS15-44, and HS20-44. Dimensions for vehicles in each class are also given in the specification. These vehicles are not selected to resemble any particular truck in existence, but are hypothetical. The lighter loads, H15-44 and H20-44, are used for design of lightly traveled state roads while HS15-44 and HS20-44 are used for national highways and bridges on the Interstate Highway System. TxDOT designs all bridge structures using the HS20-44 specification. One truck per lane for each span is to be used. In addition to truck loadings, AASHTO specifications contain equivalent loadings to be used in place of truck loadings when they produce greater response.

Live load testing was undertaken to study deflections of Brook Avenue overpass when loaded with concentrated loads from truck wheels, and to determine the accuracy of FEM and the one-way design procedure. Distributed lane loads were not used on the prototype since the one-way design procedure predicts that a single HS20-44 truck load governs the design. Also loading the bridge with the AASHTO distributed load would require enormous resources. The effects of AASHTO distributed lane loads and single concentrated loads are being studied on a laboratory model in another phase of this study.

7.2 FIELD TESTING SCHEME

In the present study, a 59.4-kip (264-kN), three-axle dump truck is used to approximate the AASHTO 72-kip (320.4-kN) load for live load testing of the bridge. Fig. 57 shows the dump truck placed on the bridge. Initial live load testing was conducted in July, 1989 (see Table 2). A three-axle dump truck was provided by TxDOT to the researchers in Wichita Falls, Texas. The truck was weighed, and approximate loads on each wheel were calculated by placing each axle on a scale. Loads on the front and rear tandem axles were 11.6 kips (51.6 kN) and 47.8 kips (212.4 kN), respectively. Wheel configurations are shown in Fig. 58.

FIG. 57. Test Truck

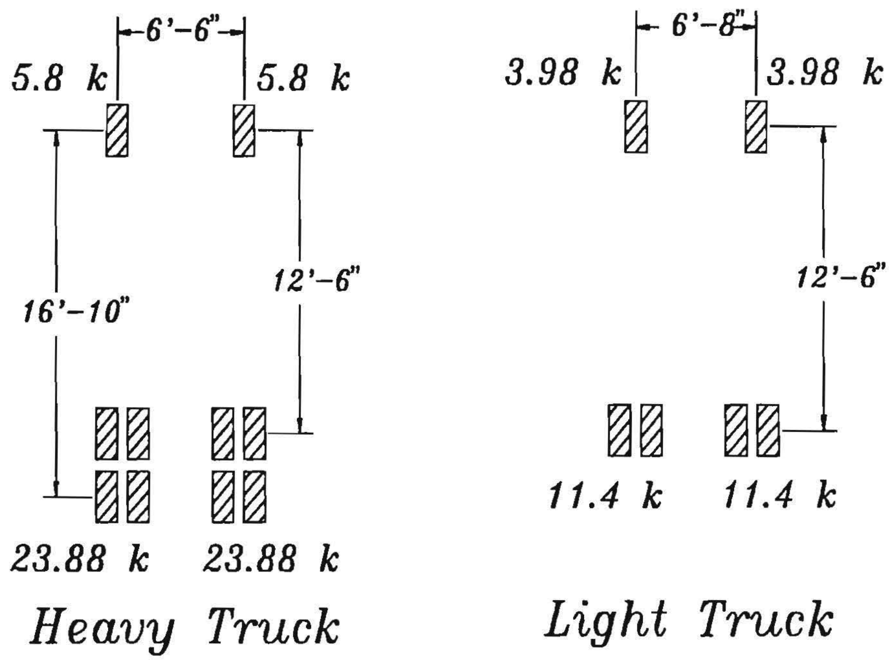

FIG. 58. Truck Wheel Loads and Measurements

A total of 5 load cases, named A, B, C, D, and E, were used (see Fig. 59). Wheels were positioned to approximate locations of finite element nodes used in the computer simulation. For case A, the right rear wheel is placed 0.4l from the abutment of the east span, where l is span length (Fig. 59). This location is also used by TxDOT engineers in the one-way design procedure to place the truck load at the critical location in the end spans. For case B, the truck is placed at the analogous location in the west span. To minimize response of the center span, the right rear wheel is located at position C. For case D, the left rear wheel is midway between second and third columns of the east column line. Finally, for case E, a second truck is added to case D. This truck weighs 30.76 kips (136.82 kN). Load on front and rear axle is 7.96 kips (35.41 kN) and 22.8 kips (101.44 kN), respectively (Fig. 58). The lighter truck's left rear wheel lies midway between the first and second columns of the east column line (Fig. 59).

A second phase of live load testing was conducted in November, 1989, using the same heavy truck as before with approximately the same weight. In this case four locations of the truck named F, G, H, and I, were used (see Fig. 59). Choice of these positions was influenced by strain gage locations in the slab. In case *F* the truck is oriented in the direction of the skew at 173.3 ft (52.8 m) from the northeast corner. Similarly, for case *G* the truck is placed on the south side of the bridge. For case *H*, the truck rests on the interior span so that the maximum number of strain gages is affected. In case *I*, the right rear wheel of the truck is placed near deflection implant 10 (Fig. 30) to create maximum deflection in the bridge at this point.

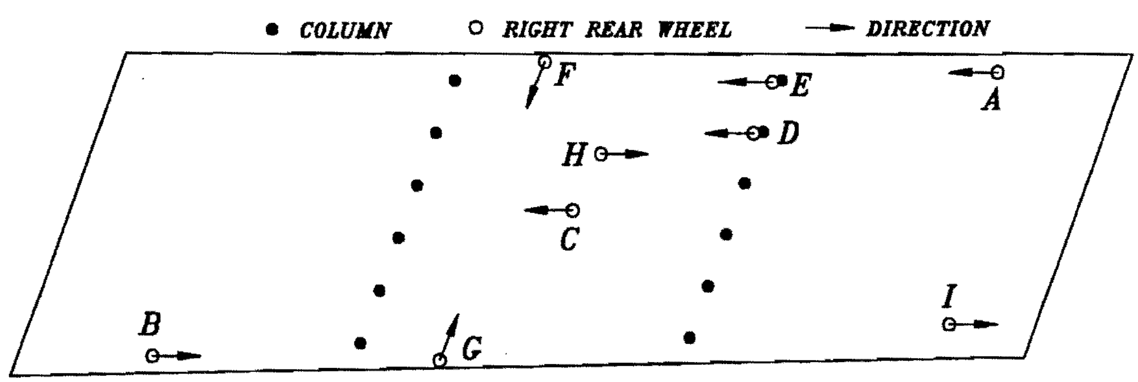

FIG. 59. Location of Right Rear Wheel and Direction of Truck for Live Load Testing

7.3 Experimental and Analytical Results

7.3.1 Deflection

A field survey of the elevation of each implant marker on the deck slab (Fig. 30) is performed in order to determine change in vertical deflection due to the addition of live load. In this section comparison of salient experimental results and numerical prediction is made by means of tabulated data, fringe, and x-y plots. Fig. 43 in section 6.3 is a gray-scale fringe plot that shows the vertical deflection of the bridge predicted by FEM on the date of live load testing but without any truck loads; effects of dead and thermal loads are not included. Deflections in this figure serve as a reference from which differential deflections are measured. A complete set of deflection data is presented in Table 5 for Cases *A*-*C* and *F*-*I*. With the truck wheels located directly on top of a column (positions *D* and *E*) the survey instrument did not offer sufficient resolution to detect vertical deflection of the slab. For this reason readings for these two locations of the truck are not included in Table 5.

With the heavy truck placed near the edge of the slab at position *A* on the 192nd day after pour, FEM predicts the distribution of differential vertical deflections shown in Fig. 60. That is, these gray-scale fringes represent deflections due only to the truck load. Predicted maximum vertical deflection is -0.26 in. (-6.6 mm) which occurs directly under the truck. Effects of skew and plate action are evident. Fig. 61 enables quantification and visualization of differential vertical deflection along a longitudinal line of the bridge with the truck at point *A*. Deflection of the slab is shown along a line from the west abutment to the east abutment that passes through point *A* in Fig. 59. Field survey deflections are compared with predictions from FEM and one-way design. The latter approach uses a simply-supported unit wide strip and concentrated loads that represent the force of the wheels. Concentrated wheel loads for the unit strip are obtained by dividing the axle loads with the width of a standard AASHTO lane. The maximum deflection reported by the survey is -0.228 in. (-5.79 mm) which occurs near the truck at implant 11. FEM predictions agree well with survey quantities in the east span but are less satisfactory in the center span. The one-way design procedure predicts a maximum deflection in the east span that is more than four times as large as the survey and FEM values.

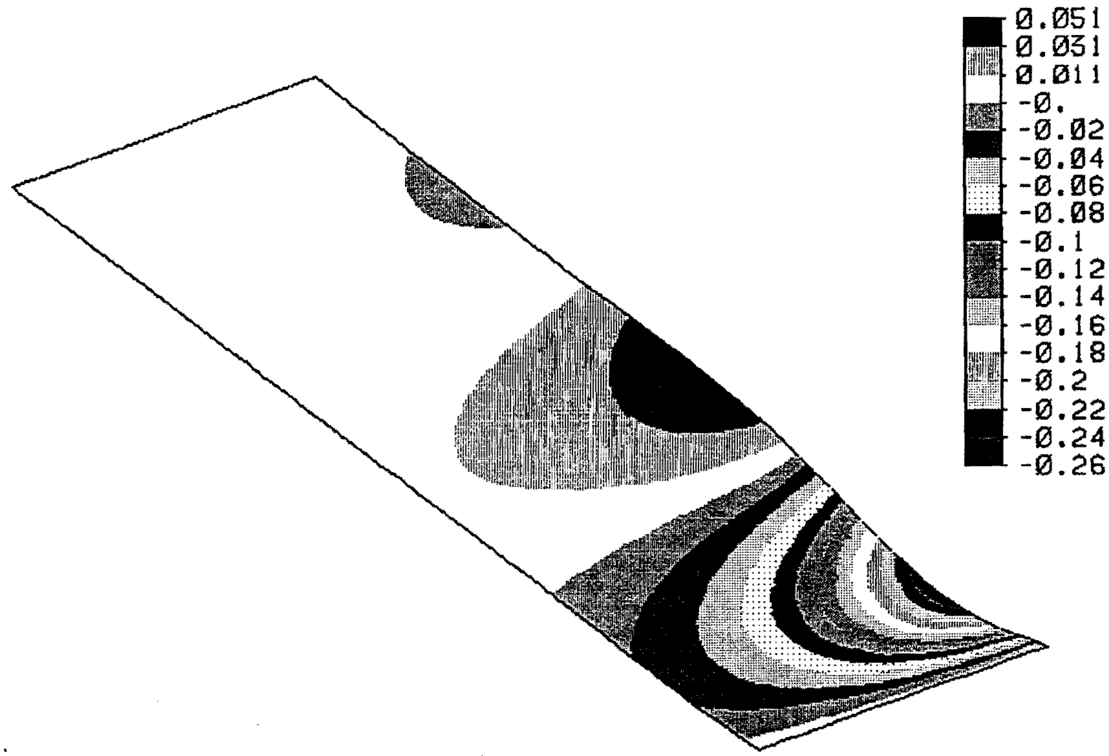

FIG. 60. Differential Vertical Deflection from FEM: Load Case A

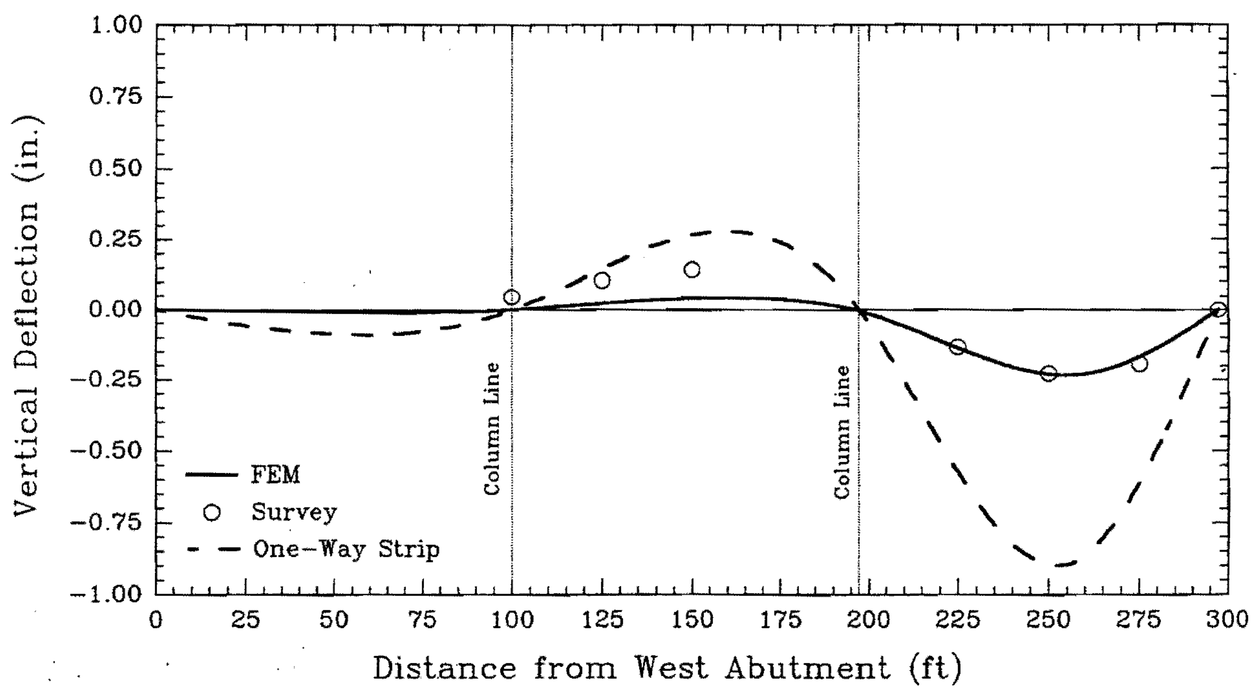

FIG. 61. Differential Vertical Deflection for Longitudinal Section A: Load Case A

In order to check predictions of deflection for a location on the plate that is stiffer than point *A*, the truck is placed at the center of the middle span in position *C* (Fig. 59). Similar to the presentation for the truck at position *A*, an FEM fringe plot of differential vertical deflection, as well as a comparison of differential deflections from the survey, FEM, and one-way design approaches, are shown in Figs. 62 and 63. Fig. 63 is constructed for a longitudinal cross-section that passes through point *C*. Maximum vertical movement recorded by the survey instrument is -0.186 in. (-4.72 mm). This is somewhat larger than the FEM prediction and much less than the -0.65 in. (-16.5 mm) obtained from the unit strip analysis. Refer to Table 5 for comparison of deflections for the remaining load cases.

One of the problems encountered during the truck load testing on the 192nd day was the large effect of thermal heating on measured vertical deflections. As Fig. 39 shows, during the middle part of a hot day, the vertical elevation of an implant changes by as much as 0.10 in. (2.54 mm) per hour. Collection of deflection data for all implants and strain gage readings takes approximately one hour. FEM analysis is conducted with the assumption that the temperature is constant throughout the slab, while gage readings shown in Fig. 45 show a variation of more than 15 °F (8.3 °C) within the top one-half of the slab thickness. This difference causes bending that is not simulated by the FEM or one-way analyses. Also the benchmark location, implant 5, was assumed to remain unmoved although, in reality, it likely had some vertical displacement. The measured deflections due to the truck loads are very small, and the experience of the surveyors and climatic conditions such as wind tend to affect accuracy when measuring such minute deflections. All of these factors contribute to the difficulty of accurate measurement of deflection, since the truck weight and the deflections it induces are small compared to the relatively large self weight and stiffness of the slab. This difficulty was observed during phase one of live load testing and reconfirmed in phase two.

7.3.2 Strain

Strain gages readings are recorded for each position of the truck live loads. Table 7 lists the total strain recorded for truck positions *A-I* and their counterpart FEM prediction. Differential strains are obtained from these values by subtracting the appropriate 192- and 319-day readings (without live load) in Table 6. The magnitudes of these differential strains are so small that they cast doubt on the reliability of the readings from the strain gages since the transducer resolution is questionable for this range of strains. For example, case *A* shows a difference of less than 30 microstrains between the loaded and unloaded states with the 59.4-kip (264-kN) truck.

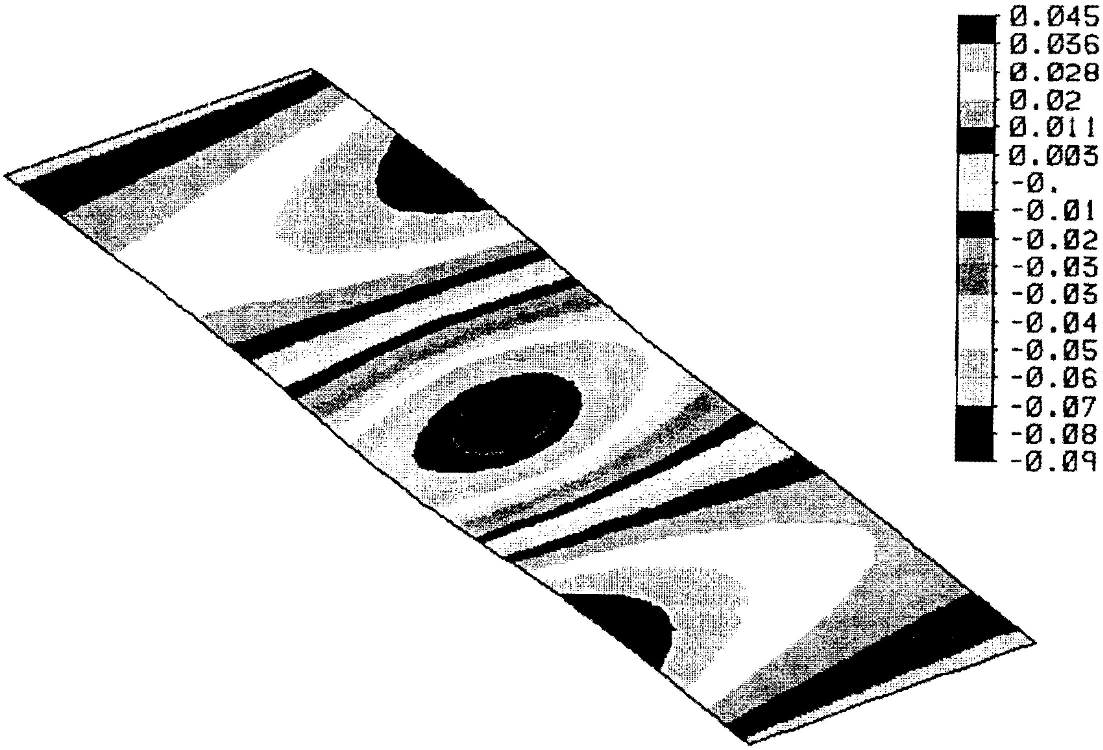

FIG. 62. Differential Deflection from FEM: Load Case C

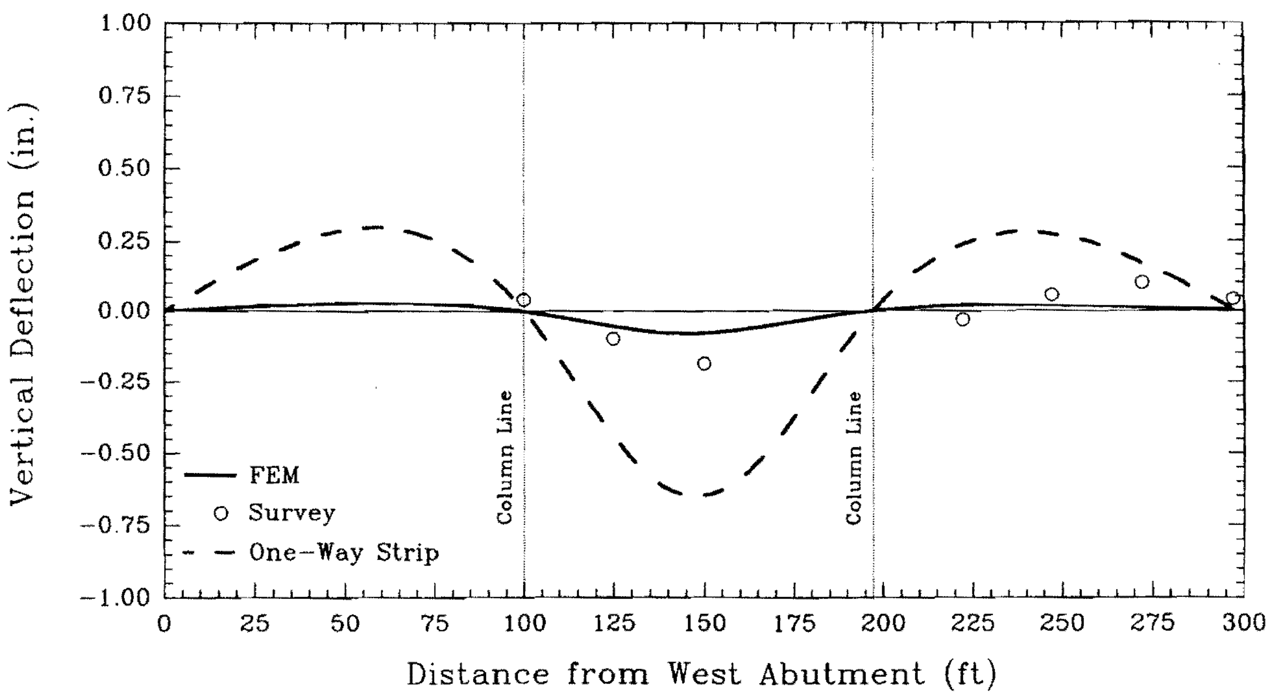

FIG. 63. Differential Deflection for Load Case C

Figs. 64-67 show differential strains for load case *H*. The gray-scale fringe patterns from FEM analysis in Fig. 64 indicate that the bottom layer of the slab undergoes a maximum differential strain in the longitudinal direction of less than 20 microstrains. The small magnitudes of longitudinal strain in the bottom layer are evident in Fig. 65 where strain recorded from gages and predicted by FEM and unit strip analyses are compared along section *C* (see Fig. 24). Strains from the one-way design procedure are calculated by a procedure that is analogous to that described in section 6.3.1 and 7.3.1. Due to long lead wires and poor RS232 connections (see Fig. 28), strain gage data obtained in the ±0-50 microstrain range are scattered and do not correlate well with either the unit strip or FEM predictions. In any case, all gages report changes in strain that are less than ±50 microstrain, which is much less than one-half of the strain predicted by the one-way design procedure. Similar small, but uncorrelated, changes in strain are reported at the top layer of reinforcing steel in Figs. 66 and 67 for the truck at position *H*.

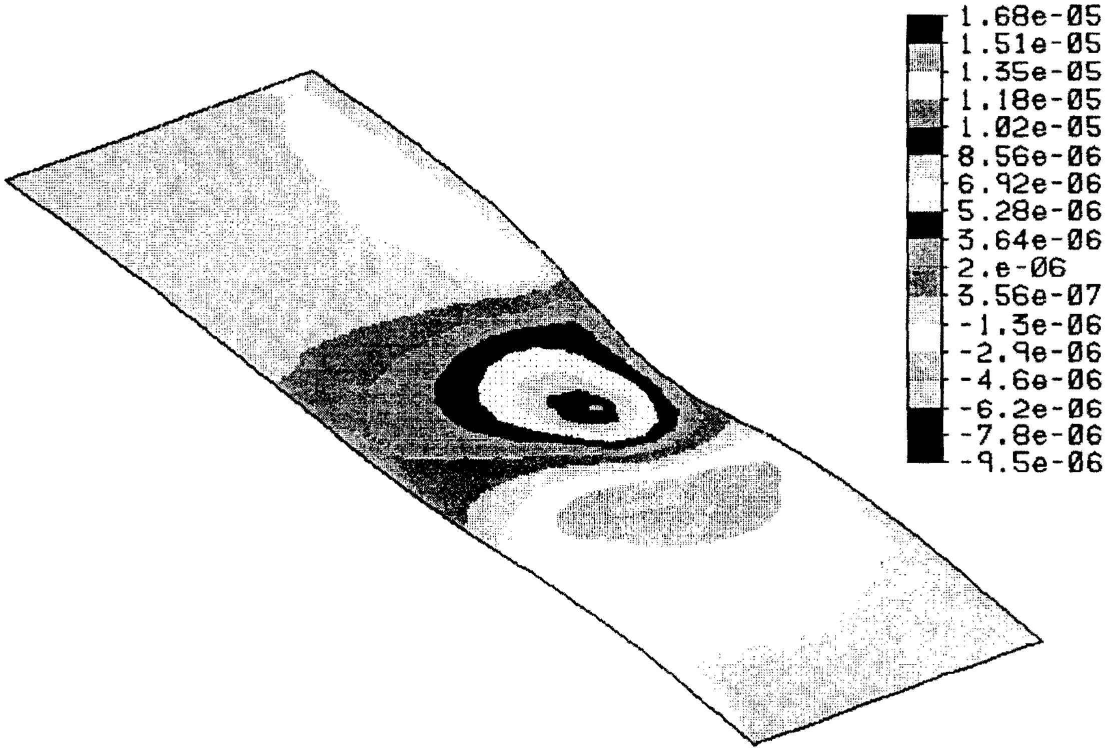

FIG. 64. Differential Bottom Layer Longitudinal Strain: Load Case H

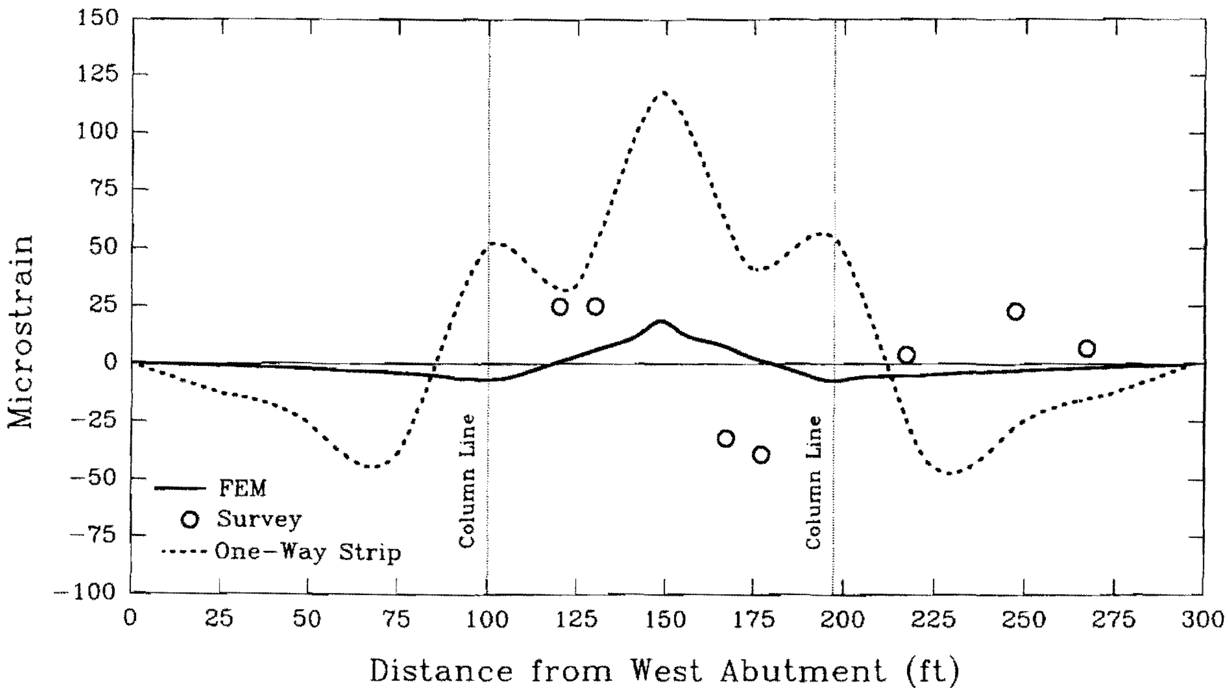

FIG. 65. Bottom Layer Longitudinal Differential Strain Along Section C: Load Case H

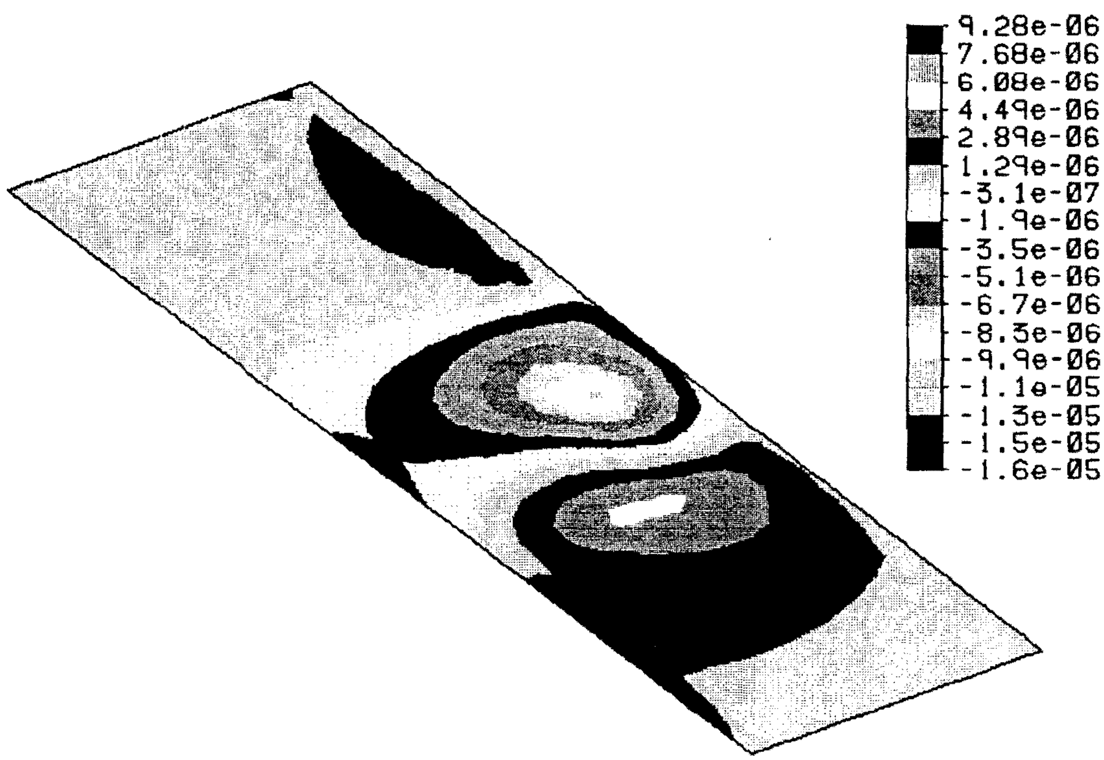

FIG. 66. Differential Top Layer Longitudinal Strain: Load Case H

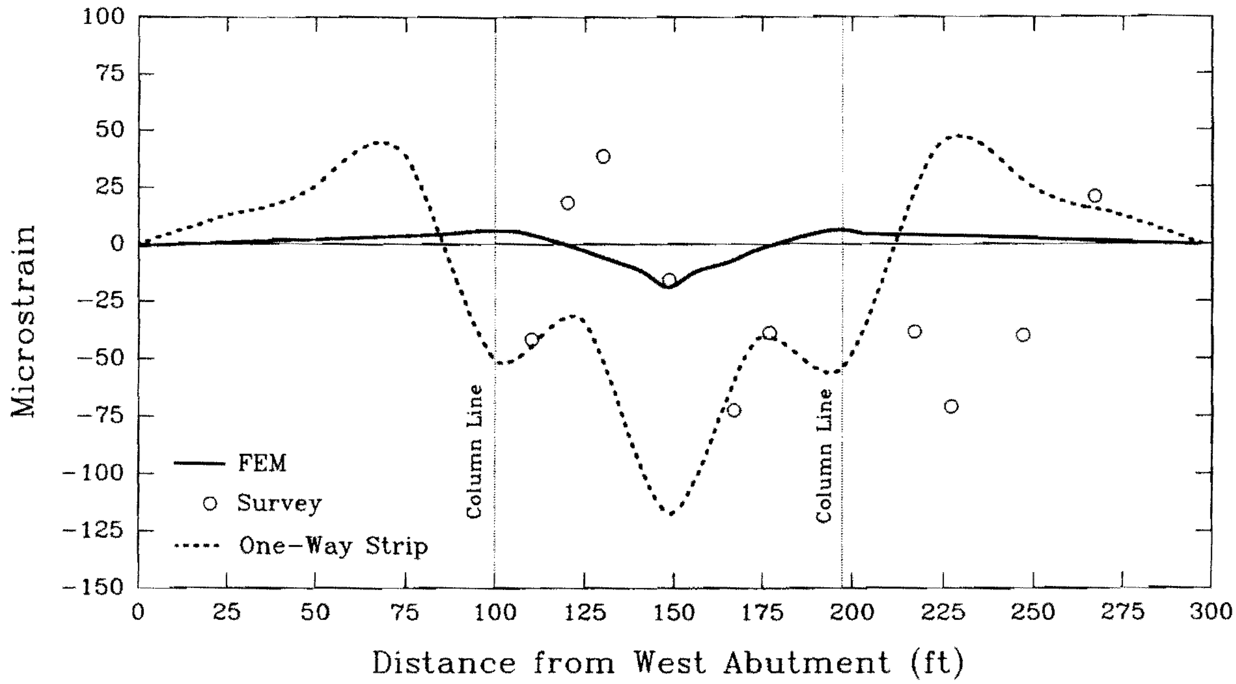

FIG. 67. Top Layer Longitudinal Differential Strain Along Section C: Load Case H

8. CONCLUSION

8.1 SUMMARY

A three-span structure in Wichita Falls, Texas, was monitored during and after construction in order to aid engineers in design of post-tensioned bridges. While longitudinal post-tensioning tendons are uniformly distributed across the roadway, transverse tendons are banded about the column lines. Effects of dead load, creep, shrinkage, and relaxation are measured for approximately 2.5 years. Live truck loads were placed on the bridge at various locations. Arrays of 35 deflection implants, 166 strain gages, and 10 thermal gages provided vertical displacement, in-plane normal strain, and temperature data, respectively. Complementary FEM analyses attempt to predict the response of the structure to time-dependent, thermal, and live loads.

In addition to seasonal variation of ambient temperature, the middle 80% of the slab thickness experiences temperature gradients of up to 15 °F (8.3 °C) due to direct solar heating. Daily heating and cooling cycles cause the middle of each span to rise and fall more than 0.2 in. (5.1 mm). As a result of these cycles, vertical displacement of the center and end spans are in opposite directions.

Vertical deflection measurements at survey points provide a simple, reliable method of measuring displacements in the east and center spans. At 56 days after the average date of concrete pour, the survey data and FEM predictions show upward deflections in excess of 1.0 in. (25.4 mm) in the center and east spans. Influence of skew is evident in both of these methods. On the other hand, the one-way design approach predicts a smaller rise in the center span and a downward deflection of approximately -0.5 in. (-12.7 mm) in the center of the end spans. At 319 days after concrete pour, the FEM and survey data show increasing center span deflection and pronounced skew effects. When monitoring of deflections ceased 2.5 years after construction, the rate of increase at the middle of the center span was small, and the maximum deflection was approaching 2.0 in. (50.8 mm). This value is approximately twice as large as that predicted by the one-way design procedure.

Strain gage transducers placed at the level of reinforcing steel worked well for short- and moderate-term measurements of concrete strains. However, they were not as helpful during tests using truck live loads since their resolution is not fine enough to reliably detect very small strains. Longitudinal normal strains in the top and bottom of the slab as reported by transducers and confirmed by FEM are substantially larger than an extrapolation of the one-way design procedure predicts. At 319 days after pour the slab has nearly 1,000 microstrains of compression, which is three times larger than the final strain predicted by a unit-wide strip analysis.

Normal strains in the skewed transverse direction are also much higher than those predicted by a modification of the one-way design procedure. Averages of strain gage readings from the top and bottom layers are consistently greater than even FEM predicts. Finally, according to FEM each transverse band of tendons imposes approximately 50 microstrains of compression on the concrete over the line of columns.

A number of FEM fringe plots show stresses in the top and bottomost layers of concrete. All values in the longitudinal direction are in compression at 56 and 319 days. However, some transverse stresses are tensile on these same dates. Magnitudes of 150 psi (1.03 MPa) normal stress occur in the top layer of the east and center spans.

Live load testing with heavy trucks was conducted on two separate dates. In both cases the stiffness of the bridge slab was so much greater than the weight of the truck that accurate surveying of the deflection implants and readings of strain gages are in doubt. A 59.4-kip (264-kN) truck placed near the outside edge of the bridge caused a vertical deflection of -0.26 in. (-6.6 mm), which is less than one-third of the deflection predicted by the unit-wide strip analysis. Strain gage readings from these tests were small and scattered.

8.2 Discussion and Recommendations

The current method of data acquisition is appropriate for measuring reasonably large magnitudes of strains (generally, above 100 microstrain) to study long-term behavior of the bridge. However, it is not applicable for measuring very minute magnitudes (less than 50 microstrain). Especially long lead wires appeared to pick up background noise. RS232 connectors sometimes lead to lack of repeatability during connecting and disconnecting. Measuring deflections with a rod level also has drawbacks when recording small deflections caused by the truck live loads. On a windy day it became difficult to make readings with the leveling rod.

The one-way design procedure leads to a conservative design in the longitudinal direction. Two-way action and skew reduce deflection and strain in the bridge compared to those anticipated by the one-way design procedure.

Contribution of passive steel to the longitudinal and transverse bending stiffness is neglected in the one-way design procedure.

Banded post-tensioning in the transverse direction provides sufficient compression in the column regions of the bridge to overcome the Poisson's ratio effect of the longitudinal post-tensioning as well as stresses due to live and time-dependent loads. While FEM and experimental strains that result from these transverse post-tensioning forces vary continuously thoughout the slab, a unit-wide strip approach generally underestimates magnitudes of strains in the transverse direction. For the one-way design procedure, the required prestressing force is based on an assumed area: the greater the assumed area, the higher is the required prestressing force. By necessity of simplicity, the one-way approach also neglects skew of the column lines and non-parallel slab edges along the roadway.

Dead loads play a predominant role in the design of this type of bridge. Use of a solid slab is by choice since TxDOT desires to exploit the benefits of simplicity in construction of this type of structure. Therefore, time-dependent effects related to dead load, such as creep, play an important role in long term behavior. For this reason a decrease in thickness (and thereby overall dead load reduction) could produce a more cost-effective structure. If a thinner slab is contemplated, deflections may govern the design, and careful deflection analysis via FEM would be warranted. Because of a relatively high ratio of span-to-depth, impact and vibrations due to dynamic loads may also require study during the design phase.

The original design of Brook Avenue Overpass is not based on two-way slab action. However, if this action is considered in future designs, ACI (1989) recommends a minimum average prestress of 125 psi (0.86 MPa) for two-way systems. In order to achieve this level of prestress designers may want to consider a combination of transverse tendons that are uniformly distributed along each span and banded tendons that are placed along the column lines. In order to have a minimum average compressive stress in the slab, there should be some limitation on the maximum allowable spacing of tendons in any direction. Since this spacing depends to some extent on the depth of the slab, the current ACI Committee 423's recommendation limiting the tendon spacing to $8h$, where h is the thickness of the slab, may be followed as a first approximation.

Problems encountered by the contractor during construction of the slab over the east column led to complications in modeling behavior of the structure. Longitudinal through-cracks were apparent and especially prevalent in the neighborhood of the construction joints between adjacent pours. Moreover, the addition of an extra 2.0-in. (50.8-mm) concrete overlay added to complications for finite element simulation. Also, the crown that was built into the slab to encourage surface drainage, can not be taken into account by the FEM analyses. In spite of these limitations, measured deflections and strains show reasonably good agreement with results predicted by the FEM analysis.

APPENDIX I. REFERENCES

ACI Committee 435. (1963). "Deflections of prestressed concrete members," *Amer. Conc. Inst. J.*, 60(12), 1697-1728.

ACI-ASCE Committee 343. (1988). "Analysis and design of reinforced concrete bridge structures," *ACI 343R-88*, Detroit, MI.

ACI-ASCE Joint Committee 423. (1974). "Tentative recommendations for prestressed concrete flat plates," *Amer. Conc. Inst. J.*, 71(2), 61-71.

ACI-ASCE Joint Committee 423. (1983). "Recommendations for prestressed concrete flat plates," *Conc. Inter. Desig. & Const.*, 5(7), 61-76.

Algor Interactive Systems, Inc. (1990). "Superview reference manual," Pittsburgh, PA.

American Concrete Institute. (1989). "Building code requirements for reinforced concrete," *ACI 318-89*, Detroit, MI.

Barry, P. H. (1971). *Limit state theory of reinforced concrete*. First Edition, John Wiley, New York, NY.

Bradberry, T. E. (1987). "Bridge design notes for Brook & Harrison Overpass," Texas Department of Transportation, Bridge Division, Austin, TX.

Burns, N. H., and Hemakom, R. (1985). "Test of post-tensioned flat plate with banded tendons," *J. Struct. Engrg.*, ASCE, 111(9), 1899-1915.

Burns, N. H., and Hemakom, R. (1977). "Test of scale model post-tensioned flat plate," *Proceedings*, ASCE, 103(6), 1237-1255.

Burns, N. H., Koust, G. M., and Winter, C. Y. (1985). "Test of a four-panel post-tensioned flat plate," *J. Struct. Engrg.*, ASCE, 111(9), 1916-1929.

Govindaswamy, R. (1990). "Kansas builds first post-tensioned bridge," *Civil Engrg.*, ASCE, 60(2), 20.

Hewlett-Packard Company (1981). "Operating and service manual for Hewlett-Packard Model 44427A, Strain Gage/Bridge Assembly (120 Ohm Gage Option 070)," Manual Part No. 44427-90001, Loveland, CO.

Inoue, M. (1989). "Effects of banded post-tensioning in a prestressed concrete flat slab," thesis presented to Texas A&M Univ., College Station, Texas, in partial fulfillment of the requirements for the degree of Master of Science.

Lacey, G. C., and Breen, J. E. (1975). "The design and optimization of segmentally precast prestressed box girder bridges." Project No. 3-5-69-121, Center for Highway Research, Austin, TX.

Lin, T. Y., and Burns, N. H. (1981). *Design of prestressed concrete structures.* Third Edition, John Wiley and Sons, New York, NY.

Lotus 1-2-3 Manual, Release 2.01. (1986). Lotus Development Corporation, Cambridge, MA.

Lotus Measure Reference Manual. (1986). Lotus Development Corporation, Cambridge, MA.

Mari, A. R., Carrascon, S., and Lopez, A. (1988). "Beam models for nonlinear and time-dependent analysis of curved prestressed box girder bridges," *Trans. Res. Record 1180.*

Microsoft Excel User's Guide, Version 3.0. (1990). Microsoft Corporation, Redmond, WA.

Mindess, S., and Young, F. (1981). *Concrete.* Prentice-Hall, Inc., Englewood Cliffs, NJ.

Nilson, A. H. (1978). *Design of prestressed concrete.* Second Edition, John Wiley, New York, NY.

Panak, J., and Hudson, M. (1972). "A discrete-element method of analysis for orthogonal slab and grid bridge floor systems," *Research Report No. 56-25,* Center for Highway Research, Austin, TX.

PATRAN Plus User's Guide. (1988). PDA Engineering, Santa Ana, CA.

Post-tensioning manual. (1985). Fourth Ed., Post-Tensioning Institute, Phoenix, AZ, 149-160, 303-304.

Roschke, P. N., and Inoue, M. (1990), "Effects of banded post-tensioning in a prestressed concrete flat slab," *Report No. 1182-1*, Texas Transportation Institute, Texas A&M Univ., College Station, TX.

Roschke, P. N., Pruski, K. R., and Smith, C. D. (1992). "Experimental and analytical study of a two-span post-tensioned bridge slab," *Report No. 1182-2*, Texas Transportation Institute, Texas A&M Univ., College Station, TX.

Roschke, P. N., and Pruski, K. R. (1992). "Graphically oriented analysis of post-tensioned bridges on microcomputers," *Report No. 1182-4F*, Texas Transportation Institute, Texas A&M Univ., College Station, TX.

Scordelis, A. C., Bouwkamp, J. G., Wasti, S. T., and Anicic, D. (1980). "Structural behavior of a skew two span reinforced concrete box girder bridge model," *UC-SESM Report No. 80-1*, College of Engineering, Office of Research Services, Univ. of California, Berkeley, CA.

Scordelis, A. C., Elfgren, L. G., and Larsen, P. K. (1979). "Time-dependent behavior of concrete box girder bridges," *Amer. Conc. Inst. J.*, 76(1), 159-179.

Scordelis, A. C., Lin, T. Y., and Itaya, R. (1959). "Behavior of continuous slab prestressed in two directions," *Amer. Conc. Inst. J.*, 56(6), 441-460.

Standard Specifications for Construction of Highways, Streets and Bridges (1982). Texas State Department of Highways and Public Transportation, Austin, TX.

Standard Specifications for Highway Bridges (1989), *Fourteenth Edition*. American Association of State Highway and Transportation Officials, Washington, DC.

Steger, N. R. (1989). TxDOT field notes. Wichita Falls, TX.

van Greunen, J. (1979). "Nonlinear geometric, material and time dependent analysis of reinforced and prestressed concrete slab and panels," *Report No. UC SESM 79-3*, Dept. of Civ. Engrg., Univ. of California, Berkeley, CA.

Timoshenko, S. P., and Goodier, J. N. (1951). *Theory of elasticity*. Second Edition, McGraw-Hill, New York, NY.

Wanders, S. P., Winslow, D. A., and Sutton, C. D. (1979). "Study of the segmental box girder bridge at Turkey Run: construction, instrumentation, and data collection," *Report No. JHRP-79-25*, School of Civ. Engrn., Purdue University, West Lafayette, IN.

Winter, G., and Nilson, A. H., (1972). *Design of concrete structures*. Eighth Edition, McGraw-Hill, New York, NY.

Zia, P., Preston, H. K., and Scott, N. L. (1979). "Estimating prestress losses," *Conc. Int. Des. & Con.*, 1(6), 43-75.

APPENDIX II. NOTATION

A	= Cross-sectional area of concrete member;
AASHTO	= American Association of State Highway and Transportation Officials;
ACI	= American Concrete Institute;
D	= Width of post-tensioning band;
E	= Elastic modulus of concrete;
f_c	= Compressive strength of concrete;
G_f	= Gage factor;
HP-3497A	= Hewlett Packard data acquisition unit;
I	= Moment of inertia;
k	= Material stiffness;
L	= Bearing pad thickness;
L_c	= Length of column;
M_d	= Moment due to dead and live load;
M_p	= Moment due to prestressing force;
MTS	= Mechanical Testing System;
P	= Reaction from concrete column;
P_e	= Total prestressing force;
Slab49	= Slab program used by TxDOT engineers;
TxDOT	= Texas Department of Transportation;
V_{ex}	= Excitation voltage;
V_{ini}	= Initial voltage;
V_{out}	= Final voltage;
V_r	= Strain gage voltage;
T	= Predicted temperature;
V	= Sensor voltage;
W	= Width of slab;
y	= Distance from the neutral axis;
Δ	= Deflection;
ε	= Measured strain in the material in microstrain;
σ	= Normal stress.

APPENDIX III. DEFLECTION DATA FROM SURVEY IMPLANTS

TABLE 4. Vertical Deflection of Implants in Top Deck of Slab

Implant	Days after Pouring of Concrete						
	30	56	102	136	193	231	294
(1)	(2)	(3)	(4)	(5)	(6)	(7)	(8)
1	0.000	-0.060	-0.180	-0.108	-0.072	-0.156	-0.156
2	0.000	0.000	-0.012	-0.024	0.012	-0.012	-0.120
3	0.000	0.024	0.012	0.024	0.024	0.012	0.000
4	0.000	0.012	0.000	0.012	0.024	0.000	-0.024
5	0.000	0.000	0.000	0.000	0.000	0.000	0.000
6	0.000	0.840	0.780	0.888	0.792	0.852	0.828
7	0.000	0.864	0.780	0.948	0.780	0.876	0.780
8	0.000	0.828	0.732	0.912	0.720	0.840	0.768
9	0.000	0.744	0.612	0.780	0.624	0.720	0.660
10	0.000	0.540	0.492	0.552	0.480	0.588	0.528
11	0.000	1.080	1.032	1.128	1.032	1.152	1.104
12	0.000	0.996	0.912	1.080	0.876	1.044	0.936
13	0.000	0.888	0.780	0.948	0.732	0.924	0.816
14	0.000	0.648	0.552	0.720	0.540	0.696	0.600
15	0.000	0.432	0.396	0.420	0.372	0.480	0.420
16	0.000	0.564	0.528	0.600	0.564	0.660	0.612
17	0.000	0.432	0.348	0.468	0.336	0.480	0.396
18	0.000	0.312	0.204	0.324	0.180	0.360	0.264
19	0.000	0.156	0.084	0.168	0.072	0.228	0.132
20	0.000	-0.060	-0.096	-0.108	-0.084	-0.024	-0.084
21	0.000	1.068	1.356	1.308	1.632	1.632	1.740
22	0.000	1.188	1.368	1.452	1.632	1.680	1.788
23	0.000	1.236	1.404	1.524	1.656	1.728	1.812
24	0.000	1.212	1.392	1.476	1.668	1.680	1.776
25	0.000	1.152	1.380	1.392	1.632	1.632	1.740
26	0.000	0.864	1.068	1.080	1.308	1.296	1.404
27	0.000	0.840	0.960	1.044	1.176	1.200	1.272
28	0.000	0.816	0.912	0.996	1.104	1.092	1.200
29	0.000	0.708	0.816	0.864	1.008	0.984	1.056
30	0.000	0.540	0.660	0.648	0.852	0.780	0.864
31	0.000	-0.048	-0.024	-0.024	0.072	0.024	0.048
32	0.000	0.000	0.000	0.000	0.000	0.000	0.000
33	0.000	0.000	-0.024	0.000	0.036	0.000	0.024
34	0.000	-0.036	-0.036	-0.036	0.000	-0.048	-0.024
35	0.000	-0.096	-0.108	-0.096	-0.060	-0.120	-0.096

Note: units = inches

TABLE 4. Vertical Deflection of Implants in Top Deck of Slab (Cont.)

	Days after Pouring of Concrete						
Implant (1)	319 (2)	320 (3)	400 (4)	472 (5)	591 (6)	681 (7)	878 (8)
1	-0.192	-0.204	-0.120	-0.072	-0.060	-0.048	-0.084
2	-0.180	-0.180	-0.072	-0.144	-0.144	-0.132	-0.096
3	-0.060	-0.060	-0.036	-0.096	-0.072	-0.048	-0.048
4	-0.060	-0.024	-0.012	-0.084	-0.012	0.024	0.048
5	0.000	0.000	0.000	0.000	0.000	0.000	0.000
6	0.792	0.708	0.912	0.756	0.720	0.792	0.852
7	0.792	0.660	0.864	0.816	0.732	0.792	0.888
8	0.780	0.672	0.852	0.732	0.708	0.780	0.876
9	0.612	0.588	0.744	0.684	0.600	0.696	0.720
10	0.540	0.528	0.588	0.516	0.456	0.528	0.492
11	1.116	1.008	1.164	1.056	0.984	1.032	1.092
12	0.984	0.864	1.068	0.972	0.876	0.936	1.056
13	0.864	0.744	0.912	0.900	0.744	0.816	0.888
14	0.660	0.600	0.684	0.600	0.504	0.600	0.636
15	0.468	0.456	0.444	0.408	0.324	0.372	0.336
16	0.636	0.552	0.564	0.516	0.456	0.468	0.552
17	0.444	0.336	0.396	0.396	0.324	0.348	0.456
18	0.312	0.252	0.252	0.312	0.192	0.216	0.300
19	0.168	0.192	0.120	0.108	0.036	0.084	0.060
20	-0.036	0.012	-0.132	-0.132	-0.180	-0.156	-0.240
21	1.740	1.836	1.668	1.608	1.692	1.716	1.692
22	1.812	1.836	1.740	1.812	1.764	1.800	1.800
23	1.836	1.884	1.800	1.836	1.848	1.896	1.932
24	1.788	1.860	1.764	1.800	1.788	1.860	1.860
25	1.752	1.872	1.704	1.728	1.728	1.752	1.752
26	1.380	1.428	1.356	1.464	1.392	1.416	1.380
27	1.272	1.320	1.236	1.248	1.260	1.308	1.344
28	1.188	1.236	1.212	1.224	1.248	1.260	1.308
29	1.056	1.140	1.068	1.056	1.128	1.152	1.188
30	0.864	0.972	0.852	0.876	0.924	0.924	0.912
31	0.000	0.012	0.024	0.072	0.072	0.060	0.096
32	0.000	0.000	0.000	-0.048	0.000	0.000	0.000
33	-0.012	0.036	0.036	0.096	0.060	0.048	0.084
34	-0.048	-0.012	-0.012	0.108	0.012	0.036	0.024
35	-0.144	-0.108	-0.084	-0.108	-0.048	-0.048	-0.024

Note: units = inches

TABLE 5. Survey Results and FEM Predictions for Implant Deflections Caused by Truck Loads

Implant Number (1)	Position of Truck					
	A		B		C	
	Survey (2)	FEM (3)	Survey (4)	FEM (5)	Survey (6)	FEM (7)
1	-0.11	-0.03	-0.04	-0.03	-0.11	-0.03
2	-0.04	-0.03	0.01	-0.03	-0.02	-0.03
3	-0.04	-0.03	0.02	-0.03	-0.02	-0.03
4	-0.02	-0.03	-0.01	-0.03	-0.02	-0.03
5	-0.02	-0.02	-0.02	-0.02	-0.02	-0.02
6	0.64	1.05	0.92	1.24	0.83	1.25
7	0.67	1.02	0.98	1.16	0.92	1.17
8	0.69	0.95	0.95	1.03	0.88	1.05
9	0.59	0.79	0.81	0.84	0.75	0.86
10	0.47	0.59	0.56	0.62	0.55	0.65
11	0.82	1.39	1.16	1.62	1.05	1.65
12	0.79	1.18	1.12	1.33	1.05	1.36
13	0.71	0.92	0.97	1.01	0.92	1.04
14	0.52	0.57	0.70	0.62	0.65	0.66
15	0.32	0.15	0.41	0.18	0.38	0.23
16	0.40	0.71	0.61	0.84	0.53	0.85
17	0.27	0.40	0.47	0.47	0.41	0.50
18	0.16	0.11	0.29	0.15	0.28	0.18
19	0.04	-0.19	0.11	-0.17	0.09	-0.14
20	-0.16	-0.51	-0.13	-0.50	-0.19	-0.46
21	1.53	1.42	1.39	1.39	1.39	1.33
22	1.58	1.63	1.54	1.61	1.54	1.53
23	1.64	1.73	1.59	1.73	1.65	1.62
24	1.60	1.71	1.58	1.72	1.58	1.61
25	1.57	1.58	1.47	1.60	1.53	1.49
26	1.23	1.24	1.16	1.22	1.12	1.17
27	1.13	1.16	1.16	1.16	1.13	1.09
28	1.07	1.05	1.11	1.05	1.09	0.98
29	0.98	0.89	0.98	0.90	0.97	0.83
30	0.79	0.61	0.75	0.64	0.75	0.56
31	0.04	-0.16	0.09	-0.16	-0.01	-0.16
32	-0.02	-0.09	-0.02	-0.09	-0.02	-0.09
33	0.05	-0.09	0.00	-0.09	0.03	-0.09
34	0.02	-0.07	0.10	-0.07	0.03	-0.07
35	-0.03	-0.06	0.03	-0.07	-0.05	-0.06

Note: units = inches

TABLE 5. Survey Results and FEM Predictions for Implant Deflections Caused by Truck Loads (Cont.)

Implant Number (1)	Position of Truck: F Survey (2)	F FEM (3)	G Survey (4)	G FEM (5)	H Survey (6)	H FEM (7)	I Survey (8)	I FEM (9)
1	-0.17	-0.03	-0.17	-0.03	-0.17	-0.03	-0.13	-0.03
2	-0.15	-0.03	-0.13	-0.03	-0.13	-0.03	-0.09	-0.03
3	-0.04	-0.03	-0.04	-0.03	-0.03	-0.03	-0.01	-0.03
4	-0.04	-0.03	-0.16	-0.03	-0.04	-0.03	-0.03	-0.03
5	-0.02	-0.02	-0.02	-0.02	-0.02	-0.02	-0.02	-0.02
6	0.82	1.23	0.82	1.22	0.82	1.24	0.88	1.19
7	0.81	1.18	0.82	1.16	0.85	1.18	0.41	1.13
8	0.83	1.06	0.83	1.05	0.85	1.07	0.92	0.99
9	0.70	0.87	0.71	0.86	0.68	0.88	0.76	0.77
10	0.55	0.64	0.55	0.64	0.44	0.65	0.58	0.52
11	1.15	1.63	1.15	1.61	1.12	1.64	1.21	1.57
12	1.05	1.37	1.05	1.35	1.03	1.38	1.12	1.29
13	0.91	1.05	0.91	1.03	0.89	1.06	0.98	0.95
14	0.68	0.66	0.68	0.64	0.63	0.67	0.71	0.54
15	0.45	0.20	0.46	0.19	0.32	0.22	0.45	0.07
16	0.63	0.85	0.64	0.84	0.63	0.86	0.65	0.80
17	0.46	0.51	0.46	0.50	0.46	0.52	0.51	0.46
18	0.32	0.18	0.34	0.17	0.31	0.20	0.34	0.12
19	0.19	-0.16	0.20	-0.16	0.15	-0.14	0.19	-0.22
20	-0.04	-0.49	-0.05	-0.49	-0.11	-0.48	-0.13	-0.56
21	1.65	1.24	1.66	1.33	1.69	1.23	1.53	1.37
22	1.75	1.54	1.77	1.60	1.79	1.51	1.63	1.64
23	1.79	1.70	1.82	1.72	1.85	1.67	1.72	1.77
24	1.75	1.67	1.75	1.65	1.78	1.65	1.72	1.72
25	1.70	1.50	1.66	1.43	1.71	1.48	1.64	1.54
26	1.30	1.07	1.31	1.17	1.34	1.10	1.25	1.20
27	1.23	1.12	1.24	1.16	1.25	1.12	1.23	1.19
28	1.16	1.03	1.16	1.03	1.19	1.02	1.16	1.07
29	1.04	0.85	1.00	0.82	1.15	0.84	1.01	0.88
30	0.82	0.55	0.76	0.48	0.81	0.55	0.79	0.57
31	0.02	-0.16	0.02	-0.16	0.02	-0.16	0.05	-0.16
32	-0.02	-0.09	-0.02	-0.09	-0.02	-0.09	-0.02	-0.09
33	0.02	-0.09	0.01	-0.09	0.01	-0.09	0.08	-0.09
34	-0.01	-0.07	-0.02	-0.07	-0.02	-0.07	-0.01	-0.07
35	-0.11	-0.06	-0.11	-0.06	-0.11	-0.06	-0.09	-0.06

Note: units = microstrain

Appendix IV. Strain Gage Data

TABLE 6. Experimental Gage Readings and FEM Predictions for Time-Dependent Strains

Gage	Days after Pouring of Concrete													
	56		71		103		135		192		231		319	
Number	Gage	FEM	Gage	FEM	Gage	FEM	Gage	FEM	Gage	FEM	Gage	FEM	Gage	FEM
(1)	(2)	(3)	(4)	(5)	(6)	(7)	(8)	(9)	(10)	(11)	(12)	(13)	(14)	(15)
1	30	-134	-87	-165	-77	-172	-106	-191	-11	-268	84	-285	-94	-200
2	22	-64	10	-75	12	-82	51	-103	-221	-138	-161	-178	-206	-161
3	-31	-56	-11	-56	-66	-61	-72	-79	-134	-124	-150	-145	-182	-122
4	*	-44	*	-49	*	-52	*	-68	*	-101	*	-123	*	-94
5	*	-52	*	-63	*	-64	*	-77	*	-100	*	-124	*	-97
6	-95	-78	-171	-95	-216	-96	-239	-108	-372	-115	-308	-161	-357	-123
7	-85	-137	-150	-157	-193	-161	-145	-174	-320	-201	-296	-249	-289	-147
8	*	-193	-103	-95	*	-96	*	-108	*	-277	*	-161	*	-159
9	-109	-262	-172	-193	-224	-200	-210	-217	-342	-367	-300	-315	-401	-189
10	*	-203	-90	-151	*	-160	*	-180	*	-382	*	-280	*	-195
11	-51	-120	-76	-89	112	-96	508	-118	-233	-251	-176	-202	-248	-199
12	-51	-66	-97	-89	-106	-96	-130	-118	-434	-160	-387	-202	-322	-167
13	-18	-53	-62	-58	-46	-64	-116	-84	-166	-123	-135	-149	-92	-132
14	68	-49	-11	-43	-49	-46	-56	-62	-163	-110	-138	-110	-141	-92
15	-47	-92	-168	-157	-179	-161	-145	-174	-341	-450	-235	-249	-269	-114
16	-188	-211	-229	-269	-344	-297	-335	-346	-607	-194	-574	-517	-496	-423
17	-151	-135	-162	-193	-223	-200	-190	-217	-349	-362	-307	-315	-334	-167
18	-73	-191	-117	-253	61	-277	187	-321	297	-236	447	-484	594	-395
19	-116	-94	-193	-151	-215	-160	-242	-180	-316	-384	-291	-280	-251	-168
20	-160	-180	-185	-223	-276	-244	-254	-282	-436	-194	-412	-439	-498	-374
21	-37	-94	-62	-120	-152	-126	-131	-144	-243	-214	-253	-224	-298	-168
22	*	-300	*	-275	*	-299	*	-341	*	-492	*	-525	*	-550
23	21	-99	-24	-80	-98	-87	-82	-109	-236	-177	-186	-191	-240	-196
24	-301	-444	-306	-347	-409	-375	-398	-421	-705	-647	-691	-657	-703	-739
25	45	-90	-14	-69	-81	-75	-66	-96	-240	-155	-191	-173	-254	-183
26	-300	-548	-460	-424	-545	-456	-505	-507	-761	-765	-751	-793	-772	-875
27	27	-89	-28	-65	-83	-69	-83	-87	-206	-142	-179	-157	-212	-156
28	-352	-549	-395	-440	-524	-472	-493	-523	-803	-794	-868	-812	-861	-839
29	59	-89	-32	-69	-146	-72	-98	-86	*	-136	*	-146	87	-130
30	-338	-429	-339	-386	-456	-414	-440	-461	-723	-669	-679	-707	-693	-677
31	-29	-86	-70	-82	-109	-84	-88	-97	-203	-143	-162	-153	-229	-119
32	-206	-318	-83	-322	-143	-349	35	-394	-644	-589	-654	-604	-585	-535
33	-41	-68	-5	-60	-70	-66	-56	-86	-180	-156	-145	-158	-230	-154
34	-173	-301	-180	-280	-250	-303	-216	-343	-364	-562	-377	-533	-374	-516
35	55	-57	-13	-48	-69	-52	-63	-70	-163	-127	-123	-126	-174	-127
36	-111	-416	-186	-364	-245	-393	-67	-439	216	-678	*	-676	*	-681
37	61	-63	0	-44	-48	-48	-46	-63	-118	-118	-185	-116	-214	-117
38	-363	-545	-385	-423	-510	-454	-485	-503	-795	-792	-802	-778	-767	-837

Note: units = microstrain; *Bad gage

TABLE 6. Experimental Gage Readings and FEM Predictions for Time-Dependent Strains (Cont.)

Gage Number	Days after Pouring of Concrete													
	56		71		103		135		192		231		319	
	Gage	FEM	Gage	FEM	Gage	FEM	Gage	FEM	Gage	FEM	Gage	FEM	Gage	FEM
(1)	(2)	(3)	(4)	(5)	(6)	(7)	(8)	(9)	(10)	(11)	(12)	(13)	(14)	(15)
39	-17	-62	-7	-44	-80	-47	-65	-63	-187	-116	-319	-115	33	-118
40	-426	-554	-447	-433	-529	-464	-561	-512	-573	-778	-644	-776	-496	-828
41	-80	-77	-94	-124	-144	-128	-131	-142	-307	-169	-226	-210	-267	-126
42	*	-205	*	-269	*	-297	*	-346	*	-409	*	-517	*	-390
43	*	-97	-98	-136	*	-141	*	-157	*	-158	*	-237	*	-161
44	*	-193	*	-253	*	-277	*	-321	*	-332	*	-484	*	-361
45	-69	-76	-61	-108	-145	-114	-120	-132	-286	-144	-290	-216	-252	-135
46	-109	-565	-194	-223	-264	-244	-281	-282	-457	-352	-422	-439	-499	-891
47	-7	-107	-52	-84	-119	-91	-105	-109	-248	-166	-239	-188	-209	-181
48	-411	-565	-408	-459	-560	-493	-518	-546	-810	-823	-892	-855	-866	-891
49	-27	-104	-56	-90	-122	-95	-83	-111	-211	-163	-180	-182	-249	-162
50	-352	-455	-363	-407	-491	-439	-475	-490	-805	-701	-810	-757	-773	-735
51	-40	-90	-78	-90	-102	-94	-85	-110	-237	-170	-247	-177	-222	-144
52	-250	-323	-276	-327	-389	-354	-381	-401	-661	-607	-600	-613	-658	-550
53	-9	-73	-87	-92	-135	-96	-139	-113	-18	-178	8	-178	-124	-133
54	-175	-215	-219	-252	-320	-275	-298	-316	-526	-417	-531	-472	-461	-394
55	0	-116	-69	-95	-123	-99	-93	-117	-236	-189	-203	-184	-189	-177
56	-175	-231	-147	-242	-235	-264	-216	-304	-520	-336	-450	-454	-486	-380
57	-44	-65	-49	-78	-104	-82	-91	-98	-172	-169	-179	-162	-255	-122
58	-250	-165	-251	-217	-348	-238	-291	-276	-490	-364	*	-426	-149	-335
59	-33	-70	-25	-61	-73	-66	-62	-85	-146	-162	-221	-150	-174	-130
60	-225	-270	-235	-268	-325	-290	-322	-329	-590	-541	-511	-504	-507	-463
61	33	-73	-4	-56	-68	-62	-67	-81	-172	-142	-174	-144	-155	-140
62	-294	-377	-321	-354	-413	-382	-418	-427	-724	-666	-661	-649	-710	-609
63	-79	-70	-78	-51	-120	-54	-92	-71	91	-126	111	-127	-118	-123
64	-340	-533	-402	-426	-449	-458	-420	-507	-762	-802	-808	-786	-816	-825
65	51	-68	-16	-50	-72	-54	-59	-70	-157	-124	-136	-123	-157	-120
66	-313	-561	-409	-444	-539	-476	-510	-527	-843	-798	-766	-805	-766	-852
67	-221	-354	-299	-332	-406	-360	-399	-406	-700	-620	-648	-622	-651	-601
68	-201	-216	-232	-255	-329	-277	-282	-318	-568	-409	-281	-476	*	-403
69	-142	-109	-215	-245	-292	-267	-283	-307	-465	-332	-473	-457	-475	-109
70	-129	-169	-132	-219	-173	-239	-72	-277	-123	-352	-2	-426	2	-332
71	-212	-247	-117	-262	-106	-284	-23	-323	-575	-516	-516	-492	-518	-429
72	-141	-150	-174	-159	-184	-163	-250	-176	-260	-152	-296	-250	-256	-154
73	-44	-60	1	-62	-79	-63	-60	-75	-184	-181	-134	-121	-158	-101
74	-3	-52	-15	-49	-63	-51	-65	-66	-119	-199	-191	-119	-183	-98
75	-19	-57	-21	-56	-61	-61	-49	-79	-159	-199	-216	-143	-179	-113
76	-83	-62	-158	-75	-136	-82	-178	-103	-308	-195	-260	-177	-200	-144
77	-83	-129	-174	-166	-203	-172	-177	-189	-364	-157	-326	-279	-302	-183
78	-128	-270	-168	-196	-236	-201	-184	-214	-377	-139	-314	-298	-339	-162
79	24	-142	-37	-149	17	-151	10	-161	100	-130	477	-222	790	-119
80	-1	-47	-8	-50	-69	-49	-58	-60	-120	-158	-169	-94	-171	-79

Note: units = microstrain; *Bad gage

TABLE 6. Experimental Gage Readings and FEM Predictions for Time-Dependent Strains (Cont.)

Gage	Days after Pouring of Concrete													
	56		71		103		135		192		231		319	
Number	Gage	FEM	Gage	FEM	Gage	FEM	Gage	FEM	Gage	FEM	Gage	FEM	Gage	FEM
(1)	(2)	(3)	(4)	(5)	(6)	(7)	(8)	(9)	(10)	(11)	(12)	(13)	(14)	(15)
81	6	-36	4	-36	-60	-37	-37	-50	-89	-158	-121	-92	-142	-69
82	-66	-105	-138	-139	-138	-146	-186	-164	-229	-247	-410	-265	-428	-177
83	31	-22	-5	-38	-59	-43	-38	-60	-186	-83	-123	-114	-171	-62
84	55	-7	9	-12	-37	-14	-8	-28	-154	-69	-74	-62	-100	-26
85	-2	-29	14	-24	-33	-24	-21	-36	-61	-77	-86	-69	-78	-41
86	26	-54	-21	-54	-55	-53	-52	-62	-106	-83	-93	-104	-210	-60
87	-34	-90	-101	-96	-137	-95	-212	-104	-161	-107	-229	-165	-183	-89
88	-86	-151	-148	-149	-159	-150	-155	-160	-293	-222	-289	-248	-281	-134
89	3	-182	-95	-96	-115	-95	-94	-104	-216	-294	-170	-165	-189	-171
90	-136	-191	-140	-173	-205	-177	-179	-191	-292	-369	-355	-295	-360	-222
91	-36	-175	-96	-149	-176	-155	-148	-172	-300	-373	-268	-274	-346	-213
92	20	-105	-49	-93	-108	-99	-98	-118	-192	-246	-262	-201	-207	-152
93	7	-49	-63	-93	*	-99	*	-118	*	-120	*	-201	*	-84
94	30	-28	-117	-48	-99	-53	-12	-71	-170	-89	-147	-135	-219	-54
95	-84	-13	-103	-20	-132	-23	-107	-39	*	-76	*	-87	*	-33
96	-164	-135	-273	-157	-262	-161	-282	-174	-519	-450	*	-249	*	-179
97	-421	-540	-429	-506	-596	-548	-606	-614	-903	-242	-927	-955	-889	-891
98	-129	-185	-142	-173	-217	-177	-165	-191	-370	-907	-317	-295	-302	-205
99	-329	-525	-415	-472	-552	-510	-567	-570	-899	-321	-930	-884	-876	-817
100	-128	-153	-87	-149	-187	-155	-170	-172	-285	-811	-352	-274	-288	-187
101	-359	-524	-417	-445	-533	-477	-515	-529	-782	-264	-834	-810	-811	-780
102	-61	-136	-79	-129	-157	-135	-151	-152	-267	-250	-284	-233	-257	-164
103	-302	-416	-320	-365	-425	-392	-420	-437	-718	-579	-722	-663	-727	-621
104	33	-59	-27	-57	-75	-62	-54	-81	-157	-140	-186	-145	-235	-103
105	-241	-311	-297	-282	-297	-302	-343	-339	-653	-438	-411	-508	-274	-507
106	18	-4	7	-15	-40	-18	-5	-34	-145	-79	-104	-73	-162	-39
107	-98	-235	-196	-219	-267	-237	-259	-271	-489	-344	-431	-400	-400	-430
108	83	12	19	-5	-11	-6	-4	-18	-106	-46	-71	-44	-129	6
109	-93	-213	-196	-220	-283	-239	-264	-275	-449	-363	-453	-411	-431	-399
110	29	-21	5	-23	-32	-22	-27	-33	-95	-62	-61	-63	-125	-22
111	-124	-320	-174	-310	-160	-336	-223	-380	-196	-555	-37	-583	*	-546
112	-5	-67	-33	-64	-77	-64	-56	-74	-182	-95	-168	-124	-161	-79
113	-370	-417	-200	-420	-140	-454	-63	-507	-796	-708	-838	-781	-785	-701
114	9	-78	-42	-70	-104	-76	-93	-96	-215	-149	-167	-173	-253	-134
115	-306	-453	-356	-388	-466	-415	-440	-460	-750	-601	-670	-694	-733	-700
116	-29	-27	-62	-28	-68	-32	-41	-49	*	-95	*	-106	*	-70
117	-267	-376	*	-320	*	-344	*	-386	-590	-519	-619	-583	-642	-608
118	47	10	8	-11	-24	-14	-1	-29	-122	-61	-108	-73	-107	-14
119	-21	-279	-149	-271	-192	-294	-184	-335	*	-453	*	-518	*	-494
120	98	9	-10	-13	61	-15	22	-30	*	-63	*	-72	*	-14
121	-210	-268	-237	-265	-341	-289	-309	-330	-549	-484	-508	-536	-521	-484
122	-86	-131	-125	-134	-170	-137	-149	-151	-281	-204	-231	-235	-244	-167

Note: units = microstrain; *Bad gage

TABLE 6. Experimental Gage Readings and FEM Predictions for Time-Dependent Strains (Cont.)

Gage	Days after Pouring of Concrete													
	56		71		103		135		192		231		319	
Number	Gage	FEM	Gage	FEM	Gage	FEM	Gage	FEM	Gage	FEM	Gage	FEM	Gage	FEM
(1)	(2)	(3)	(4)	(5)	(6)	(7)	(8)	(9)	(10)	(11)	(12)	(13)	(14)	(15)
123	-426	-507	-428	-506	-606	-548	-612	-614	-963	-787	-935	-955	-956	-825
124	-53	-146	-117	-147	-169	-151	-155	-166	-245	-237	-235	-252	-254	-174
125	-342	-501	-400	-472	-549	-510	-539	-570	-915	-844	-927	-884	-862	-783
126	-105	-144	-101	-141	-183	-146	-161	-163	-244	-234	-279	-251	-254	-176
127	*	-523	*	-445	*	-477	*	-529	*	-842	*	-810	*	-782
128	24	14	16	-5	-32	-6	-18	-20	-148	-40	-104	-49	-121	-10
129	-235	-214	-240	-231	-232	-250	-310	-286	-355	-376	-266	-426	*	-414
130	80	-21	-3	-26	-37	-26	-10	-38	-102	-63	-60	-72	-100	-31
131	*	-289	-273	-306	*	-332	*	-375	*	-546	*	-576	*	-500
132	39	-73	-38	-68	-81	-69	-70	-81	-133	-105	-154	-129	-208	-86
133	-295	-381	-353	-397	-469	-430	-462	-484	-791	-683	-718	-748	-727	-622
134	-5	-118	-74	-111	-119	-112	-100	-126	-197	-225	-249	-191	-218	-145
135	-368	-474	-488	-450	-399	-487	*	-549	8250	-910	*	-851	*	-753
136	-24	-95	-93	-115	-137	-117	-100	-130	-236	-266	-267	-193	-277	-128
137	-386	-458	-391	-437	-503	-471	-515	-526	-843	-907	-858	-814	-829	-748
138	-104	-133	-90	-123	-155	-126	-139	-140	-270	-246	-270	-209	-287	-163
139	-352	-530	-409	-445	-517	-477	-497	-527	-829	-811	-829	-809	-820	-807
140	-48	-88	-49	-88	-98	-93	-104	-111	-230	-166	-165	-187	-233	-129
141	-345	-465	-365	-408	-480	-438	-457	-485	-721	-666	-712	-736	-719	-723
142	32	-43	-10	-42	-68	-47	-47	-64	-142	-112	-142	-128	-146	-88
143	-322	-395	-431	-342	-435	-368	-270	-411	*	-569	*	-623	*	-631
144	81	10	-16	-12	-31	-15	-58	-30	-108	-57	-76	-75	480	-21
145	-168	-304	-153	-286	-136	-310	288	-351	-543	-475	-566	-540	-538	-528
146	86	11	-44	-11	-11	-13	23	-28	*	-56	*	-68	*	-15
147	-168	-278	-237	-276	-327	-300	-312	-342	-555	-496	-554	-548	-581	-492
148	-108	-343	-252	-268	179	-288	411	-325	488	-580	545	-487	615	-553
149	-352	-460	-398	-357	-392	-384	-267	-429	-201	-754	278	-649	810	-713
150	-412	-460	-511	-429	-451	-463	-547	-517	-247	-832	195	-799	484	-742
151	-376	-533	-500	-511	-602	-551	-589	-614	-911	-850	-975	-952	-943	-832
152	-365	-485	-455	-493	-589	-531	-576	-588	-925	-742	-884	-905	-939	-767
153	-61	-162	-87	-147	-171	-147	-135	-155	-228	-198	-237	-238	-317	-117
154	*	-57	*	-59	*	-57	*	-66	*	-149	*	-107	*	-50
155	67	-28	-13	-28	-39	-28	-20	-39	-160	-99	-60	-71	-123	-32
156	85	-9	8	-15	-22	-17	-22	-30	-131	-72	-91	-63	-83	-28
157	69	-24	-12	-40	-60	-44	-52	-61	-120	-108	-171	-114	-132	-58
158	-242	-101	-144	-144	-64	-151	*	-168	*	-193	*	-269	*	-160
159	*	-189	*	-171	*	-176	*	-190	*	-223	*	-298	*	-214
160	-98	-155	-93	-152	-175	-154	-159	-165	-310	-223	-338	-260	-296	-151
161	-32	-60	-39	-65	-57	-65	-62	-77	-202	-167	-160	-131	-170	-80
162	66	-39	-5	-38	-67	-39	-31	-53	-172	-124	-137	-98	-129	-62

Note: units = microstrain; *Bad gage

TABLE 7. Experimental Gage Readings and FEM Predictions for Strains Due to Truck Loads

Gage Number	Position of Truck									
	A		B		C		D		E	
	Gage	FEM	Gage	FEM	Gage	FEM	Gage	FEM	Gage	FEM
(1)	(2)	(3)	(4)	(5)	(6)	(7)	(8)	(9)	(10)	(11)
1	-618	-236	-13	-235	5	-235	18	-236	55	-236
2	-213	-165	-221	-164	-175	-164	-184	-165	-236	-164
3	-147	-135	-188	-134	-196	-134	-159	-134	-178	-134
4	*	-114	*	-113	*	-114	*	-113	*	-113
5	*	-120	*	-120	*	-121	*	-119	*	-119
6	-329	-149	-302	-149	491	-149	525	-148	-381	-148
7	-268	-198	-257	-198	-291	-199	-261	-198	-268	-198
8	*	-240	*	-240	*	-240	*	-239	*	-240
9	-393	-301	-312	-300	-349	-300	-321	-299	-372	-300
10	*	-273	*	-274	*	-275	*	-274	*	-275
11	-220	-223	-232	-227	-236	-227	-212	-226	-256	-227
12	-395	-166	-463	-171	-463	-171	-472	-171	-502	-171
13	-178	-136	-186	-141	-187	-141	-193	-141	-245	-141
14	-107	-107	-129	-113	-167	-113	-175	-113	-128	-113
15	-287	-152	-259	-152	-311	-153	-294	-153	-278	-152
16	-598	-411	-557	-403	-586	-401	-556	-405	-542	-404
17	-377	-203	-356	-204	-350	-205	-353	-204	-324	-204
18	273	-389	287	-377	299	-375	253	-376	265	-376
19	-305	-181	-357	-185	-337	-185	-389	-185	-336	-186
20	-514	-364	-424	-355	-461	-353	-451	-354	-443	-355
21	-220	-181	-218	-185	-257	-185	-222	-185	-268	-186
22	*	-527	*	-530	*	-529	*	-528	*	-528
23	-232	-211	-214	-209	-245	-209	-220	-210	-195	-210
24	-682	-718	-653	-720	-660	-723	-686	-718	-680	-718
25	-207	-194	-205	-193	-164	-193	-208	-193	-212	-193
26	-775	-856	-768	-856	-774	-863	-814	-855	-790	-855
27	-182	-176	-147	-175	-207	-177	-219	-175	-220	-175
28	-831	-836	-741	-834	-766	-842	-840	-835	-793	-834
29	*	-158	*	-158	*	-161	*	-159	*	-159
30	-713	-674	-685	-670	-689	-673	-753	-672	-748	-671
31	-217	-151	-198	-150	-168	-152	-174	-152	-165	-152
32	-634	-532	-598	-526	-631	-526	-629	-528	-587	-527
33	-156	-162	-210	-167	-193	-167	-214	-167	-172	-168
34	-315	-512	-282	-509	-365	-506	-381	-508	-243	-509
35	-182	-138	-186	-144	-186	-143	-201	-144	-156	-144
36	227	-667	261	-670	226	-668	252	-669	248	-670
37	-130	-131	-178	-136	-174	-136	-189	-136	-134	-136
38	-762	-813	-752	-828	-746	-826	-818	-827	-812	-828

Note: units = microstrain; *Bad gage

TABLE 7. Experimental Gage Readings and FEM Predictions for Strains Due to Truck Loads (Cont.)

Gage Number (1)	Position of Truck: A Gage (2)	A FEM (3)	B Gage (4)	B FEM (5)	C Gage (6)	C FEM (7)	D Gage (8)	D FEM (9)	E Gage (10)	E FEM (11)
39	-121	-139	-134	-137	-88	-136	-94	-137	-118	-137
40	-543	-803	-579	-824	-590	-824	-618	-824	-568	-824
41	-279	-149	-256	-150	-239	-151	-280	-152	-285	-153
42	*	-388	*	-381	*	-379	*	-383	*	-382
43	*	-178	*	-180	*	-180	*	-182	*	-184
44	*	-368	*	-360	*	-357	*	-362	*	-362
45	-211	-151	-228	-155	-256	-155	-243	-155	-257	-156
46	-481	-874	-476	-873	-509	-885	-500	-873	-492	-872
47	-185	-201	-225	-201	-238	-207	-205	-201	-215	-201
48	-838	-874	-839	-873	-849	-885	-861	-873	-864	-872
49	-217	-187	-180	-188	-210	-192	-255	-188	-209	-188
50	-740	-724	-760	-721	-768	-724	-776	-722	-798	-721
51	-176	-167	-239	-168	-215	-170	-250	-167	-239	-168
52	-670	-544	-624	-540	-651	-540	-595	-541	-660	-541
53	0	-150	25	-151	44	-153	52	-150	20	-151
54	-523	-394	-477	-389	-491	-387	-474	-391	-512	-390
55	-200	-200	-230	-203	-182	-202	-189	-200	-254	-201
56	-516	-398	-463	-393	-500	-388	-476	-391	-501	-391
57	-169	-137	-188	-140	-205	-139	-234	-139	-231	-140
58	*	-330	-487	-325	-502	-321	-493	-325	-432	-325
59	-167	-146	-194	-150	-197	-150	-195	-150	-173	-150
60	-522	-459	-486	-457	-509	-454	-537	-456	-511	-457
61	-141	-155	-190	-159	-163	-158	-183	-159	-217	-159
62	-664	-601	-623	-602	-640	-600	-640	-602	-708	-602
63	100	-143	108	-145	135	-145	94	-145	137	-146
64	-800	-806	-767	-815	-816	-813	-815	-815	-789	-815
65	-142	-143	-179	-140	-123	-140	-148	-140	-202	-140
66	-804	-831	-771	-845	-790	-844	-809	-845	-846	-845
67	-612	-591	-636	-588	-615	-589	-639	-589	-624	-589
68	-552	-400	-559	-396	-498	-393	-554	-397	-498	-397
69	-536	-109	-516	-109	-504	-109	-479	-109	-449	-109
70	-120	-330	-92	-326	-76	-322	-87	-326	-59	-326
71	-511	-426	-538	-424	-556	-421	-522	-424	-551	-424
72	-282	-209	-266	-209	-306	-210	-222	-209	-268	-209
73	-168	-124	-158	-125	-129	-125	-139	-124	-157	-124
74	-147	-119	-136	-119	-124	-120	-179	-118	-151	-118
75	-142	-130	-196	-131	-157	-130	-212	-130	-196	-130
76	-215	-153	-277	-154	-305	-154	-340	-154	-320	-154
77	-282	-223	-286	-224	-291	-223	-320	-223	-302	-223
78	-314	-283	-332	-284	-336	-283	-336	-284	-361	-284
79	195	-180	108	-181	158	-180	153	-180	185	-180
80	-124	-104	-131	-105	-154	-105	-107	-105	-117	-105

Note: units = microstrain; *Bad gage

TABLE 7. Experimental Gage Readings and FEM Predictions for Strains Due to Truck Loads (Cont.)

Gage Number (1)	A Gage (2)	A FEM (3)	B Gage (4)	B FEM (5)	C Gage (6)	C FEM (7)	D Gage (8)	D FEM (9)	E Gage (10)	E FEM (11)
81	-153	-93	-99	-94	-151	-94	-118	-94	-121	-94
82	-234	-198	-245	-199	-280	-199	-263	-199	-290	-199
83	-147	-81	-171	-82	-156	-82	-153	-82	-201	-82
84	-134	-53	-132	-54	-104	-54	-92	-54	-82	-54
85	-120	-71	-105	-71	-90	-70	-146	-71	-122	-72
86	-154	-93	-106	-93	-91	-92	-159	-93	-174	-94
87	-191	-128	-159	-128	-169	-128	-222	-129	-234	-129
88	-246	-187	-270	-187	-290	-187	-287	-188	-314	-188
89	-165	-224	-144	-224	-211	-224	-280	-224	-324	-224
90	-307	-263	-327	-264	-329	-264	-362	-264	-361	-263
91	-331	-256	-289	-255	-263	-255	-348	-256	-281	-255
92	-224	-188	-192	-185	-262	-185	-222	-185	-251	-185
93	*	-120	*	-116	*	-116	*	-116	*	-116
94	-192	-91	-141	-86	-171	-86	-157	-86	-191	-86
95	226	-71	255	-65	189	-65	174	-65	150	-65
96	-302	-204	-481	-204	-542	-203	-548	-203	-553	-203
97	-952	-848	-899	-855	-905	-857	-941	-853	-976	-854
98	-293	-250	-334	-248	-299	-248	-310	-248	-326	-248
99	-852	-793	-799	-803	-831	-806	-875	-805	-890	-805
100	-273	-230	-273	-226	-321	-226	-331	-226	-325	-225
101	-821	-774	-797	-782	-785	-784	-837	-784	-785	-783
102	-261	-201	-273	-203	-257	-204	-293	-202	-289	-202
103	-639	-631	-634	-628	-674	-629	-652	-630	-633	-629
104	-176	-130	-177	-131	-168	-132	-209	-131	-191	-131
105	-517	-505	-619	-503	-650	-501	-616	-505	-687	-505
106	-83	-61	-120	-62	-144	-62	-98	-62	-108	-62
107	-414	-415	-420	-415	-447	-408	-411	-416	-442	-416
108	-94	-25	-103	-26	-108	-23	-104	-25	-112	-25
109	-450	-385	-484	-386	-457	-380	-446	-386	-460	-387
110	-87	-55	-90	-56	-65	-53	-126	-55	-99	-55
111	-161	-536	-190	-540	-303	-538	-284	-539	-279	-540
112	-111	-111	-180	-111	-121	-109	-164	-109	-174	-109
113	-754	-679	-747	-684	-797	-684	-833	-682	-779	-683
114	-167	-163	-213	-158	-218	-159	-195	-158	-236	-158
115	-672	-695	-700	-698	-669	-700	-728	-699	-719	-698
116	315	-101	352	-96	306	-96	290	-96	237	-95
117	-632	-604	-578	-602	-607	-604	-634	-603	-628	-602
118	-121	-46	-97	-41	-78	-41	-110	-41	-132	-41
119	*	-498	*	-484	*	-485	*	-484	*	-484
120	355	-38	345	-40	323	-41	335	-40	301	-40
121	-574	-499	-529	-476	-572	-477	-536	-477	-577	-477
122	-277	-196	-266	-195	-265	-194	-285	-193	-243	-192

Note: units = microstrain; *Bad gage

TABLE 7. Experimental Gage Readings and FEM Predictions for Strains Due to Truck Loads (Cont.)

Gage Number (1)	Position of Truck									
	A		B		C		D		E	
	Gage (2)	FEM (3)	Gage (4)	FEM (5)	Gage (6)	FEM (7)	Gage (8)	FEM (9)	Gage (10)	FEM (11)
123	-931	-792	-909	-798	-892	-800	-989	-796	-944	-797
124	-289	-206	-285	-204	-274	-204	-271	-202	-319	-201
125	-818	-761	-835	-768	-898	-771	-907	-766	-857	-766
126	-257	-212	-262	-208	-275	-209	-310	-208	-285	-207
127	*	-777	*	-783	*	-786	*	-784	*	-784
128	-76	-35	-57	-35	-124	-29	-125	-35	-101	-35
129	-315	-395	-362	-395	-421	-385	-436	-396	-402	-396
130	-113	-64	-128	-64	-99	-60	-141	-64	-87	-64
131	*	-489	*	-492	*	-490	*	-491	*	-492
132	-132	-120	-130	-119	-162	-117	-158	-119	-188	-119
133	-738	-612	-696	-615	-793	-616	-747	-614	-806	-614
134	-186	-175	-234	-174	-222	-172	-209	-174	-241	-174
135	*	-734	*	-739	*	-741	*	-737	*	-738
136	-180	-149	-176	-147	-246	-147	-262	-150	-201	-149
137	-826	-718	-782	-722	-808	-726	-805	-724	-833	-724
138	-258	-196	-214	-193	-217	-193	-244	-194	-248	-193
139	-799	-796	-751	-801	-806	-804	-851	-801	-796	-801
140										
141	-750	-718	-708	-721	-755	-723	-719	-721	-731	-721
142	-135	-116	-173	-112	-158	-113	-163	-112	-148	-112
143	*	-631	*	-631	*	-633	*	-631	*	-631
144	-27	-49	-21	-47	-101	-47	-114	-47	-81	-46
145	-578	-528	-571	-519	-549	-521	-575	-520	-543	-519
146	*	-37	*	-41	*	-41	*	-41	*	-40
147	-585	-500	-545	-485	-539	-486	-549	-486	-559	-485
148	506	-550	469	-553	545	-552	575	-551	566	-552
149	-215	-705	-222	-708	-11	-710	3	-707	9	-707
150	-212	-717	-265	-720	-283	-725	-328	-720	-337	-721
151	-911	-813	-890	-817	-920	-820	-935	-817	-961	-816
152	-878	-755	-877	-758	-919	-761	-921	-758	-899	-758
153	-279	-181	-224	-181	-214	-180	-245	-181	-266	-181
154	*	-87	*	-86	*	-86	*	-87	*	-87
155	-121	-64	-120	-64	-133	-63	-104	-64	-137	-64
156	-75	-55	-110	-54	-110	-55	-149	-55	-129	-55
157	-148	-80	-147	-79	-161	-80	-199	-80	-199	-80
158	575	-185	647	-184	691	-185	671	-184	704	-184
159	*	-260	*	-260	*	-261	*	-260	*	-260
160	-240	-200	-226	-200	-231	-200	-283	-200	-240	-200
161	-173	-109	-154	-108	-184	-108	-175	-108	-205	-108
162	-133	-90	-96	-88	-92	-89	-134	-88	-167	-88

Note: units = microstrain; *Bad gage

TABLE 7. Experimental Gage Readings and FEM Predictions for Strains Due to Truck Loads (Cont.)

Gage Number (1)	F Gage (2)	F FEM (3)	G Gage (4)	G FEM (5)	H Gage (6)	H FEM (7)	I Gage (8)	I FEM (9)
1	-97	-194	-77	-200	-95	-198	-81	-199
2	-196	-154	-200	-161	-215	-158	-180	-161
3	-207	-122	-202	-121	-184	-119	-142	-122
4	*	-96	*	-93	*	-93	*	-94
5	*	-99	*	-97	*	-97	*	-97
6	-330	-125	-329	-122	-301	-123	-339	-123
7	-281	-149	-286	-146	-317	-147	-302	-147
8	*	-161	*	-159	*	-160	*	-160
9	-322	-191	-371	-189	-318	-190	-326	-190
10	*	-197	*	-195	*	-197	*	-196
11	-275	-200	-233	-198	-248	-200	-218	-199
12	-323	-167	-279	-166	-315	-167	-317	-167
13	-58	-133	-99	-132	-45	-133	-67	-132
14	-134	-93	-154	-92	-172	-93	-151	-92
15	-322	-116	-252	-113	-263	-114	-285	-114
16	-523	-425	-536	-423	-542	-426	-535	-425
17	-357	-169	-337	-166	-368	-168	-362	-168
18	637	-399	610	-395	606	-401	661	-396
19	-212	-170	-255	-168	-239	-170	-242	-169
20	-431	-378	-462	-374	-484	-379	-466	-373
21	-268	-170	-285	-168	-250	-170	-250	-169
22	*	-552	*	-547	*	-553	*	-549
23	-200	-191	-252	-197	-218	-191	-224	-196
24	-661	-732	-681	-736	-678	-738	-665	-739
25	-189	-182	-214	-183	-207	-177	-187	-183
26	-779	-864	-767	-873	-747	-869	-763	-876
27	-164	-159	-217	-156	-184	-145	-165	-156
28	-817	-831	-793	-837	-755	-819	-781	-841
29	94	-132	113	-129	71	-124	90	-130
30	-702	-674	-673	-677	-725	-669	-736	-680
31	-225	-121	-222	-117	-177	-116	-156	-119
32	-635	-534	-621	-534	-624	-533	-590	-537
33	-184	-156	-183	-154	-212	-156	-202	-155
34	-337	-519	-335	-516	-370	-520	-359	-513
35	-187	-128	-155	-127	-188	-128	-180	-128
36	*	-684	*	-682	*	-685	*	-677
37	-123	-117	-122	-116	-122	-117	-178	-116
38	-816	-839	-794	-837	-744	-839	-799	-832

Note: units = microstrain; *Bad gage

TABLE 7. Experimental Gage Readings and FEM Predictions for Strains Due to Truck Loads (Cont.)

Gage Number (1)	F Gage (2)	F FEM (3)	G Gage (4)	G FEM (5)	H Gage (6)	H FEM (7)	I Gage (8)	I FEM (9)
39	26	-118	52	-117	66	-118	44	-115
40	-461	-829	-468	-829	-489	-830	-482	-825
41	-265	-129	-278	-125	-261	-127	-251	-127
42	*	-392	*	-391	*	-393	*	-393
43	*	-163	*	-160	*	-163	*	-162
44	*	-364	*	-361	*	-367	*	-363
45	-231	-137	-230	-135	-247	-137	-254	-137
46	-475	-885	-455	-889	-425	-880	-422	-893
47	-216	-183	-229	-181	-237	-176	-247	-182
48	-885	-885	-802	-889	-793	-880	-827	-893
49	-247	-164	-234	-161	-199	-161	-216	-163
50	-749	-731	-737	-734	-725	-725	-756	-737
51	-251	-147	-212	-143	-240	-145	-250	-145
52	-622	-549	-586	-551	-602	-547	-587	-554
53	-98	-136	-100	-132	-101	-135	-93	-134
54	-514	-394	-447	-394	-521	-395	-462	-397
55	-258	-180	-246	-176	-192	-181	-211	-179
56	-470	-382	-476	-380	-438	-386	-449	-383
57	-227	-124	-196	-121	-222	-124	-203	-124
58	-100	-338	-112	-335	-114	-340	-139	-336
59	-185	-131	-159	-130	-200	-132	-212	-132
60	-522	-465	-501	-463	-516	-467	-496	-461
61	-181	-140	-167	-139	-173	-141	-197	-141
62	-676	-612	-637	-610	-685	-613	-638	-606
63								
64	-806	-827	-780	-826	-758	-828	-736	-818
65	-199	-120	-124	-120	-160	-120	-152	-117
66	-816	-853	-825	-852	-825	-854	-776	-847
67	-608	-599	-628	-602	-626	-596	-652	-604
68								
69	-477	-109	-456	-109	-485	-109	-479	-109
70	51	-334	14	-333	-7	-337	32	-334
71	-518	-431	-470	-430	-502	-433	-508	-428
72	-237	-154	-305	-162	-253	-153	-263	-154
73	-140	-99	-170	-103	-170	-99	-127	-100
74	-160	-97	-140	-97	-164	-97	-119	-98
75	-204	-112	-194	-109	-146	-112	-155	-113
76	-201	-144	-242	-141	-171	-144	-187	-144
77	-280	-183	-350	-181	-348	-184	-297	-184
78	-371	-163	-336	-163	-345	-163	-350	-164
79	866	-120	831	-119	870	-120	820	-120
80	-103	-79	-109	-79	-104	-80	-158	-80

Note: units = microstrain; *Bad gage

TABLE 7. Experimental Gage Readings and FEM Predictions for Strains Due to Truck Loads (Cont.)

Gage Number (1)	F Gage (2)	F FEM (3)	G Gage (4)	G FEM (5)	H Gage (6)	H FEM (7)	I Gage (8)	I FEM (9)
81	-113	-70	-121	-70	-161	-70	-119	-70
82	-438	-182	-468	-176	-419	-178	-449	-177
83	-145	-67	-163	-61	-184	-64	-168	-61
84	-149	-24	-121	-25	-118	-27	-131	-25
85	-91	-38	-144	-41	-144	-42	-133	-40
86	-124	-58	-141	-60	-118	-60	-165	-59
87	-184	-87	-176	-89	-174	-89	-210	-88
88	-300	-132	-287	-134	-284	-134	-276	-134
89	-308	-169	-179	-171	-178	-170	-245	-170
90	-320	-220	-323	-223	-323	-221	-305	-222
91	-306	-211	-318	-213	-280	-212	-303	-212
92	-249	-150	-221	-152	-220	-151	-237	-151
93	*	-82	*	-83	*	-82	*	-83
94	-149	-53	-173	-54	-159	-53	-160	-53
95	*	-32	*	-33	*	-32	*	-32
96	*	-175	*	-178	*	-177	*	-177
97	-970	-888	-946	-891	-944	-887	-910	-889
98	-348	-203	-364	-206	-333	-203	-374	-204
99	-858	-813	-859	-817	-850	-811	-833	-815
100	-331	-185	-310	-187	-319	-185	-314	-185
101	-846	-776	-802	-779	-796	-775	-780	-779
102	-236	-169	-239	-162	-250	-166	-278	-163
103	-653	-617	-630	-622	-685	-616	-648	-621
104	-169	-107	-163	-101	-175	-107	-189	-102
105	-342	-513	-313	-510	-292	-508	-307	-507
106	-90	-38	-113	-37	-123	-44	-113	-38
107	-410	-441	-415	-432	-438	-436	-403	-429
108	-66	9	-118	6	-114	-4	-94	6
109	-439	-407	-439	-400	-415	-418	-400	-397
110	-131	-19	-139	-22	-125	-26	-126	-21
111	591	-549	598	-546	591	-553	527	-543
112	-139	-76	-166	-79	-135	-80	-169	-78
113	-810	-700	-762	-700	-746	-701	-782	-698
114	-185	-132	-230	-134	-172	-132	-228	-132
115	-728	-697	-663	-700	-695	-696	-726	-702
116	*	-69	*	-70	*	-68	*	-69
117	-574	-605	-585	-607	-571	-604	-603	-611
118	-93	-12	-74	-13	-144	-12	-130	-13
119	*	-492	*	-493	*	-491	*	-499
120	*	-13	*	-13	*	-13	*	-15
121	-583	-482	-527	-483	-541	-482	-529	-487
122	-241	-164	-309	-168	-306	-166	-286	-166

Note: units = microstrain; *Bad gage

TABLE 7. Experimental Gage Readings and FEM Predictions for Strains Due to Truck Loads (Cont.)

Gage Number (1)	Position of Truck: F Gage (2)	F FEM (3)	G Gage (4)	G FEM (5)	H Gage (6)	H FEM (7)	I Gage (8)	I FEM (9)
123	-938	-823	-923	-824	-929	-822	-937	-822
124	-258	-170	-297	-174	-262	-171	-300	-172
125	-927	-780	-831	-783	-876	-777	-872	-781
126	-327	-174	-269	-176	-266	-174	-271	-174
127	*	-778	*	-781	*	-777	*	-781
128	-116	-7	-128	-9	-100	-14	-101	-9
129	*	-420	*	-416	*	-425	*	-412
130	-109	-28	-103	-31	-111	-31	-113	-29
131	*	-504	*	-500	*	-508	*	-497
132	-189	-82	-151	-86	-194	-84	-138	-84
133	-766	-623	-717	-622	-708	-625	-757	-619
134	-268	-141	-243	-145	-196	-142	-234	-143
135	*	-752	*	-752	*	-751	*	-750
136	-205	-125	-242	-128	-209	-124	-231	-125
137	-826	-746	-802	-747	-768	-742	-792	-745
138								
139	-825	-804	-837	-806	-829	-802	-775	-805
140	-192	-127	-198	-129	-195	-127	-216	-127
141	-712	-720	-768	-722	-716	-718	-720	-723
142	-167	-87	-133	-88	-151	-86	-145	-86
143	5631	-629	5607	-630	5606	-627	5628	-634
144	482	-20	461	-21	461	-20	418	-20
145								
146	2073	-14	2059	-14	2101	-13	2072	-17
147	-582	-491	-583	-491	-564	-490	-541	-497
148	609	-554	636	-552	623	-557	609	-550
149	778	-713	787	-712	788	-713	829	-710
150	441	-740	437	-741	460	-738	437	-738
151	-941	-830	-894	-831	-890	-828	-897	-829
152	-917	-764	-892	-766	-861	-763	-871	-766
153	-233	-117	-288	-110	-256	-117	-291	-117
154	*	-50	*	-47	*	-51	*	-49
155	-129	-32	-106	-33	-145	-33	-135	-32
156	-89	-27	-122	-30	-96	-28	-122	-27
157	-179	-57	-139	-60	-188	-57	-134	-57
158	-938	-159	-947	-161	-899	-159	-878	-159
159	*	-213	*	-213	*	-213	*	-212
160	-274	-150	-328	-150	-336	-150	-312	-149
161	-196	-79	-145	-80	-166	-79	-136	-79
162	-172	-62	-140	-62	-158	-61	-155	-61

Note: units = microstrain; *Bad gage

APPENDIX V. LIST OF FEM ANALYSES

NO.	DESCRIPTION	TIME (day)	TEMP. (°F)	LOAD (lb)	NODE NUMBERS
1	February, 1989	56	47.8	None	
2	March	70	42.	None	
3	April	102	52.5	None	
4	May	136	72.8	None	
5	July	192	78.8	None	
6	Truck A	192	78.8	-5,800	80
				-5,800	81
				-23,880	106
				-23,880	107
7	Truck B	192	81.2	-5,800	531
				-5,800	532
				-23,880	557
				-23,880	558
8	Truck C	192	84.4	-5,800	345
				-5,800	346
				-23,880	319
				-23,880	320
9	Truck D	192	87.3	-5,800	239
				-5,800	238
				-23,880	213
				-23,880	212
10	Truck E	192	90.2	-5,800	239
				-5,800	238
				-23,880	213
				-23,880	213
				-11,400	210
				-11,400	211
				-3,980	236
				-3,980	237
11	August	231	82.5	None	
12	October	294	54.2	None	
13	November	319	50.1	None	

14	Truck F	320	50.1	-6,060	367
				-6,060	380
				-11,395	366
				-11,395	379
				-11,395	365
				-11,395	378
15	Truck G	320	50.1	-6,060	375
				-6,060	388
				-11,395	376
				-11,395	389
				-11,395	377
				-11,395	390
16	Truck H	320	50.1	-6,060	290
				-6,060	291
				-22,790	316
				-22,790	317
17	Truck I	320	50.1	-6,060	90
				-6,060	89
				-22,790	116
				-22,790	115
18	February, 1990	400	47.2	None	
19	April	472		None	
20	August	591		None	
21	November	681	70.0	None	
22	May, 1991	878	80.0	None	

Appendix VI. Example FEM Input Data File

```
 BROOK AVENUE OVERPASS   TIME-DEPENDENT ANALYSIS
 637   2   3   0   0   0   1   1   1   0
   2   0   0   1   0   2   0   1
     0.0       0.0      .005      .01
  1000.00   1000.00     15.0      1.0
     47.       75.      211.
   1   0   0   0   0   0   10.0000E+000.0000E+000.0000E+00
   2   0   0   0   0   0   10.3179E+020.8490E+020.0000E+00
   3   0   0   0   0   0   10.6358E+020.1698E+030.0000E+00
   4   0   0   0   0   0   10.9538E+020.2547E+030.0000E+00
   5   0   0   0   0   0   10.1272E+030.3396E+030.0000E+00
   6   0   0   0   0   0   10.1590E+030.4245E+030.0000E+00
   7   0   0   0   0   0   10.1908E+030.5094E+030.0000E+00
   8   0   0   0   0   0   10.2225E+030.5943E+030.0000E+00
   9   0   0   0   0   0   10.2543E+030.6792E+030.0000E+00
  10   0   0   0   0   0   10.2861E+030.7641E+030.0000E+00
. . .
. . .
. . .
 630   0   0   0   0   0   10.3736E+040.4525E+030.0000E+00
 631   0   0   0   0   0   10.3770E+040.5430E+030.0000E+00
 632   0   0   0   0   0   10.3804E+040.6335E+030.0000E+00
 633   0   0   0   0   0   10.3838E+040.7240E+030.0000E+00
 634   0   0   0   0   0   10.3871E+040.8145E+030.0000E+00
 635   0   0   0   0   0   10.3905E+040.9050E+030.0000E+00
 636   0   0   0   0   0   10.3939E+040.9955E+030.0000E+00
 637   0   0   0   0   0   10.3973E+040.1086E+040.0000E+00
   1   1   2   1   1
   1   2   2   2    6300.      .15      .087      10.      1.0
              7.12      30.
   1 29000000.   60000.  346000.       .18
   1   1     2.907  .000017      .25   225000.      10.   4
  170520.    .0058  220000.      .01   240000.      .03  253000.      .067

   2   1     1.071  .000017      .25   225000.      10.   4
  170520.    .0058  220000.      .01   240000.      .03  253000.      .067

   1  10
    -15.0    -14.90    -12.25     -8.0      -4.0       0.0       4.0       8.0
    12.25     16.40     16.5
   1   4   1
   1   1  -12.5625     .026
   2   1  -13.1875     .052      69.5
   3   1   12.5625     .026
   4   1   13.1875     .052      69.5
   1 1152   0   0
     0.0       0.0       -1.
   1  15   2   1   1   1   1   1 0.0     0 0.00  0.00  0.00  0.00 60.00
   2   1  14  15   1   1   1   1 0.0     0 0.00  0.00  0.00  0.00 60.00
   3  28  15  14   1   1   1   1 0.0     0 0.00  0.00  0.00  0.00 60.00
   4  14  27  28   1   1   1   1 0.0     0 0.00  0.00  0.00  0.00 60.00
```

```
   5   41   28   27    1    1    1    1  0.0     0  0.00  0.00  0.00  0.00 60.00
   6   27   40   41    1    1    1    1  0.0     0  0.00  0.00  0.00  0.00 60.00
   7   54   41   40    1    1    1    1  0.0     0  0.00  0.00  0.00  0.00 60.00
   8   40   53   54    1    1    1    1  0.0     0  0.00  0.00  0.00  0.00 60.00
   9   67   54   53    1    1    1    1  0.0     0  0.00  0.00  0.00  0.00 60.00
. . .
. . .
. . .
1140  545  558  559    1    1    1    1  0.0     0  0.00  0.00  0.00  0.00 60.00
1141  572  559  558    1    1    1    1  0.0     0  0.00  0.00  0.00  0.00 60.00
1142  558  571  572    1    1    1    1  0.0     0  0.00  0.00  0.00  0.00 60.00
1143  585  572  571    1    1    1    1  0.0     0  0.00  0.00  0.00  0.00 60.00
1144  571  584  585    1    1    1    1  0.0     0  0.00  0.00  0.00  0.00 60.00
1145  598  585  584    1    1    1    1  0.0     0  0.00  0.00  0.00  0.00 60.00
1146  584  597  598    1    1    1    1  0.0     0  0.00  0.00  0.00  0.00 60.00
1147  611  598  597    1    1    1    1  0.0     0  0.00  0.00  0.00  0.00 60.00
1148  597  610  611    1    1    1    1  0.0     0  0.00  0.00  0.00  0.00 60.00
1149  624  611  610    1    1    1    1  0.0     0  0.00  0.00  0.00  0.00 60.00
1150  610  623  624    1    1    1    1  0.0     0  0.00  0.00  0.00  0.00 60.00
1151  637  624  623    1    1    1    1  0.0     0  0.00  0.00  0.00  0.00 60.00
1152  623  636  637    1    1    1    1  0.0     0  0.00  0.00  0.00  0.00 60.00
   2   62
 210  209                     1    0               0.           56620.5
 220  219                     1    0    2          0.           56620.5
 210  197                     1    0               0.           56620.5
 220  207                     1    0    2          0.           56620.5
 418  417                     1    0               0.           56620.5
 428  427                     1    0    2          0.           56620.5
 418  405                     1    0               0.           56620.5
 428  415                     1    0    2          0.           56620.5
 210  196  224  222  198      1    0               0.           6.5E+06
 220  206  234  232  208      1    0    2          0.           6.5E+06
 418  404  432  430  406      1    0               0.           6.5E+06
 428  414  442  440  416      1    0    2          0.           6.5E+06
   1    1   15   14    2      1    0               0.          9.81E+06
  13   12   26   25   13      1    0    1          0.          9.81E+06
 625  612  626  625  613      1    0               0.          9.81E+06
 637  623  637  636  624      1    0    1          0.          9.81E+06
  99   96    6   13
   1    0    0    1   96    6    1    2  625  626    0    0    1    5
    .2500   588700.  -588700.
   1    2    3    4    5    6    7    8    9   10   11   12   13   14   15   16
  17   18   19   20   21   22   23   24   25   26   27   28   29   30   31   32
  33   34   35   36   37   38   39   40   41   42   43   44   45   46   47   48
  49   50   51   52   53   54   55   56   57   58   59   60   61   62   63   64
  65   66   67   68   69   70   71   72   73   74   75   76   77   78   79   80
  81   82   83   84   85   86   87   88   89   90   91   92   93   94   95   96
     5.383    14.375      .000     1.000   477.500   -10.000
  1085.883    14.261     5.800     1.000   119.500     9.000
  1321.883    14.237     5.800     1.000   466.500    -7.000
  2255.283    14.138     5.800     1.000   119.500     9.000
  2491.283    14.114     5.800     1.000   603.000   -10.000
  3571.600    14.000      .000     1.000      .000      .000
    31.129    83.128      .000     1.000   477.500   -10.000
```

```
 1111.629    84.444     5.800     1.000   119.500     9.000
 1347.629    84.731     5.800     1.000   466.500    -7.000
 2281.029    85.868     5.800     1.000   119.500     9.000
 2517.029    86.155     5.800     1.000   603.000   -10.000
 3599.114    87.472      .000     1.000      .000      .000
   68    0    0    1   96    6   12   13  636  637    0    0    1    5
    .2500   588700.  -588700.
 1057 1058 1059 1060 1061 1062 1063 1064 1065 1066 1067 1068 1069 1070 1071 1072
 1073 1074 1075 1076 1077 1078 1079 1080 1081 1082 1083 1084 1085 1086 1087 1088
 1089 1090 1091 1092 1093 1094 1095 1096 1097 1098 1099 1100 1101 1102 1103 1104
 1105 1106 1107 1108 1109 1110 1111 1112 1113 1114 1115 1116 1117 1118 1119 1120
 1121 1122 1123 1124 1125 1126 1127 1128 1129 1130 1131 1132 1133 1134 1135 1136
 1137 1138 1139 1140 1141 1142 1143 1144 1145 1146 1147 1148 1149 1150 1151 1152
  350.376   935.672      .000     1.000   477.500   -10.000
 1430.876   954.590     5.800     1.000   119.500     9.000
 1666.876   958.722     5.800     1.000   466.500    -7.000
 2600.276   975.065     5.800     1.000   119.500     9.000
 2836.276   979.198     5.800     1.000   603.000   -10.000
 3940.286   998.528      .000     1.000      .000      .000
  376.122  1004.425      .000     1.000   477.500   -10.000
 1456.622  1024.754     5.800     1.000   119.500     9.000
 1692.622  1029.194     5.800     1.000   466.500    -7.000
 2626.022  1046.755     5.800     1.000   119.500     9.000
 2862.022  1051.196     5.800     1.000   603.000   -10.000
 3967.800  1072.000      .000     1.000      .000      .000
   74    0    0    1   24    2  196  209  208  221   -1
    .2500   588700.
   32   31  128  127  224  223  320  319  416  415  512  511  608  607  704  703
  800  799  896  895  992  991 1088 1087
     1130.        0.        0.        1.      510.      1.75
  1519.45   1040.05         0.

    .2500   588700.
   68   67  164  163  260  259  356  355  452  451  548  547  644  643  740  739
  836  835  932  931 1028 1027 1124 1123
   2446.4        0.        0.
  2845.14   1064.80        0.
   96    0    0    2   24    2    1   14   13   26   -1
    .2500            -400000.
    2    1   98   97  194  193  290  289  386  385  482  481  578  577  674  673
  770  769  866  865  962  961 1058 1057
      38.        0.        6.
   421.27   1022.02        6.
   97    0    0    2   24    2    1   14   13   26   -1
    .2500            -400000.
    2    1   98   97  194  193  290  289  386  385  482  481  578  577  674  673
  770  769  866  865  962  961 1058 1057
      38.        0.       -6.
   421.27   1022.02       -6.
   98    0    0    2   24    2  612  625  624  637   -1
    .2500    400000.
   96   95  192  191  288  287  384  383  480  479  576  575  672  671  768  767
  864  863  960  959 1056 1055 1152 1151
     3528.        0.        6.
```

```
  3936.8    1085.5         6.
 99    0    0    2   24    2  612  625  624  637   -1
   .2500   400000.
 96   95  192  191  288  287  384  383  480  479  576  575  672  671  768  767
864  863  960  959 1056 1055 1152 1151
   3528.        0.        -6.
  3936.8    1085.5        -6.
  1   20        1.         .5   1.  0.0    1   20       1152
  1 1152       41.         0.
                                           1   20       1152
  1 1152      89.9
  1   20    4                                           1152
319                     -23880.
320                     -23880.
345                      -5800.
346                      -5880.
  1 1152      89.3         0.
```

Appendix VII. Example FEM Output Data File

```
1  BROOK TRUCK-C


 NUMBER OF NODAL POINTS                          637

 NUMBER OF ELEMENT TYPES                           2

 NUMBER OF TIME STEPS                              3

 ITERATION TYPE CODE                               0
    -1 = INITIAL STIFFNESS ONLY
     0 = CONSTANT STIFFNESS IN LOAD STEPS
     N = REFORM STIFFNESS EACH N ITERATIONS

 CODE FOR NONLINEAR GEOMETRY                       0
 GEOMETRIC STIFFNESS CODE                          0
     0 = NOT CONSIDERED
     1 = INCLUDED

 CREEP ANALYSIS CODE                               1
 SHRINKAGE ANALYSIS CODE                           1
     0 = ANALYSIS NOT REQUIRED
     1 = ANALYSIS REQUIRED


 CONVERGENCE NORM CODE                             1
     0 = FORCE NORM USED
     1 = DISPLACEMENT NORM USED
     2 = BOTH FORCE AND DISPL NORMS

 CONVERGENGE TOLERANCE TYPE CODE                   0
     0 = ABSOLUTE VALUES
     1 = FRACTIONS

 PRINCIPAL AXES DIRECTION CODE                     0
     0 = CALCULATED IN PROGRAM
     1 = COINCIDE WITH ELEMENT LOCAL AXES



 OUTPUT CONTROL CODES
     0 = NO
     1 = YES

 DISPL, UNBAL FORCES + STRESSES FOR EACH ITER      2
     2 = ONLY AT END OF TIME STEPS
 NODAL DISPL IN LOCAL COORD SYSTEM                 0
 STRESS RESULTANTS                                 0
 STRAINS                                           1
 DISPL FOR EACH ITERATION                          0
```

UNBAL FORCES FOR EACH ITERATION 2
CODE TO START STOP PRINTING OF PATRAN OUTPUT 0
CODE TO SUPPRESS STRAIN, STRESS, TENDON FORCE 1

TOLERANCES TO GET CONVERGENCE

FORCES	.00000D+00
MOMENTS	.00000D+00
TRANSLATIONS	.50000D-02
ROTATIONS	.10000D-01

UPPER LIMITS ON UNBALANCE

FORCES	0.10D+04
MOMENTS	0.10D+04
TRANSLATIONS	0.15D+02
ROTATIONS	0.10D+01

ANALYSIS REQD. AT FOLLOWING DAYS AFTER CASTING
47. 75. 211.
1STORAGE REQUIRED = 5734
1COMPLETE NODAL POINT DATA

ONODE NUMBER	BOUNDARY CONDITION CODES X	Y	Z	XX	YY	ZZ	NODAL POINT COORDINATES X	Y	Z
1	0	0	0	0	0	1	0.000D+00	0.000D+00	0.000D+00
2	0	0	0	0	0	1	3.179D+01	8.490D+01	0.000D+00
3	0	0	0	0	0	1	6.358D+01	1.698D+02	0.000D+00
4	0	0	0	0	0	1	9.538D+01	2.547D+02	0.000D+00
5	0	0	0	0	0	1	1.272D+02	3.396D+02	0.000D+00
6	0	0	0	0	0	1	1.590D+02	4.245D+02	0.000D+00
7	0	0	0	0	0	1	1.908D+02	5.094D+02	0.000D+00
8	0	0	0	0	0	1	2.225D+02	5.943D+02	0.000D+00
9	0	0	0	0	0	1	2.543D+02	6.792D+02	0.000D+00
10	0	0	0	0	0	1	2.861D+02	7.641D+02	0.000D+00
630	0	0	0	0	0	1	3.736D+03	4.525D+02	0.000D+00
631	0	0	0	0	0	1	3.770D+03	5.430D+02	0.000D+00
632	0	0	0	0	0	1	3.804D+03	6.335D+02	0.000D+00
633	0	0	0	0	0	1	3.838D+03	7.240D+02	0.000D+00
634	0	0	0	0	0	1	3.871D+03	8.145D+02	0.000D+00
635	0	0	0	0	0	1	3.905D+03	9.050D+02	0.000D+00
636	0	0	0	0	0	1	3.939D+03	9.955D+02	0.000D+00
637	0	0	0	0	0	1	3.973D+03	1.086D+03	0.000D+00

1 MATERIAL PROPERTIES - CONCRETE , REINFORCING STEEL AND PRESTRESSING STEEL

NUMBER OF CONCRETE TYPES 1
NUMBER OF RE STEEL TYPES 1
NUMBER OF PRE STEEL TYPES 2

NUMBER OF CONCRETE LAYER SYSTEMS	1
NUMBER OF RE STEEL LAYER SYSTEMS	1

CONCRETE MATERIAL PROPERTIES

TYPE NO.	1
ELASTIC MATERIAL DATA INPUT INDICATOR	2
CREEP DATA INPUT INDICATOR	2
SHRINKAGE DATA INPUT INDICATOR	2

DATA INPUT INDICATORS - 1 = READ IN VALUES
2 = USE ACI DATA

COMPRESSIVE STRENGTH AT 28 DAYS	0.63000D+04
POISSONS RATIO	0.15000D+00
WEIGHT PER UNIT VOLUME	0.87000D-01
CRACKED SHEAR CONSTANT	0.10000D+01

DAYS AFTER CASTING	47.
COMPRESSIVE STRENGTH	0.67372D+04
TENSILE STRENGTH	0.65416D+03
MODULUS OF ELASTICITY	0.49928D+07
STRAIN AT COMPRESSIVE STRENGTH	0.26987D-02
ULTIMATE STRAIN IN COMPRESSION	0.10795D-01
ULTIMATE STRAIN IN TENSION	0.13102D-02

TENSION STIFFENING MODEL - UNLOADING IN CONCRETE

ULTIMATE SHRINKAGE	-0.80000D-03
SLUMP OF MIX	0.71200D+01
SIZE OF MEMBER	0.30000D+02
RELATIVE HUMIDITY	0.40000D+02
TEMPERATURE COEFFICIENT	0.55000D-05

STEEL MATERIAL PROPERTIES

TYPE	MODULUS	YIELD STRENGTH	BI-MODULUS	ULT STRAIN
1	0.29000D+08	0.60000D+05	0.34600D+06	0.18000D+00

1

PRESTRESSING STEEL PROPERTIES

BOND CODE 0 = POST-TENSIONED - UNBONDED
1 = POST TENSIONED - BONDED
2 = PRETENSIONED

TYPE NO	BOND CODE	AREA	WOBBLE COEF	FRICTION COEF	0.1 PERC. FY	RELAX COEF
1	1	2.907D+00	1.70000D-05	2.50000D-01	2.25000D+05	1.00D+01

```
        2          1 1.071D+00    1.70000D-05    2.50000D-01    2.25000D+05     1.00D+01

 POINTS ON THE STRESS-STRAIN CURVE  -  TYPE NO    1
    SECTION      E-MODULUS     MAX STRESS     MAX STRAIN
         1     2.94000D+07    1.70520D+05    5.80000D-03
         2     1.17810D+07    2.20000D+05    1.00000D-02
         3     1.00000D+06    2.40000D+05    3.00000D-02
         4     3.51351D+05    2.53000D+05    6.70000D-02

 POINTS ON THE STRESS-STRAIN CURVE  -  TYPE NO    2
    SECTION      E-MODULUS     MAX STRESS     MAX STRAIN
         1     2.94000D+07    1.70520D+05    5.80000D-03
         2     1.17810D+07    2.20000D+05    1.00000D-02
         3     1.00000D+06    2.40000D+05    3.00000D-02
         4     3.51351D+05    2.53000D+05    6.70000D-02
1CONCRETE LAYER SYSTEMS

 TYPE NO.    1
 Z-COORDINATES =
 -15.00000 -14.90000 -12.25000  -8.00000  -4.00000   0.00000   4.00000   8.00000  12.25000  16.40000
16.50000


 STEEL LAYER SYSTEMS

 TYPE NO.                      1
 NO. OF LAYERS                 4
 ANGLE CODE                    1


    LAYER  MATERIAL       Z-COORD.  SMEARED THK.        ANGLE
        1         1  -1.25625D+01   2.60000D-02   0.00000D+00
        2         1  -1.31875D+01   5.20000D-02   6.95000D+01
        3         1   1.25625D+01   2.60000D-02   0.00000D+00
        4         1   1.31875D+01   5.20000D-02   6.95000D+01
  2STORAGE REQUIRED =     11494
1TRIANGULAR SHELL ELEMENT DATA

 NUMBER OF ELEMENTS                       1152
 ELEMENT TYPE OPTION                         0
      0 = SHELL
      1 = MEMBRANE (CST)
      2 = PLATE BENDING (RAZZAQUE)
 OPTION FOR ELEMENT NODAL LOADS              0
      0 = CONSISTENT
      1 = TRIBUTARY AREA


 GRAVITY LOAD MULTIPLIERS
           X              Y              Z
        0.000          0.000         -1.000
```

```
 ELEMENT  NODE I  NODE J  NODE K   CONCR   C L S  ST L S   LOCO      ANLO     PLAT          PX
PY          PZ        TEMP


      1      15       2       1       1       1       1       1      0.00 0.00000D+00 0.00000D+00
0.00000D+00 0.00000D+00600.00
      2       1      14      15       1       1       1       1      0.00 0.00000D+00 0.00000D+00
0.00000D+00 0.00000D+00600.00
      3      28      15      14       1       1       1       1      0.00 0.00000D+00 0.00000D+00
0.00000D+00 0.00000D+00600.00
      4      14      27      28       1       1       1       1      0.00 0.00000D+00 0.00000D+00
0.00000D+00 0.00000D+00600.00
      5      41      28      27       1       1       1       1      0.00 0.00000D+00 0.00000D+00
0.00000D+00 0.00000D+00600.00
      6      27      40      41       1       1       1       1      0.00 0.00000D+00 0.00000D+00
0.00000D+00 0.00000D+00600.00
      7      54      41      40       1       1       1       1      0.00 0.00000D+00 0.00000D+00
0.00000D+00 0.00000D+00600.00
      8      40      53      54       1       1       1       1      0.00 0.00000D+00 0.00000D+00
0.00000D+00 0.00000D+00600.00
      9      67      54      53       1       1       1       1      0.00 0.00000D+00 0.00000D+00
0.00000D+00 0.00000D+00600.00
     10      53      66      67       1       1       1       1      0.00 0.00000D+00 0.00000D+00
0.00000D+00 0.00000D+00600.00

   1140     545     558     559       1       1       1       1      0.00 0.00000D+00 0.00000D+00
0.00000D+00 0.00000D+00600.00
   1141     572     559     558       1       1       1       1      0.00 0.00000D+00 0.00000D+00
0.00000D+00 0.00000D+00600.00
   1142     558     571     572       1       1       1       1      0.00 0.00000D+00 0.00000D+00
0.00000D+00 0.00000D+00600.00
   1143     585     572     571       1       1       1       1      0.00 0.00000D+00 0.00000D+00
0.00000D+00 0.00000D+00600.00
   1144     571     584     585       1       1       1       1      0.00 0.00000D+00 0.00000D+00
0.00000D+00 0.00000D+00600.00
   1145     598     585     584       1       1       1       1      0.00 0.00000D+00 0.00000D+00
0.00000D+00 0.00000D+00600.00
   1146     584     597     598       1       1       1       1      0.00 0.00000D+00 0.00000D+00
0.00000D+00 0.00000D+00600.00
   1147     611     598     597       1       1       1       1      0.00 0.00000D+00 0.00000D+00
0.00000D+00 0.00000D+00600.00
   1148     597     610     611       1       1       1       1      0.00 0.00000D+00 0.00000D+00
0.00000D+00 0.00000D+00600.00
   1149     624     611     610       1       1       1       1      0.00 0.00000D+00 0.00000D+00
0.00000D+00 0.00000D+00600.00
   1150     610     623     624       1       1       1       1      0.00 0.00000D+00 0.00000D+00
0.00000D+00 0.00000D+00600.00
   1151     637     624     623       1       1       1       1      0.00 0.00000D+00 0.00000D+00
0.00000D+00 0.00000D+00600.00
   1152     623     636     637       1       1       1       1      0.00 0.00000D+00 0.00000D+00
0.00000D+00 0.00000D+00600.00
1BOUNDARY ELEMENTS
```

NODE..NODES DEFINING CONSTRAINT DIRECTION... CODES DISPLACEMENT ROTATION STIFFNESS

N	NI	NJ	NK	NL	KD	KR	KN	DISPLACEMENT	ROTATION	STIFFNESS
210	209	0	0	0	1	0	0	0.000000D+00	0.000000D+00	5.66205D+04
212	209	0	0	0	1	0	2	0.000000D+00	0.000000D+00	5.66205D+04
214	209	0	0	0	1	0	2	0.000000D+00	0.000000D+00	5.66205D+04
216	209	0	0	0	1	0	2	0.000000D+00	0.000000D+00	5.66205D+04
218	209	0	0	0	1	0	2	0.000000D+00	0.000000D+00	5.66205D+04
220	209	0	0	0	1	0	2	0.000000D+00	0.000000D+00	5.66205D+04
210	197	0	0	0	1	0	0	0.000000D+00	0.000000D+00	5.66205D+04
212	197	0	0	0	1	0	2	0.000000D+00	0.000000D+00	5.66205D+04
214	197	0	0	0	1	0	2	0.000000D+00	0.000000D+00	5.66205D+04
216	197	0	0	0	1	0	2	0.000000D+00	0.000000D+00	5.66205D+04
218	197	0	0	0	1	0	2	0.000000D+00	0.000000D+00	5.66205D+04
220	197	0	0	0	1	0	2	0.000000D+00	0.000000D+00	5.66205D+04
418	417	0	0	0	1	0	0	0.000000D+00	0.000000D+00	5.66205D+04
420	417	0	0	0	1	0	2	0.000000D+00	0.000000D+00	5.66205D+04
422	417	0	0	0	1	0	2	0.000000D+00	0.000000D+00	5.66205D+04
424	417	0	0	0	1	0	2	0.000000D+00	0.000000D+00	5.66205D+04
426	417	0	0	0	1	0	2	0.000000D+00	0.000000D+00	5.66205D+04
428	417	0	0	0	1	0	2	0.000000D+00	0.000000D+00	5.66205D+04
418	405	0	0	0	1	0	0	0.000000D+00	0.000000D+00	5.66205D+04
420	405	0	0	0	1	0	2	0.000000D+00	0.000000D+00	5.66205D+04
422	405	0	0	0	1	0	2	0.000000D+00	0.000000D+00	5.66205D+04
424	405	0	0	0	1	0	2	0.000000D+00	0.000000D+00	5.66205D+04
426	405	0	0	0	1	0	2	0.000000D+00	0.000000D+00	5.66205D+04
428	405	0	0	0	1	0	2	0.000000D+00	0.000000D+00	5.66205D+04
210	196	224	222	198	1	0	0	0.000000D+00	0.000000D+00	6.50000D+06

212	196	224	222	198	1	0	2	0.00000D+00	0.00000D+00	6.50000D+06
214	196	224	222	198	1	0	2	0.00000D+00	0.00000D+00	6.50000D+06
216	196	224	222	198	1	0	2	0.00000D+00	0.00000D+00	6.50000D+06
218	196	224	222	198	1	0	2	0.00000D+00	0.00000D+00	6.50000D+06
220	196	224	222	198	1	0	2	0.00000D+00	0.00000D+00	6.50000D+06
418	404	432	430	406	1	0	0	0.00000D+00	0.00000D+00	6.50000D+06
420	404	432	430	406	1	0	2	0.00000D+00	0.00000D+00	6.50000D+06
422	404	432	430	406	1	0	2	0.00000D+00	0.00000D+00	6.50000D+06
424	404	432	430	406	1	0	2	0.00000D+00	0.00000D+00	6.50000D+06
426	404	432	430	406	1	0	2	0.00000D+00	0.00000D+00	6.50000D+06
428	404	432	430	406	1	0	2	0.00000D+00	0.00000D+00	6.50000D+06
1	1	15	14	2	1	0	0	0.00000D+00	0.00000D+00	9.81000D+06
2	1	15	14	2	1	0	1	0.00000D+00	0.00000D+00	9.81000D+06
3	1	15	14	2	1	0	1	0.00000D+00	0.00000D+00	9.81000D+06
4	1	15	14	2	1	0	1	0.00000D+00	0.00000D+00	9.81000D+06
5	1	15	14	2	1	0	1	0.00000D+00	0.00000D+00	9.81000D+06
6	1	15	14	2	1	0	1	0.00000D+00	0.00000D+00	9.81000D+06
7	1	15	14	2	1	0	1	0.00000D+00	0.00000D+00	9.81000D+06
8	1	15	14	2	1	0	1	0.00000D+00	0.00000D+00	9.81000D+06
9	1	15	14	2	1	0	1	0.00000D+00	0.00000D+00	9.81000D+06
10	1	15	14	2	1	0	1	0.00000D+00	0.00000D+00	9.81000D+06
11	1	15	14	2	1	0	1	0.00000D+00	0.00000D+00	9.81000D+06
12	1	15	14	2	1	0	1	0.00000D+00	0.00000D+00	9.81000D+06
13	1	15	14	2	1	0	1	0.00000D+00	0.00000D+00	9.81000D+06
625	612	626	625	613	1	0	0	0.00000D+00	0.00000D+00	9.81000D+06
626	612	626	625	613	1	0	1	0.00000D+00	0.00000D+00	9.81000D+06
627	612	626	625	613	1	0	1	0.00000D+00	0.00000D+00	9.81000D+06

```
      628        612        626        625        613     1     0     1   0.00000D+00    0.00000D+00
9.81000D+06
      629        612        626        625        613     1     0     1   0.00000D+00    0.00000D+00
9.81000D+06
      630        612        626        625        613     1     0     1   0.00000D+00    0.00000D+00
9.81000D+06
      631        612        626        625        613     1     0     1   0.00000D+00    0.00000D+00
9.81000D+06
      632        612        626        625        613     1     0     1   0.00000D+00    0.00000D+00
9.81000D+06
      633        612        626        625        613     1     0     1   0.00000D+00    0.00000D+00
9.81000D+06
      634        612        626        625        613     1     0     1   0.00000D+00    0.00000D+00
9.81000D+06
      635        612        626        625        613     1     0     1   0.00000D+00    0.00000D+00
9.81000D+06
      636        612        626        625        613     1     0     1   0.00000D+00    0.00000D+00
9.81000D+06
      637        612        626        625        613     1     0     1   0.00000D+00    0.00000D+00
9.81000D+06
1 PRESTRESSING TENDON DATA

 NUMBER OF TENDONS                          99
 MAX NO OF ELEMENTS CROSSED BY A TENDON     96
 MAX NO OF INFLEXION POINTS PER TENDON       6
 MAX NO OF TENDONS IN ONE ELEMENT           13



  3STORAGE REQUIRED =   356786

 TENDON INFORMATION
      TCODE - 0 = SLAB TENDON - IN ELEMENTS
              1 = SLAB TENDON - ON NODES
              2 = PANEL TENDON - IN ELEMENTS
      JCODE - 0 = JACKING FROM ONE END OR SEQUENTIAL
              1 = JACKING SYMMETRICALLY

 TENDON NO    TCODE    JCODE     TYPE    NO EL   NO I P   NODE A   NODE B   NODE Y   NODE Z    ANCH SLIP
FORCE JS     FORCE JE
         1        0        0        1       96        6        1        2      625      626 2.50000D-01
5.89D+05   -5.89D+05
         2        0        0        1       96        6        1        2      625      626 2.50000D-01
5.89D+05   -5.89D+05
         3        0        0        1       96        6        1        2      625      626 2.50000D-01
5.89D+05   -5.89D+05
         4        0        0        1       96        6        1        2      625      626 2.50000D-01
5.89D+05   -5.89D+05
         5        0        0        1       96        6        1        2      625      626 2.50000D-01
5.89D+05   -5.89D+05
         6        0        0        1       96        6        1        2      625      626 2.50000D-01
5.89D+05   -5.89D+05
         7        0        0        1       96        6        2        3      626      627 2.50000D-01
5.89D+05   -5.89D+05
```

```
      8      0      0      1     96      6      2      3    626    627 2.50000D-01
5.89D+05  -5.89D+05
      9      0      0      1     96      6      2      3    626    627 2.50000D-01
5.89D+05  -5.89D+05
     10      0      0      1     96      6      2      3    626    627 2.50000D-01
5.89D+05  -5.89D+05

     90      0      0      1     24      2    417    430    429    442 2.50000D-01
0.00D+00  -5.89D+05
     91      0      0      1     24      2    417    430    429    442 2.50000D-01
5.89D+05   0.00D+00
     92      0      0      1     24      2    417    430    429    442 2.50000D-01
0.00D+00  -5.89D+05
     93      0      0      1     24      2    417    430    429    442 2.50000D-01
5.89D+05   0.00D+00
     94      0      0      1     24      2    417    430    429    442 2.50000D-01
0.00D+00  -5.89D+05
     95      0      0      1     24      2    430    443    442    455 2.50000D-01
5.89D+05   0.00D+00
     96      0      0      2     24      2      1     14     13     26 2.50000D-01
0.00D+00  -4.00D+05
     97      0      0      2     24      2      1     14     13     26 2.50000D-01
0.00D+00  -4.00D+05
     98      0      0      2     24      2    612    625    624    637 2.50000D-01
4.00D+05   0.00D+00
     99      0      0      2     24      2    612    625    624    637 2.50000D-01
4.00D+05   0.00D+00


 NUMBERS OF ELEMENTS CROSSED BY -------------------


 TENDON NO   1
    1    2    3    4    5    6    7    8    9   10   11   12   13   14   15   16   17   18   19   20
21   22   23   24   25   26
   27   28   29   30   31   32   33   34   35   36   37   38   39   40   41   42   43   44   45   46
47   48   49   50   51   52
   53   54   55   56   57   58   59   60   61   62   63   64   65   66   67   68   69   70   71   72
73   74   75   76   77   78
   79   80   81   82   83   84   85   86   87   88   89   90   91   92   93   94   95   96


 TENDON NO  99
   96   95  192  191  288  287  384  383  480  479  576  575  672  671  768  767  864  863  960  959
1056 1055 1152 1151


 TENDON INFLEXION POINT DATA FOR ------------------

   I P NO      X-COORD       Y-COORD       ECCENTR  CURVE TYPE  DISTANCE AA       MAX ECC
```

```
TENDON NO   1
        1   0.5383D+01   0.1438D+02   0.0000D+00          1.   0.4775D+03   -0.1000D+02
        2   0.1086D+04   0.1426D+02   0.5800D+01          1.   0.1195D+03    0.9000D+01
        3   0.1322D+04   0.1424D+02   0.5800D+01          1.   0.4665D+03   -0.7000D+01
        4   0.2255D+04   0.1414D+02   0.5800D+01          1.   0.1195D+03    0.9000D+01
        5   0.2491D+04   0.1411D+02   0.5800D+01          1.   0.6030D+03   -0.1000D+02
        6   0.3572D+04   0.1400D+02   0.0000D+00          1.   0.0000D+00    0.0000D+00


TENDON NO  99
        1   0.3528D+04   0.0000D+00  -0.6000D+01          0.   0.0000D+00    0.0000D+00
        2   0.3937D+04   0.1086D+04  -0.6000D+01          0.   0.0000D+00    0.0000D+00


TENDON PROFILE FOR -------------------------------

             DISTANCE     CUM.  TENDON         PRESTRESS            TENDON               TENDON
PART OF LOAD TAKEN BY
  POINT NO   FROM START SLOPE CHANGE       FORCE ECCENTRICITY       SLOPE   PLAN ANGLE    NODE P
NODE Q      NODE P      NODE Q


 7.25885850D+02  7.26885850D+02    1   97
 3.69229418D+04  1.26736710D+01    2   97
 6.29896798D+03  7.49915520D+01    3   97
 5.40461685D+03  8.76551730D+01    4   97
 3.21891481D+03  1.49997890D+02    5   97
 2.98324267D+03  1.62621980D+02    6   97
 2.21732677D+03  2.24987990D+02    7   97
 2.11325643D+03  2.37603580D+02    8   97
 1.73495196D+03  2.99994280D+02    9   97
 1.67847954D+03  3.12568430D+02   10   97
 1.46034964D+03  3.74983770D+02   11   97
 1.42612125D+03  3.87550130D+02   12   97
 1.28948300D+03  4.49990030D+02   13   97
 1.26750718D+03  4.62515150D+02   14   97
 1.17790780D+03  5.24979550D+02   15   97
 1.16332457D+03  5.37480260D+02   16   97
 1.10332064D+03  5.99969100D+02   17   97
 1.09353108D+03  6.12464200D+02   18   97
 1.05334700D+03  6.74975930D+02   19   97
 1.04686825D+03  6.87429470D+02   20   97
 1.02058925D+03  7.49965510D+02   21   97


TENDON NO    1          ( ANCHOR SLIP DISTANCE =0.81D+03)

      1   4.1753D-04   0.0000D+00   5.5487D+05  -1.7443D-05  -4.1777D-02  -6.0451D-03          1
2  8.3068D-01  1.6932D-01
```

```
         2   1.2674D+01   1.1059D-03   5.5514D+05  -5.2246D-01  -4.0671D-02  -6.0451D-03          1
15  8.3094D-01  1.6906D-01
         3   7.4992D+01   6.5441D-03   5.5648D+05  -2.8875D+00  -3.5233D-02  -6.0451D-03         15
14  1.6898D-01  8.3102D-01
         4   8.7655D+01   7.6492D-03   5.5676D+05  -3.3267D+00  -3.4128D-02  -6.0451D-03         14
28  8.3127D-01  1.6873D-01
         5   1.5000D+02   1.3089D-02   5.5811D+05  -5.2847D+00  -2.8687D-02  -6.0451D-03         28
27  1.6865D-01  8.3135D-01
         6   1.6262D+02   1.4191D-02   5.5838D+05  -5.6399D+00  -2.7586D-02  -6.0451D-03         27
41  8.3158D-01  1.6842D-01
         7   2.2499D+02   1.9633D-02   5.5973D+05  -7.1906D+00  -2.2143D-02  -6.0451D-03         41
40  1.6834D-01  8.3166D-01
         8   2.3760D+02   2.0734D-02   5.6001D+05  -7.4630D+00  -2.1042D-02  -6.0451D-03         40
54  8.3191D-01  1.6809D-01
         9   2.9999D+02   2.6179D-02   5.6137D+05  -8.6061D+00  -1.5598D-02  -6.0451D-03         54
53  1.6801D-01  8.3199D-01
        10   3.1257D+02   2.7276D-02   5.6164D+05  -8.7953D+00  -1.4501D-02  -6.0451D-03         53
67  8.3224D-01  1.6776D-01


 TENDON NO   99          ( ANCHOR SLIP DISTANCE =0.10D+04)

         1   5.6843D-14   0.0000D+00   3.8641D+05  -6.0000D+00   0.0000D+00   6.9364D+01        612
625  5.0667D-01  4.9333D-01
         2   4.7760D+01   0.0000D+00   3.8673D+05  -6.0000D+00   0.0000D+00   6.9364D+01        612
626  5.0612D-01  4.9388D-01
         3   9.6640D+01   0.0000D+00   3.8705D+05  -6.0000D+00   0.0000D+00   6.9364D+01        626
613  4.9413D-01  5.0587D-01
         4   1.4448D+02   0.0000D+00   3.8737D+05  -6.0000D+00   0.0000D+00   6.9364D+01        613
627  5.0533D-01  4.9467D-01
         5   1.9330D+02   0.0000D+00   3.8769D+05  -6.0000D+00   0.0000D+00   6.9364D+01        627
614  4.9502D-01  5.0498D-01
         6   2.4123D+02   0.0000D+00   3.8800D+05  -6.0000D+00   0.0000D+00   6.9364D+01        614
628  5.0443D-01  4.9557D-01
         7   2.8990D+02   0.0000D+00   3.8832D+05  -6.0000D+00   0.0000D+00   6.9364D+01        628
615  4.9561D-01  5.0439D-01
         8   3.3788D+02   0.0000D+00   3.8864D+05  -6.0000D+00   0.0000D+00   6.9364D+01        615
629  5.0384D-01  4.9616D-01
         9   3.8655D+02   0.0000D+00   3.8896D+05  -6.0000D+00   0.0000D+00   6.9364D+01        629
616  4.9646D-01  5.0354D-01
        10   4.3461D+02   0.0000D+00   3.8928D+05  -6.0000D+00   0.0000D+00   6.9364D+01        616
630  5.0299D-01  4.9701D-01

  4STORAGE REQUIRED =     13378


 NUMBER OF EQUATIONS      3185
 BANDWIDTH                  75


  6STORAGE REQUIRED =    346456
  5STORAGE REQUIRED =     13378
1LOAD CONTROL DATA
```

```
NUMBER OF LOAD STEPS                           1
NUMBER OF ITERATIONS PERMITTED                20
NUMBER OF LOADED JOINTS                        0
FRACTION OF DEAD LOAD                     0.1000D+01
FRACTION OF SURFACE LOAD                  0.0000D+00
FRACTION OF SPRING LOAD                   0.5000D+00
FRACTION OF PRESTRESS LOAD                0.1000D+01
PRESTRESS - FRACTION OF EL DEF ALLOWED    0.0000D+00
NUMBER OF LOAD STEPS FOR TIME DEP. ANAL.       1
NUMBER OF ITERATIONS FOR TIME DEP. ANAL.      20
ITERATION TYPE CODE                            0
NUMBER OF ELEMENTS WITH TEMP CHANGE         1152

 5STORAGE REQUIRED =    13378
 7STORAGE REQUIRED =   242698

ELEMENT AND TOTAL STIFFNESS MATRICES FORMED AND TRIANGULARIZED
TIME STEP NO    1     LOAD STEP NO    1     ITERATION NO    1

 8STORAGE REQUIRED =   245883
 8STORAGE REQUIRED =   245883
 9STORAGE REQUIRED =   356302


CONVERGENCE CRITERIA NOT SATISFIED FOR THIS ITER

 8STORAGE REQUIRED =   245883
 9STORAGE REQUIRED =   356302


CONVERGENCE CRITERIA NOT SATISFIED FOR THIS ITER

 8STORAGE REQUIRED =   245883
 9STORAGE REQUIRED =   356302


CONVERGENCE CRITERIA NOT SATISFIED FOR THIS ITER

 8STORAGE REQUIRED =   245883
 9STORAGE REQUIRED =   356302
1  BROOK TRUCK-C                                                     ====     RESULTS

TIME STEP NUMBER                               1
LOAD STEP NUMBER                               1
ITERATION NUMBER                               4



TOTAL EXTERNAL NODAL FORCES

NODE          PX           PY           PZ           MX           MY           MZ
```

1	1.55372D+06	3.63553D+05	-5.85694D+04	-9.26962D+04	1.13830D+05	0.00000D+00
2	3.41778D+06	4.58028D+03	-1.40279D+05	-6.20241D+04	1.29275D+05	0.00000D+00
3	3.41791D+06	9.30455D+03	-1.40304D+05	-6.22053D+04	1.29376D+05	0.00000D+00
4	3.41830D+06	1.48689D+04	-1.40331D+05	-6.23309D+04	1.28557D+05	0.00000D+00
5	3.41873D+06	2.04277D+04	-1.40353D+05	-6.25036D+04	1.25607D+05	0.00000D+00
6	3.41911D+06	2.59799D+04	-1.40374D+05	-6.25958D+04	1.24133D+05	0.00000D+00
7	3.40214D+06	3.13898D+04	-1.39495D+05	-6.24860D+04	8.40214D+04	0.00000D+00
8	3.44943D+06	3.73921D+04	-1.41556D+05	-6.29507D+04	1.23062D+05	0.00000D+00
9	3.41698D+06	4.26143D+04	-1.40221D+05	-6.31494D+04	1.24987D+05	0.00000D+00

JOINT DISPLACEMENTS

NODE	DISPL-X	DISPL-Y	DISPL-Z	ROTAT-X	ROTAT-Y	ROTAT-Z
1	5.26243D-01	-7.53111D-02	-6.29144D-03	-9.04459D-04	-2.17704D-03	0.00000D+00
2	5.21744D-01	-7.74369D-02	-1.15441D-02	-8.45360D-04	-2.14738D-03	0.00000D+00
3	5.13295D-01	-7.88105D-02	-1.29212D-02	-7.89226D-04	-2.09079D-03	0.00000D+00
4	5.02487D-01	-7.90631D-02	-1.27148D-02	-7.57817D-04	-2.01842D-03	0.00000D+00
5	4.90179D-01	-7.82699D-02	-1.24380D-02	-7.31148D-04	-1.94239D-03	0.00000D+00
6	4.76928D-01	-7.66323D-02	-1.23348D-02	-7.02174D-04	-1.86301D-03	0.00000D+00
7	4.63052D-01	-7.43850D-02	-1.22749D-02	-6.70446D-04	-1.77987D-03	0.00000D+00
8	4.49076D-01	-7.17376D-02	-1.23862D-02	-6.37114D-04	-1.69011D-03	0.00000D+00
9	4.34308D-01	-6.89823D-02	-1.23873D-02	-6.03085D-04	-1.59603D-03	0.00000D+00
10	4.19150D-01	-6.62104D-02	-1.25230D-02	-5.68632D-04	-1.49992D-03	0.00000D+00
630	-4.32380D-01	8.20650D-02	-1.29354D-02	4.71503D-04	1.24593D-03	0.00000D+00
631	-4.48016D-01	8.54012D-02	-1.29044D-02	4.96439D-04	1.31142D-03	0.00000D+00
632	-4.63803D-01	8.82805D-02	-1.29772D-02	5.18432D-04	1.37444D-03	0.00000D+00
633	-4.78818D-01	9.05762D-02	-1.34118D-02	5.34828D-04	1.43587D-03	0.00000D+00
634	-4.92954D-01	9.19594D-02	-1.29471D-02	5.55076D-04	1.49728D-03	0.00000D+00
635	-5.06089D-01	9.22609D-02	-1.35288D-02	5.86370D-04	1.55265D-03	0.00000D+00
636	-5.17104D-01	9.13599D-02	-1.21767D-02	6.38409D-04	1.59452D-03	0.00000D+00
637	-5.24614D-01	8.95149D-02	-6.54852D-03	6.95754D-04	1.61162D-03	0.00000D+00

ELEMENT NUMBER 1
==============

STRAINS AT CENTROIDS OF STEEL LAYERS

	INT. PT. 1			INT. PT. 2			INT. PT. 3		
NO.	STRAIN-XX	STRAIN-YY	STRAIN-XY	STRAIN-XX	STRAIN-YY	STRAIN-XY	STRAIN-XX	STRAIN-YY	STRAIN-XY
1	-2.8884D-04	-9.7923D-07	-1.4616D-05	-2.9431D-04	-3.6265D-06	-1.7893D-05	-2.9477D-04	-3.9800D-06	-1.3290D-05
2	-2.9024D-04	-6.5826D-07	-1.5226D-05	-2.9598D-04	-3.4372D-06	-1.8665D-05	-2.9646D-04	-3.8083D-06	-1.3833D-05

```
   3   -2.3270D-04    -1.3882D-05     9.8808D-06    -2.2723D-04    -1.1235D-05     1.3157D-05     -
2.2677D-04   -1.0882D-05    8.5545D-06
   4   -2.3130D-04    -1.4203D-05     1.0490D-05    -2.2556D-04    -1.1424D-05     1.3930D-05     -
2.2508D-04   -1.1053D-05    9.0979D-06

 ELEMENT NUMBER    2
 ==============


 STRAINS AT CENTROIDS OF STEEL LAYERS
                    INT. PT. 1                                                        INT. PT. 2
INT. PT. 3
  NO.        STRAIN-XX        STRAIN-YY        STRAIN-XY        STRAIN-XX        STRAIN-YY        STRAIN-XY
STRAIN-XX     STRAIN-YY     STRAIN-XY

   1   -2.7772D-04     2.4534D-05    -5.5428D-05    -2.7403D-04     2.6088D-05    -5.5156D-05     -
2.7262D-04    2.7726D-05   -5.8562D-05
   2   -2.7945D-04     2.4832D-05    -5.5918D-05    -2.7558D-04     2.6462D-05    -5.5633D-05     -
2.7410D-04    2.8182D-05   -5.9209D-05
   3   -2.0799D-04     1.2579D-05    -3.5702D-05    -2.1167D-04     1.1025D-05    -3.5973D-05     -
2.1308D-04    9.3868D-06   -3.2567D-05
   4   -2.0625D-04     1.2281D-05    -3.5211D-05    -2.1012D-04     1.0651D-05    -3.5496D-05     -
2.1160D-04    8.9306D-06   -3.1920D-05



 ELEMENT NUMBER 1152
 ==============


 STRAINS AT CENTROIDS OF STEEL LAYERS
                    INT. PT. 1                                                        INT. PT. 2
INT. PT. 3
  NO.        STRAIN-XX        STRAIN-YY        STRAIN-XY        STRAIN-XX        STRAIN-YY        STRAIN-XY
STRAIN-XX     STRAIN-YY     STRAIN-XY

   1   -2.7222D-04    -4.5078D-06    -3.2451D-05    -2.7577D-04    -6.1502D-06    -3.4098D-05     -
2.7635D-04   -6.7814D-06   -3.0903D-05
   2   -2.7347D-04    -4.2440D-06    -3.3155D-05    -2.7720D-04    -5.9681D-06    -3.4884D-05     -
2.7781D-04   -6.6307D-06   -3.1530D-05
   3   -2.2193D-04    -1.5114D-05    -4.1609D-06    -2.1839D-04    -1.3471D-05    -2.5138D-06     -
2.1780D-04   -1.2840D-05   -5.7090D-06
   4   -2.2068D-04    -1.5378D-05    -3.4571D-06    -2.1696D-04    -1.3653D-05    -1.7282D-06     -
2.1634D-04   -1.2991D-05   -5.0822D-06
1INTERNAL STRESSES IN THE BOUNDARY ELEMENTS



 NODE    EXTENSIONAL STRESS     ROTATIONAL STRESS


  210         4.060215970+03         0.00000000D+00
  212         2.87557095D+03         0.00000000D+00
  214         2.06752088D+03         0.00000000D+00
```

216	1.35148214D+03	0.00000000D+00
218	5.37392161D+02	0.00000000D+00
220	-6.63450202D+02	0.00000000D+00
210	1.25146423D+04	0.00000000D+00
212	1.06902163D+04	0.00000000D+00
214	9.03378297D+03	0.00000000D+00
216	7.38601719D+03	0.00000000D+00
218	5.71970899D+03	0.00000000D+00
220	3.85553922D+03	0.00000000D+00
418	6.60569067D+02	0.00000000D+00
420	-5.25940565D+02	0.00000000D+00
422	-1.33137771D+03	0.00000000D+00
424	-2.05553562D+03	0.00000000D+00
426	-2.88232097D+03	0.00000000D+00

424	-6.21338008D+05	0.00000000D+00
426	-6.09312865D+05	0.00000000D+00
428	-6.26085673D+05	0.00000000D+00
1	-6.17190578D+04	0.00000000D+00
2	-1.13247200D+05	0.00000000D+00
3	-1.26756733D+05	0.00000000D+00
4	-1.24732407D+05	0.00000000D+00
5	-1.22016930D+05	0.00000000D+00
6	-1.21003967D+05	0.00000000D+00
7	-1.20416410D+05	0.00000000D+00
8	-1.21508922D+05	0.00000000D+00
9	-1.21519195D+05	0.00000000D+00
10	-1.22850971D+05	0.00000000D+00
11	-1.22486885D+05	0.00000000D+00
12	-1.05240851D+05	0.00000000D+00
13	-5.91274711D+04	0.00000000D+00
625	-6.63206446D+04	0.00000000D+00
626	-1.12075569D+05	0.00000000D+00
627	-1.28802546D+05	0.00000000D+00
628	-1.28860215D+05	0.00000000D+00
629	-1.27469095D+05	0.00000000D+00
630	-1.26896187D+05	0.00000000D+00
631	-1.26591886D+05	0.00000000D+00
632	-1.27306771D+05	0.00000000D+00
633	-1.31569352D+05	0.00000000D+00
634	-1.27011440D+05	0.00000000D+00
635	-1.32717147D+05	0.00000000D+00
636	-1.19453212D+05	0.00000000D+00
637	-6.42410013D+04	0.00000000D+00

1 BROOK TRUCK-C

TIME DEPENDENT ANALYSIS - CONCRETE PROPERTIES AT NEW TIME

DAYS AFTER CASTING	0.75000D+02
COMPRESSIVE STRENGTH	0.69742D+04
TENSILE STRENGTH	0.66557D+03
MODULUS OF ELASTICITY	0.50799D+07
STRAIN AT COMPRESSIVE STRENGTH	0.27458D-02

ELEMENT TEMPERATURE CHANGES

ELEMENT NO	TEMPERATURE REF LEVEL	GRADIENT
1	4.10D+01	0.00D+00
2	4.10D+01	0.00D+00
3	4.10D+01	0.00D+00
4	4.10D+01	0.00D+00
5	4.10D+01	0.00D+00
6	4.10D+01	0.00D+00
7	4.10D+01	0.00D+00
8	4.10D+01	0.00D+00
9	4.10D+01	0.00D+00
10	4.10D+01	0.00D+00
1146	4.10D+01	0.00D+00
1147	4.10D+01	0.00D+00
1148	4.10D+01	0.00D+00
1149	4.10D+01	0.00D+00
1150	4.10D+01	0.00D+00
1151	4.10D+01	0.00D+00
1152	4.10D+01	0.00D+00

TIME-DEPENDENT EQUIVALENT FORCES

NODE	PX	PY	PZ	MX	MY	MZ
1	1.73439D+06	6.61695D+05	-1.60106D+04	-5.24733D+05	7.65949D+05	0.00000D+00
2	3.50606D+06	-8.20891D+05	-3.10858D+04	5.25477D+05	1.58994D+06	0.00000D+00
3	3.52728D+06	-8.43068D+05	-3.01819D+04	5.37915D+05	1.54607D+06	0.00000D+00
4	3.53355D+06	-8.40844D+05	-3.08279D+04	5.33660D+05	1.53059D+06	0.00000D+00
5	3.53624D+06	-8.31329D+05	-3.12297D+04	5.30028D+05	1.52640D+06	0.00000D+00
6	3.53750D+06	-8.20235D+05	-3.13573D+04	5.26148D+05	1.51684D+06	0.00000D+00
7	3.53555D+06	-8.09102D+05	-3.13272D+04	5.17392D+05	1.49679D+06	0.00000D+00
8	3.54231D+06	-7.96955D+05	-3.16686D+04	5.13372D+05	1.49529D+06	0.00000D+00
9	3.53207D+06	-7.97830D+05	-3.17348D+04	5.02780D+05	1.48539D+06	0.00000D+00
10	3.52480D+06	-7.92260D+05	-3.22843D+04	4.80045D+05	1.48152D+06	0.00000D+00
631	-3.67860D+06	8.67619D+05	-3.11817D+04	-6.04340D+05	-1.71022D+06	0.00000D+00
632	-3.69294D+06	8.72705D+05	-3.13771D+04	-6.12984D+05	-1.71691D+06	0.00000D+00
633	-3.68658D+06	8.73420D+05	-3.07078D+04	-6.04751D+05	-1.70407D+06	0.00000D+00
634	-3.68500D+06	8.85179D+05	-3.05777D+04	-6.13676D+05	-1.68600D+06	0.00000D+00
635	-3.68190D+06	9.02770D+05	-2.97717D+04	-6.14601D+05	-1.68172D+06	0.00000D+00
636	-3.66826D+06	8.87851D+05	-3.04812D+04	-6.00176D+05	-1.72125D+06	0.00000D+00
637	-1.80816D+06	-6.38777D+05	-1.56714D+04	4.84905D+05	-8.15128D+05	0.00000D+00

5STORAGE REQUIRED = 13378
6STORAGE REQUIRED = 346456
7STORAGE REQUIRED = 242698

ELEMENT AND TOTAL STIFFNESS MATRICES FORMED AND TRIANGULARIZED
TIME STEP NO 1 LOAD STEP NO 1 ITERATION NO 1

8STORAGE REQUIRED = 245883

8STORAGE REQUIRED = 245883
9STORAGE REQUIRED = 356302

CONVERGENCE CRITERIA NOT SATISFIED FOR THIS ITER

8STORAGE REQUIRED = 245883
9STORAGE REQUIRED = 356302

CONVERGENCE CRITERIA NOT SATISFIED FOR THIS ITER

8STORAGE REQUIRED = 245883
9STORAGE REQUIRED = 356302

CONVERGENCE CRITERIA NOT SATISFIED FOR THIS ITER

8STORAGE REQUIRED = 245883
9STORAGE REQUIRED = 356302

1 BROOK TRUCK-C ==== RESULTS

TIME STEP NUMBER 1
LOAD STEP NUMBER 1
ITERATION NUMBER 4

TIME DEPENDENT ANALYSIS

TOTAL EXTERNAL NODAL FORCES

NODE	PX	PY	PZ	MX	MY	MZ
1	1.52051D+06	3.18022D+05	-5.79689D+04	-9.27024D+04	1.13809D+05	0.00000D+00
2	3.37877D+06	4.50136D+03	-1.38778D+05	-6.20229D+04	1.29254D+05	0.00000D+00
3	3.37889D+06	9.25211D+03	-1.38801D+05	-6.22051D+04	1.29356D+05	0.00000D+00
4	3.37922D+06	1.47529D+04	-1.38826D+05	-6.23316D+04	1.28544D+05	0.00000D+00
5	3.37961D+06	2.02483D+04	-1.38846D+05	-6.25068D+04	1.25631D+05	0.00000D+00
6	3.37998D+06	2.57373D+04	-1.38866D+05	-6.25984D+04	1.24173D+05	0.00000D+00
7	3.36319D+06	3.10849D+04	-1.37997D+05	-6.24926D+04	8.45216D+04	0.00000D+00
8	3.40991D+06	3.70183D+04	-1.40033D+05	-6.29550D+04	1.23121D+05	0.00000D+00
9	3.37785D+06	4.21812D+04	-1.38714D+05	-6.31556D+04	1.25025D+05	0.00000D+00
10	3.37817D+06	4.76446D+04	-1.38741D+05	-6.33871D+04	1.26103D+05	0.00000D+00
630	-3.37188D+06	-2.56522D+04	-1.38005D+05	7.09620D+04	-1.66043D+05	0.00000D+00
631	-3.35560D+06	-3.09677D+04	-1.37374D+05	7.16596D+04	-2.23858D+05	0.00000D+00
632	-3.40501D+06	-3.69015D+04	-1.38832D+05	7.26845D+04	-2.11039D+05	0.00000D+00
633	-3.37459D+06	-4.20554D+04	-1.37505D+05	7.27756D+04	-2.02249D+05	0.00000D+00
634	-3.37445D+06	-4.74840D+04	-1.37108D+05	7.18994D+04	-1.19060D+05	0.00000D+00
635	-3.37391D+06	-5.29036D+04	-1.36833D+05	7.09676D+04	-1.08309D+05	0.00000D+00

636	-3.37391D+06	-5.91454D+04	-1.36618D+05	7.13234D+04	-1.24639D+05	0.00000D+00
637	-1.57266D+06	-3.59295D+05	-5.90444D+04	1.06070D+05	-1.24898D+05	0.00000D+00

JOINT DISPLACEMENTS

NODE	DISPL-X	DISPL-Y	DISPL-Z	ROTAT-X	ROTAT-Y	ROTAT-Z
1	8.90254D-01	-7.98375D-02	-6.59793D-03	-9.88883D-04	-2.39592D-03	0.00000D+00
2	8.77700D-01	-9.11148D-02	-1.17764D-02	-9.22669D-04	-2.35888D-03	0.00000D+00
3	8.61465D-01	-1.01717D-01	-1.29624D-02	-8.65654D-04	-2.29940D-03	0.00000D+00
4	8.42865D-01	-1.11195D-01	-1.26470D-02	-8.34474D-04	-2.22453D-03	0.00000D+00
5	8.22714D-01	-1.19608D-01	-1.23290D-02	-8.06429D-04	-2.14362D-03	0.00000D+00
6	8.01573D-01	-1.27158D-01	-1.22070D-02	-7.74506D-04	-2.05633D-03	0.00000D+00
7	7.79784D-01	-1.34089D-01	-1.21297D-02	-7.38573D-04	-1.96207D-03	0.00000D+00
8	7.57872D-01	-1.40630D-01	-1.22407D-02	-6.99826D-04	-1.85781D-03	0.00000D+00
9	7.35179D-01	-1.47112D-01	-1.22369D-02	-6.59359D-04	-1.74599D-03	0.00000D+00
10	7.12068D-01	-1.53629D-01	-1.23821D-02	-6.17033D-04	-1.62840D-03	0.00000D+00
630	-7.38295D-01	1.53478D-01	-1.27990D-02	5.07746D-04	1.34285D-03	0.00000D+00
631	-7.62525D-01	1.47082D-01	-1.27726D-02	5.37067D-04	1.41985D-03	0.00000D+00
632	-7.86838D-01	1.40221D-01	-1.28560D-02	5.62169D-04	1.49167D-03	0.00000D+00
633	-8.10344D-01	1.32781D-01	-1.33391D-02	5.80377D-04	1.55962D-03	0.00000D+00
634	-8.32699D-01	1.24379D-01	-1.28405D-02	6.01777D-04	1.62482D-03	0.00000D+00
635	-8.54150D-01	1.14927D-01	-1.35322D-02	6.33798D-04	1.68282D-03	0.00000D+00
636	-8.73467D-01	1.04279D-01	-1.23461D-02	6.86949D-04	1.72862D-03	0.00000D+00
637	-8.89493D-01	9.27525D-02	-6.81325D-03	7.51006D-04	1.75474D-03	0.00000D+00

ELEMENT NUMBER 1
==============

STRAINS AT CENTROIDS OF STEEL LAYERS

	INT. PT. 1			INT. PT. 2			INT. PT. 3		
NO.	STRAIN-XX	STRAIN-YY	STRAIN-XY	STRAIN-XX	STRAIN-YY	STRAIN-XY	STRAIN-XX	STRAIN-YY	STRAIN-XY
1	-3.4532D-04	9.8206D-07	-4.5993D-06	-3.5051D-04	-1.1623D-06	-7.3969D-06	-3.5112D-04	-2.8076D-06	-3.7337D-06
2	-3.4689D-04	1.3511D-06	-5.2316D-06	-3.5234D-04	-8.9988D-07	-8.1683D-06	-3.5298D-04	-2.6270D-06	-4.3229D-06
3	-2.8210D-04	-1.3854D-05	2.0818D-05	-2.7691D-04	-1.1710D-05	2.3616D-05	-2.7630D-04	-1.0065D-05	1.9953D-05
4	-2.8053D-04	-1.4223D-05	2.1451D-05	-2.7508D-04	-1.1972D-05	2.4387D-05	-2.7444D-04	-1.0245D-05	2.0542D-05

ELEMENT NUMBER 2
==============

STRAINS AT CENTROIDS OF STEEL LAYERS

```
                    INT. PT. 1                                                    INT. PT. 2
INT. PT. 3
  NO.      STRAIN-XX      STRAIN-YY      STRAIN-XY      STRAIN-XX      STRAIN-YY      STRAIN-XY
STRAIN-XX    STRAIN-YY    STRAIN-XY

    1   -3.3401D-04    2.5193D-05   -4.6344D-05   -3.3026D-04    2.6465D-05   -4.5977D-05    -
3.2887D-04    2.9118D-05   -4.8706D-05
    2   -3.3594D-04    2.5530D-05   -4.6914D-05   -3.3200D-04    2.6866D-05   -4.6528D-05    -
3.3055D-04    2.9651D-05   -4.9393D-05
    3   -2.5643D-04    1.1628D-05   -2.3452D-05   -2.6018D-04    1.0356D-05   -2.3819D-05    -
2.6157D-04    7.7027D-06   -2.1090D-05
    4   -2.5450D-04    1.1291D-05   -2.2883D-05   -2.5844D-04    9.9551D-06   -2.3268D-05    -
2.5989D-04    7.1699D-06   -2.0403D-05


 ELEMENT NUMBER 1152
 ==============


 STRAINS AT CENTROIDS OF STEEL LAYERS
                    INT. PT. 1                                                    INT. PT. 2
INT. PT. 3
  NO.      STRAIN-XX      STRAIN-YY      STRAIN-XY      STRAIN-XX      STRAIN-YY      STRAIN-XY
STRAIN-XX    STRAIN-YY    STRAIN-XY

    1   -3.2602D-04   -2.9194D-06   -1.8747D-05   -3.2921D-04   -4.1216D-06   -1.9978D-05    -
3.2989D-04   -5.7206D-06   -1.7690D-05
    2   -3.2743D-04   -2.6082D-06   -1.9445D-05   -3.3077D-04   -3.8701D-06   -2.0738D-05    -
3.3149D-04   -5.5487D-06   -1.8336D-05
    3   -2.6936D-04   -1.5431D-05    9.3220D-06   -2.6617D-04   -1.4228D-05    1.0553D-05    -
2.6549D-04   -1.2629D-05    8.2652D-06
    4   -2.6795D-04   -1.5742D-05    1.0020D-05   -2.6461D-04   -1.4480D-05    1.1312D-05    -
2.6389D-04   -1.2801D-05    8.9108D-06
1INTERNAL STRESSES IN THE BOUNDARY ELEMENTS



 NODE    EXTENSIONAL STRESS     ROTATIONAL STRESS


  210         8.48808282D+03         0.00000000D+00
  212         5.86872967D+03         0.00000000D+00
  214         3.69811492D+03         0.00000000D+00
  216         1.63541535D+03         0.00000000D+00
  218        -5.37962521D+02         0.00000000D+00
  220        -3.16453547D+03         0.00000000D+00
  210         2.07155533D+04         0.00000000D+00
  212         1.78936242D+04         0.00000000D+00
  214         1.52915922D+04         0.00000000D+00
  216         1.27130792D+04         0.00000000D+00
  218         1.01140933D+04         0.00000000D+00
  220         7.27701952D+03         0.00000000D+00
  418         3.24159865D+03         0.00000000D+00
```

```
 420       5.92142045D+02       0.00000000D+00
 422      -1.60457642D+03       0.00000000D+00
 424      -3.70590694D+03       0.00000000D+00
 426      -5.92252829D+03       0.00000000D+00
 428      -8.60112425D+03       0.00000000D+00
 418      -7.13937848D+03       0.00000000D+00
 420      -9.97951351D+03       0.00000000D+00
 422      -1.26169770D+04       0.00000000D+00
 424      -1.52879087D+04       0.00000000D+00
 426      -1.79885124D+04       0.00000000D+00
 428      -2.09434461D+04       0.00000000D+00
 210      -5.68249723D+05       0.00000000D+00
 212      -6.12402444D+05       0.00000000D+00
 214      -6.26423064D+05       0.00000000D+00

 633      -1.30856629D+05       0.00000000D+00
 634      -1.25965762D+05       0.00000000D+00
 635      -1.32750800D+05       0.00000000D+00
 636      -1.21115604D+05       0.00000000D+00
 637      -6.68379386D+04       0.00000000D+00
 5STORAGE REQUIRED =    13378
1LOAD CONTROL DATA

 NUMBER OF LOAD STEPS                          0
 NUMBER OF ITERATIONS PERMITTED                0
 NUMBER OF LOADED JOINTS                       0
 FRACTION OF DEAD LOAD                    0.0000D+00
 FRACTION OF SURFACE LOAD                 0.0000D+00
 FRACTION OF SPRING LOAD                  0.0000D+00
 FRACTION OF PRESTRESS LOAD               0.0000D+00
 PRESTRESS - FRACTION OF EL DEF ALLOWED   0.0000D+00
 NUMBER OF LOAD STEPS FOR TIME DEP. ANAL.      1
 NUMBER OF ITERATIONS FOR TIME DEP. ANAL.     20
 ITERATION TYPE CODE                           0
 NUMBER OF ELEMENTS WITH TEMP CHANGE        1152

 9STORAGE REQUIRED =   356302
1  BROOK TRUCK-C

 TIME DEPENDENT ANALYSIS   - CONCRETE PROPERTIES AT NEW TIME


 DAYS AFTER CASTING                            0.21100D+03
 COMPRESSIVE STRENGTH                          0.72501D+04
 TENSILE STRENGTH                              0.67860D+03
 MODULUS OF ELASTICITY                         0.51794D+07
 STRAIN AT COMPRESSIVE STRENGTH                0.27996D-02
 ELEMENT TEMPERATURE CHANGES

 ELEMENT     TEMPERATURE
     NO   REF LEVEL    GRADIENT
      1   8.99D+01     0.00D+00
      2   8.99D+01     0.00D+00
      3   8.99D+01     0.00D+00
```

4	8.99D+01	0.00D+00
5	8.99D+01	0.00D+00
6	8.99D+01	0.00D+00
7	8.99D+01	0.00D+00
8	8.99D+01	0.00D+00
9	8.99D+01	0.00D+00
10	8.99D+01	0.00D+00
1151	8.99D+01	0.00D+00
1152	8.99D+01	0.00D+00

TIME-DEPENDENT EQUIVALENT FORCES

NODE	PX	PY	PZ	MX	MY	MZ
1	-1.46955D+05	-9.08626D+05	-1.35732D+04	3.47199D+05	-1.12372D+06	0.00000D+00
2	-1.56333D+05	1.11902D+06	-2.85402D+03	-1.19392D+06	-2.22447D+06	0.00000D+00
3	-5.73038D+04	1.01987D+06	-7.17031D+02	-1.24268D+06	-2.57694D+06	0.00000D+00
4	-3.55578D+04	1.02274D+06	-4.01333D+03	-1.28472D+06	-2.73396D+06	0.00000D+00
5	-3.78715D+04	1.05318D+06	-5.84180D+03	-1.28465D+06	-2.78103D+06	0.00000D+00
6	-4.90467D+04	1.08860D+06	-6.44457D+03	-1.28387D+06	-2.83520D+06	0.00000D+00
7	-5.35925D+04	1.12230D+06	-6.91183D+03	-1.30510D+06	-2.90689D+06	0.00000D+00
8	-6.19864D+04	1.16069D+06	-6.50988D+03	-1.31785D+06	-2.95500D+06	0.00000D+00
9	-5.95010D+04	1.16048D+06	-7.25650D+03	-1.36453D+06	-3.01855D+06	0.00000D+00
10	-6.94565D+04	1.17786D+06	-7.78300D+03	-1.43604D+06	-3.04051D+06	0.00000D+00
633	2.45579D+05	-1.11190D+06	-2.93140D+03	1.19564D+06	2.74940D+06	0.00000D+00
634	2.34146D+05	-1.06158D+06	-3.29036D+03	1.15530D+06	2.70304D+06	0.00000D+00
635	2.35341D+05	-1.05793D+06	9.10005D+02	1.16739D+06	2.60730D+06	0.00000D+00
636	2.97062D+05	-1.11195D+06	-1.31900D+03	1.12685D+06	2.30681D+06	0.00000D+00
637	2.32226D+05	9.01337D+05	-1.14855D+04	-3.73972D+05	1.16932D+06	0.00000D+00

5STORAGE REQUIRED = 13378
6STORAGE REQUIRED = 346456
7STORAGE REQUIRED = 242698

ELEMENT AND TOTAL STIFFNESS MATRICES FORMED AND TRIANGULARIZED
TIME STEP NO 2 LOAD STEP NO 1 ITERATION NO 1

8STORAGE REQUIRED = 245883
8STORAGE REQUIRED = 245883
9STORAGE REQUIRED = 356302

CONVERGENCE CRITERIA NOT SATISFIED FOR THIS ITER

8STORAGE REQUIRED = 245883
9STORAGE REQUIRED = 356302

CONVERGENCE CRITERIA NOT SATISFIED FOR THIS ITER

8STORAGE REQUIRED = 245883
9STORAGE REQUIRED = 356302

CONVERGENCE CRITERIA NOT SATISFIED FOR THIS ITER

8STORAGE REQUIRED = 245883
9STORAGE REQUIRED = 356302

1 BROOK TRUCK-C ==== RESULTS

TIME STEP NUMBER 2
LOAD STEP NUMBER 1
ITERATION NUMBER 4

TIME DEPENDENT ANALYSIS

TOTAL EXTERNAL NODAL FORCES

NODE	PX	PY	PZ	MX	MY	MZ
1	1.47999D+06	3.47074D+05	-5.60555D+04	-9.22889D+04	1.16252D+05	0.00000D+00
2	3.25696D+06	4.83487D+03	-1.34085D+05	-6.25484D+04	1.31083D+05	0.00000D+00
3	3.25522D+06	8.98119D+03	-1.34042D+05	-6.22903D+04	1.31404D+05	0.00000D+00
4	3.25439D+06	1.42224D+04	-1.34022D+05	-6.22255D+04	1.30791D+05	0.00000D+00
5	3.25366D+06	1.94588D+04	-1.34000D+05	-6.24770D+04	1.28180D+05	0.00000D+00
6	3.25275D+06	2.46784D+04	-1.33972D+05	-6.26198D+04	1.26860D+05	0.00000D+00
7	3.23486D+06	2.96710D+04	-1.33071D+05	-6.25640D+04	8.89331D+04	0.00000D+00
8	3.27781D+06	3.51957D+04	-1.34957D+05	-6.30090D+04	1.26268D+05	0.00000D+00
9	3.24513D+06	4.00166D+04	-1.33619D+05	-6.31894D+04	1.28301D+05	0.00000D+00
10	3.24360D+06	4.49880D+04	-1.33577D+05	-6.35262D+04	1.29889D+05	0.00000D+00
630	-3.24411D+06	-2.42514D+04	-1.33136D+05	7.09754D+04	-1.67158D+05	0.00000D+00
631	-3.22975D+06	-2.95787D+04	-1.32579D+05	7.16243D+04	-2.22810D+05	0.00000D+00
632	-3.27807D+06	-3.53490D+04	-1.34011D+05	7.25496D+04	-2.10669D+05	0.00000D+00
633	-3.24975D+06	-4.03577D+04	-1.32769D+05	7.28938D+04	-2.01960D+05	0.00000D+00
634	-3.25049D+06	-4.56758D+04	-1.32415D+05	7.20644D+04	-1.21572D+05	0.00000D+00
635	-3.25068D+06	-5.09880D+04	-1.32174D+05	7.08684D+04	-1.11023D+05	0.00000D+00
636	-3.25173D+06	-5.76063D+04	-1.31999D+05	7.17465D+04	-1.26882D+05	0.00000D+00
637	-1.53049D+06	-3.88933D+05	-5.70831D+04	1.05815D+05	-1.27476D+05	0.00000D+00

JOINT DISPLACEMENTS

NODE	DISPL-X	DISPL-Y	DISPL-Z	ROTAT-X	ROTAT-Y	ROTAT-Z
1	8.77298D-01	-1.89576D-01	-8.01515D-03	-1.48372D-03	-3.69939D-03	0.00000D+00
2	8.69022D-01	-1.81329D-01	-1.25996D-02	-1.39067D-03	-3.62751D-03	0.00000D+00

3	8.57800D-01	-1.72219D-01	-1.29942D-02	-1.33057D-03	-3.55243D-03	0.00000D+00
4	8.43762D-01	-1.61515D-01	-1.23252D-02	-1.29876D-03	-3.46304D-03	0.00000D+00
5	8.27604D-01	-1.49292D-01	-1.18824D-02	-1.26203D-03	-3.35647D-03	0.00000D+00
6	8.09973D-01	-1.35839D-01	-1.16797D-02	-1.21436D-03	-3.22849D-03	0.00000D+00
7	7.91364D-01	-1.21519D-01	-1.14997D-02	-1.15685D-03	-3.07805D-03	0.00000D+00
8	7.72285D-01	-1.06705D-01	-1.16086D-02	-1.09102D-03	-2.90095D-03	0.00000D+00
9	7.52349D-01	-9.20065D-02	-1.15590D-02	-1.01837D-03	-2.70102D-03	0.00000D+00
10	7.31685D-01	-7.75627D-02	-1.17153D-02	-9.36897D-04	-2.47811D-03	0.00000D+00
630	-7.41413D-01	1.26998D-01	-1.21915D-02	7.77678D-04	2.06038D-03	0.00000D+00
631	-7.63149D-01	1.43712D-01	-1.21897D-02	8.29684D-04	2.19717D-03	0.00000D+00
632	-7.84506D-01	1.59798D-01	-1.23256D-02	8.71606D-04	2.31572D-03	0.00000D+00
633	-8.04688D-01	1.75119D-01	-1.30987D-02	8.98885D-04	2.41985D-03	0.00000D+00
634	-8.23035D-01	1.89132D-01	-1.23199D-02	9.28422D-04	2.50905D-03	0.00000D+00
635	-8.39783D-01	2.01657D-01	-1.34955D-02	9.68556D-04	2.58367D-03	0.00000D+00
636	-8.53864D-01	2.12514D-01	-1.29638D-02	1.02793D-03	2.65225D-03	0.00000D+00
637	-8.65178D-01	2.22106D-01	-7.98712D-03	1.11969D-03	2.72417D-03	0.00000D+00

ELEMENT NUMBER 1
==============

STRAINS AT CENTROIDS OF STEEL LAYERS

	INT. PT. 1			INT. PT. 2			INT. PT. 3		
NO.	STRAIN-XX	STRAIN-YY	STRAIN-XY	STRAIN-XX	STRAIN-YY	STRAIN-XY	STRAIN-XX	STRAIN-YY	STRAIN-XY
1	-6.9069D-04	-7.2828D-05	1.6028D-05	-6.9577D-04	-7.3016D-05	1.4457D-05	-6.9704D-04	-8.1275D-05	1.4190D-05
2	-6.9321D-04	-7.2298D-05	1.5198D-05	-6.9855D-04	-7.2495D-05	1.3549D-05	-6.9987D-04	-8.1166D-05	1.3268D-05
3	-5.8934D-04	-9.4119D-05	4.9382D-05	-5.8426D-04	-9.3932D-05	5.0953D-05	-5.8300D-04	-8.5672D-05	5.1220D-05
4	-5.8682D-04	-9.4649D-05	5.0212D-05	-5.8149D-04	-9.4452D-05	5.1861D-05	-5.8016D-04	-8.5782D-05	5.2141D-05

ELEMENT NUMBER 2
==============

STRAINS AT CENTROIDS OF STEEL LAYERS

	INT. PT. 1			INT. PT. 2			INT. PT. 3		
NO.	STRAIN-XX	STRAIN-YY	STRAIN-XY	STRAIN-XX	STRAIN-YY	STRAIN-XY	STRAIN-XX	STRAIN-YY	STRAIN-XY
1	-6.8377D-04	-4.1085D-05	-3.5358D-05	-6.7886D-04	-4.1003D-05	-3.4082D-05	-6.7751D-04	-3.2627D-05	-3.3728D-05
2	-6.8681D-04	-4.0598D-05	-3.6375D-05	-6.8166D-04	-4.0511D-05	-3.5035D-05	-6.8023D-04	-3.1718D-05	-3.4663D-05
3	-5.6172D-04	-6.0696D-05	5.5060D-06	-5.6663D-04	-6.0779D-05	4.2294D-06	-5.6799D-04	-6.9155D-05	3.8753D-06

```
    4  -5.5869D-04    -6.1184D-05     6.5225D-06    -5.6384D-04    -6.1271D-05     5.1824D-06     -
5.6527D-04   -7.0064D-05     4.8107D-06


 ELEMENT NUMBER 1152
 ==============


 STRAINS AT CENTROIDS OF STEEL LAYERS
                   INT. PT. 1                                                              INT. PT. 2
INT. PT. 3
  NO.      STRAIN-XX      STRAIN-YY      STRAIN-XY      STRAIN-XX      STRAIN-YY      STRAIN-XY
STRAIN-XX     STRAIN-YY     STRAIN-XY

    1  -6.5878D-04    -7.8577D-05     1.7772D-05    -6.6135D-04    -7.8063D-05     1.7355D-05     -
6.6228D-04   -8.4592D-05     1.5700D-05
    2  -6.6108D-04    -7.8082D-05     1.7036D-05    -6.6378D-04    -7.7542D-05     1.6599D-05     -
6.6475D-04   -8.4395D-05     1.4861D-05
    3  -5.6626D-04    -9.8494D-05     4.7358D-05    -5.6369D-04    -9.9008D-05     4.7775D-05     -
5.6276D-04   -9.2480D-05     4.9430D-05
    4  -5.6396D-04    -9.8990D-05     4.8094D-05    -5.6126D-04    -9.9529D-05     4.8531D-05     -
5.6028D-04   -9.2676D-05     5.0269D-05
1INTERNAL STRESSES IN THE BOUNDARY ELEMENTS



 NODE    EXTENSIONAL STRESS     ROTATIONAL STRESS


  210        2.634737240+03         0.000000000+00
  212        2.10055014D+03         0.00000000D+00
  214        2.29378530D+03         0.00000000D+00
  216        2.64763417D+03         0.00000000D+00
  218        2.84232216D+03         0.00000000D+00
  220        2.32700100D+03         0.00000000D+00
  210        2.02815974D+04         0.00000000D+00
  212        1.74561791D+04         0.00000000D+00
  214        1.50690200D+04         0.00000000D+00

  637       -7.835369540+04         0.000000000+00
  5STORAGE REQUIRED =     13378
1LOAD CONTROL DATA

 NUMBER OF LOAD STEPS                            1
 NUMBER OF ITERATIONS PERMITTED                 20
 NUMBER OF LOADED JOINTS                         4
 FRACTION OF DEAD LOAD                      0.0000D+00
 FRACTION OF SURFACE LOAD                   0.0000D+00
 FRACTION OF SPRING LOAD                    0.0000D+00
 FRACTION OF PRESTRESS LOAD                 0.0000D+00
 PRESTRESS - FRACTION OF EL DEF ALLOWED     0.0000D+00
 NUMBER OF LOAD STEPS FOR TIME DEP. ANAL.        0
 NUMBER OF ITERATIONS FOR TIME DEP. ANAL.        0
 ITERATION TYPE CODE                             0
```

NUMBER OF ELEMENTS WITH TEMP CHANGE 1152

1 CONCENTRATED JOINT LOADS

NODE	PX	PY	PZ	MX	MY	MZ
319	0.0000D+00	0.0000D+00	-2.3880D+04	0.0000D+00	0.0000D+00	0.0000D+00
320	0.0000D+00	0.0000D+00	-2.3880D+04	0.0000D+00	0.0000D+00	0.0000D+00
345	0.0000D+00	0.0000D+00	-5.8000D+03	0.0000D+00	0.0000D+00	0.0000D+00
346	0.0000D+00	0.0000D+00	-5.8800D+03	0.0000D+00	0.0000D+00	0.0000D+00

5STORAGE REQUIRED = 13378
6STORAGE REQUIRED = 346456
7STORAGE REQUIRED = 242698

ELEMENT AND TOTAL STIFFNESS MATRICES FORMED AND TRIANGULARIZED
TIME STEP NO 3 LOAD STEP NO 1 ITERATION NO 1

8STORAGE REQUIRED = 245883
8STORAGE REQUIRED = 245883
9STORAGE REQUIRED = 356302

CONVERGENCE CRITERIA NOT SATISFIED FOR THIS ITER

8STORAGE REQUIRED = 245883
9STORAGE REQUIRED = 356302

1 BROOK TRUCK-C ==== RESULTS

TIME STEP NUMBER 3
LOAD STEP NUMBER 1
ITERATION NUMBER 2

TOTAL EXTERNAL NODAL FORCES

NODE	PX	PY	PZ	MX	MY	MZ
1	1.48290D+06	3.54622D+05	-5.60584D+04	-4.64943D+04	9.92929D+04	0.00000D+00
2	3.25473D+06	-2.76008D+03	-1.34108D+05	-1.08270D+05	1.48201D+05	0.00000D+00
3	3.25576D+06	8.99402D+03	-1.34063D+05	-6.22966D+04	1.31451D+05	0.00000D+00
4	3.25500D+06	1.42316D+04	-1.34046D+05	-6.22284D+04	1.30820D+05	0.00000D+00
5	3.25432D+06	1.94679D+04	-1.34025D+05	-6.24804D+04	1.28210D+05	0.00000D+00
6	3.25346D+06	2.46876D+04	-1.33999D+05	-6.26183D+04	1.26890D+05	0.00000D+00
7	3.23563D+06	2.96806D+04	-1.33101D+05	-6.25654D+04	8.89532D+04	0.00000D+00
8	3.27866D+06	3.52061D+04	-1.34989D+05	-6.30095D+04	1.26296D+05	0.00000D+00
9	3.24605D+06	4.00273D+04	-1.33654D+05	-6.31873D+04	1.28344D+05	0.00000D+00
10	3.24465D+06	4.49934D+04	-1.33618D+05	-6.35281D+04	1.29865D+05	0.00000D+00
630	-3.24507D+06	-2.42600D+04	-1.33173D+05	7.09767D+04	-1.67198D+05	0.00000D+00
631	-3.23065D+06	-2.95896D+04	-1.32613D+05	7.16235D+04	-2.22864D+05	0.00000D+00

632	-3.27891D+06	-3.53623D+04	-1.34043D+05	7.25501D+04	-2.10723D+05	0.00000D+00
633	-3.25054D+06	-4.03738D+04	-1.32799D+05	7.28983D+04	-2.02008D+05	0.00000D+00
634	-3.25119D+06	-4.56988D+04	-1.32442D+05	7.20597D+04	-1.21622D+05	0.00000D+00
635	-3.25139D+06	-5.10092D+04	-1.32201D+05	7.08591D+04	-1.11026D+05	0.00000D+00
636	-3.24946D+06	-4.96667D+04	-1.32026D+05	1.19617D+05	-1.44910D+05	0.00000D+00
637	-1.53357D+06	-3.96859D+05	-5.70868D+04	5.77335D+04	-1.09612D+05	0.00000D+00

JOINT DISPLACEMENTS

NODE	DISPL-X	DISPL-Y	DISPL-Z	ROTAT-X	ROTAT-Y	ROTAT-Z
1	8.77039D-01	-1.87816D-01	-8.08800D-03	-1.48972D-03	-3.72810D-03	0.00000D+00
2	8.68882D-01	-1.79938D-01	-1.25256D-02	-1.40287D-03	-3.65600D-03	0.00000D+00
3	8.57784D-01	-1.71071D-01	-1.29803D-02	-1.34269D-03	-3.58337D-03	0.00000D+00
4	8.43834D-01	-1.60560D-01	-1.23314D-02	-1.31103D-03	-3.49549D-03	0.00000D+00
5	8.27731D-01	-1.48495D-01	-1.18792D-02	-1.27490D-03	-3.39094D-03	0.00000D+00
6	8.10134D-01	-1.35175D-01	-1.16673D-02	-1.22816D-03	-3.26517D-03	0.00000D+00
7	7.91543D-01	-1.20970D-01	-1.14838D-02	-1.17164D-03	-3.11728D-03	0.00000D+00
8	7.72474D-01	-1.06258D-01	-1.15969D-02	-1.10697D-03	-2.94304D-03	0.00000D+00
9	7.52537D-01	-9.16557D-02	-1.15603D-02	-1.03576D-03	-2.74661D-03	0.00000D+00
10	7.31861D-01	-7.73063D-02	-1.17312D-02	-9.55794D-04	-2.52801D-03	0.00000D+00
630	-7.41614D-01	1.26549D-01	-1.21694D-02	7.96314D-04	2.10948D-03	0.00000D+00
631	-7.63343D-01	1.43158D-01	-1.21670D-02	8.47195D-04	2.24353D-03	0.00000D+00
632	-7.84681D-01	1.59127D-01	-1.23117D-02	8.88065D-04	2.35965D-03	0.00000D+00
633	-8.04829D-01	1.74311D-01	-1.31043D-02	9.14457D-04	2.46161D-03	0.00000D+00
634	-8.23118D-01	1.88158D-01	-1.22924D-02	9.43677D-04	2.54914D-03	0.00000D+00
635	-8.39785D-01	2.00461D-01	-1.34775D-02	9.83098D-04	2.62219D-03	0.00000D+00
636	-8.53731D-01	2.11057D-01	-1.28931D-02	1.04304D-03	2.68799D-03	0.00000D+00
637	-8.64913D-01	2.20251D-01	-8.06178D-03	1.12833D-03	2.76005D-03	0.00000D+00

ELEMENT NUMBER 1
==============

STRAINS AT CENTROIDS OF STEEL LAYERS

	INT. PT. 1			INT. PT. 2			INT. PT. 3		
NO.	STRAIN-XX	STRAIN-YY	STRAIN-XY	STRAIN-XX	STRAIN-YY	STRAIN-XY	STRAIN-XX	STRAIN-YY	STRAIN-XY
1	-6.9083D-04	-7.6862D-05	1.4031D-05	-6.9584D-04	-7.6972D-05	1.2096D-05	-6.9687D-04	-8.5229D-05	1.1500D-05
2	-6.9336D-04	-7.6378D-05	1.3198D-05	-6.9862D-04	-7.6495D-05	1.1167D-05	-6.9970D-04	-8.5161D-05	1.0541D-05
3	-5.8912D-04	-9.6292D-05	4.7525D-05	-5.8411D-04	-9.6182D-05	4.9460D-05	-5.8308D-04	-8.7926D-05	5.0056D-05
4	-5.8659D-04	-9.6776D-05	4.8358D-05	-5.8133D-04	-9.6660D-05	5.0390D-05	-5.8025D-04	-8.7993D-05	5.1015D-05

ELEMENT NUMBER 2

==============

STRAINS AT CENTROIDS OF STEEL LAYERS

	INT. PT. 1			INT. PT. 2			INT. PT. 3		
NO.	STRAIN-XX	STRAIN-YY	STRAIN-XY	STRAIN-XX	STRAIN-YY	STRAIN-XY	STRAIN-XX	STRAIN-YY	STRAIN-XY
1	-6.8414D-04	-4.2865D-05	-3.7746D-05	-6.7953D-04	-4.2926D-05	-3.6557D-05	-6.7825D-04	-3.4598D-05	-3.5917D-05
2	-6.8716D-04	-4.2401D-05	-3.8760D-05	-6.8232D-04	-4.2464D-05	-3.7513D-05	-6.8097D-04	-3.3722D-05	-3.6841D-05
3	-5.6276D-04	-6.1530D-05	3.0538D-06	-5.6738D-04	-6.1470D-05	1.8655D-06	-5.6866D-04	-6.9798D-05	1.2248D-06
4	-5.5974D-04	-6.1995D-05	4.0687D-06	-5.6459D-04	-6.1931D-05	2.8213D-06	-5.6593D-04	-7.0673D-05	2.1488D-06

ELEMENT NUMBER 1152

==============

STRAINS AT CENTROIDS OF STEEL LAYERS

	INT. PT. 1			INT. PT. 2			INT. PT. 3		
NO.	STRAIN-XX	STRAIN-YY	STRAIN-XY	STRAIN-XX	STRAIN-YY	STRAIN-XY	STRAIN-XX	STRAIN-YY	STRAIN-XY
1	-6.5897D-04	-8.2657D-05	1.5760D-05	-6.6142D-04	-8.2052D-05	1.5043D-05	-6.6212D-04	-8.8538D-05	1.3032D-05
2	-6.6128D-04	-8.2207D-05	1.5018D-05	-6.6386D-04	-8.1572D-05	1.4265D-05	-6.6459D-04	-8.8381D-05	1.2154D-05
3	-5.6600D-04	-1.0073D-04	4.5598D-05	-5.6355D-04	-1.0133D-04	4.6315D-05	-5.6285D-04	-9.4847D-05	4.8326D-05
4	-5.6369D-04	-1.0118D-04	4.6340D-05	-5.6111D-04	-1.0181D-04	4.7093D-05	-5.6038D-04	-9.5004D-05	4.9204D-05

1INTERNAL STRESSES IN THE BOUNDARY ELEMENTS

NODE	EXTENSIONAL STRESS	ROTATIONAL STRESS
210	2.632895350+03	0.000000000D+00
212	2.09910236D+03	0.000000000D+00
214	2.29292592D+03	0.000000000D+00
216	2.64726213D+03	0.000000000D+00
218	2.84201253D+03	0.000000000D+00
220	2.32628820D+03	0.000000000D+00
210	2.02730853D+04	0.000000000D+00
212	1.74500087D+04	0.000000000D+00
214	1.50647989D+04	0.000000000D+00

216	1.27600611D+04	0.00000000D+00
218	1.04214439D+04	0.00000000D+00
630	-1.19381393D+05	0.00000000D+00
631	-1.19358416D+05	0.00000000D+00
632	-1.20777973D+05	0.00000000D+00
633	-1.28553347D+05	0.00000000D+00
634	-1.20588494D+05	0.00000000D+00
635	-1.32214373D+05	0.00000000D+00
636	-1.26481417D+05	0.00000000D+00
637	-7.90860367D+04	0.00000000D+00